

# **Nonlinear optical properties of modified Bacteriorhodopsins**

A Dissertation

Submitted to the Department of Physics  
in Partial Fulfilment of the Requirements for the  
Degree of *Doctor Rerum Naturalium*

by

**Aliaksei Krasnaberski**



January, 2008

# **Nonlinear optical properties of modified Bacteriorhodopsins**

Referee:

Prof. Dr. H.-J. Steinhoff

Prof. Dr. K. Betzler

# Contents

<b>1. Introduction.....</b>	<b>1</b>
1.1. New materials for nonlinear optic.....	1
1.2. Scope of this thesis.....	2
<b>2. Bacteriorhodopsin.....</b>	<b>4</b>
2.1. Structure and function of bR.....	5
2.2. The photocycle of bR.....	10
2.3. Methods of bacteriorhodopsins modification.....	14
2.4. Nonlinear optical properties of bacteriorhodopsin. State of the art.....	21
<b>3. Theoretical Background.....</b>	<b>23</b>
3.1. Nonlinear polarization. The Anharmonic Oscillator Model.....	23
3.2. Local field correction factors .....	27
3.3. The theory of the Hyper-Raleigh-scattering.....	29
3.4. Calculation of the electronic structure of molecules. Methods of modern quantum physics.....	32
3.4.1. The adiabatic and Born-Oppenheimer Approximations.....	32
3.4.2. Hartree-Fock Theory.....	35
3.4.2.1. Molecular orbitals.....	35
3.4.2.2. The variation principle. The Roothaan-Hall equation.....	36
3.4.2.3. Electron correlation effects. Configuration Interaction method.....	42
3.4.2.4. The semiempirical INDO/S method.....	42
3.4.3. Calculation of the hyperpolarizabilities.....	43
3.4.3.1 The coupled methods (Finite field method).....	43
3.4.3.2 The Sum Over States method. Two state model.....	46
3.4.4. Solvation models.....	50
3.4.4.1 Continuum salvation models. Polarizable Continuum Model (PCM). Conductor-like Screening Model(COSMO) SMx.....	50
3.4.4.2 The hybrid QM/MM method.....	52
<b>4 Calculation of Linear and Nonlinear Optical Properties of Modified Bacteriorhodopsins.....</b>	<b>59</b>
4.1 The origin of the nonlinear optical properties of bacteriorhodopsin.....	59

4.2	Calculations for bacteriorhodopsin mutants and variants.....	66
<b>5</b>	<b>Experimental Part.....</b>	<b>72</b>
5.1	Time-resolve optical spectroscopy setup.....	72
5.1.1	Sample preparation.....	72
5.1.2	Optical part.....	72
5.1.3	Data evaluation. Global Fit procedure.....	74
5.2	Hyper-Raleigh-scattering setup.....	76
5.2.1	Sample preparation.....	76
5.2.2	Optical part.....	76
5.2.3	Electronic part.....	78
<b>6</b>	<b>Experimental Results and Discussions.....</b>	<b>80</b>
6.1	pH dependence of the first hyperpolarizability of bacteriorhodopsin.....	80
6.2	Determination of the first hyperpolarizability of the bR mutants W86F, D85C.....	83
6.2.1	Extinction coefficient determination.....	84
6.2.2	Size distribution measurements.....	88
6.2.3	HRS measurement of the mutants W86F, D85C.....	90
6.3	Examination of the photocycles of bR mutants by means of the absorption spectroscopy and HRS techniques.....	93
6.3.1	Time-resolved absorption spectroscopy measurements.....	94
6.3.2	Time-resolved HRS measurements.....	102
<b>7</b>	<b>Summary.....</b>	<b>109</b>
	<b>Bibliography.....</b>	<b>111</b>

# Chapter 1

## Introduction

### 1.1. New materials for nonlinear optic

Recent years have shown a dramatic growth of research activity in searching of materials that exhibit nonlinear optical (NLO) behaviours. NLO properties have been found in semiconductors and inorganic crystals such as  $\text{LiNbO}_3$  and  $\text{KH}_2\text{PO}_4$ . Later investigations have shown that molecule-based organic materials and biomaterials possess advantages in NLO characteristics. The ultra fast response due to fully electronic polarization, enhanced NLO properties and better processability are advantages with respect to conventional inorganic materials. Moreover, the investigations of materials, which exhibit switchability are of importance for optical computing.

A number of proteins have been explored for technical application[1-4]. But, only one of them, the membrane protein bacteriorhodopsin (BR), has received considerable attention. Owing to its unique stability toward chemical and thermal degradation, switchability and high NLO-properties (BR possesses the unusually high optical nonlinearities of  $2100 \times 10^{30}$ esu which is two order of magnitude larger than 4-methyl-4-methoxy nitrostilbene which is 120 times larger than KTP[5]) a broad range of applications has been proposed for BR. These include random access thin film memories[6], photon counters and photovoltaic converters[7], picosecond photodetectors[8], neutral-type logic gates[9], reversible holographic media[10], spatial light modulators[2], associative memories[2], two-photon volumetric memories[11], nonlinear optical filters[12], real-time holographic imaging systems[12], and optical computing[13].

This thesis is devoted to the theoretical and experimental study of the second-order nonlinear optical properties of native and modified bacteriorhodopsins.

For the theoretical calculations of the absorption maxima and the first hyperpolarizabilities of modified bacteriorhodopsins and of the M-like intermediate, a hybrid quantum mechanical/molecular mechanical-configuration interaction (QM/MM-CI) method of the molecular orbital package MOS-F from the Mopac program has been used as self-consistent reaction field model. This method is more suitable than the conventional Onsager, PMC (Polarizable Continuum Model) and COSMO (Conductor-like Screening Model) continuum solvation models for protein investigations.

The measurements of the first hyperpolarizabilities of modified BR have been performed by means of the Hyper-Raleigh scattering (HRS) technique. Due to its inherent simplicity this is a useful tool for the experimental determination of the second-order nonlinear properties of charged organic materials in solutions. Being dependent on the intramolecular charges movements, the second-order nonlinear processes may provide insight into BR charge redistribution, which determines structural changes required for biological function. HRS polarization measurements can also give additional information on the conformation of the retinal molecule in BR as well as on the correlation between the chromophores.

## **1.2. Scope of this thesis**

This thesis is organized as follows. Chapter 2 describes the main structural and functional properties of bacteriorhodopsin as well as its nonlinear characteristics. Chapter 3 provides the theoretical background of computational methods which are used to obtain the (non)linear properties of modified bacteriorhodopsins. The theory of Hyper-Raleigh scattering is described as well. In Chapter 4 the origin of the unusually high nonlinearity of BR is discussed. The results of theoretical calculations of the first hyperpolarizability of several BR mutants and variants are presented. Chapter 5 is devoted to the experimental

determination of the first hyperpolarizability of two BR mutants, W86F and D85C. pH dependence of the first-order nonlinearity of wild type BR is also presented. The kinetics of time-resolved HRS and flash spectroscopy measurements of several BR mutants are compared.

## Chapter 2

# Bacteriorhodopsin

Bacteriorhodopsin is a membrane protein discovered in 1971 in *Halobacterium halobium* (since 1990 named *Halobacterium salinarum*) [14], a primitive organism living in salt lakes (Fig. 2.1).



Figure 2.1: A saline in the Arabian desert. Red colour is due to the presence of *Halobacterium salinarum*. Taken from [www.biochem.mpg.de](http://www.biochem.mpg.de)

The halobacteria belong to prokaryotes, but morphologically differ from them. Their cell walls are quite different from those of bacteria and consist mainly of glycoprotein as ordinary lipoprotein membranes fail in high salt concentrations. Halobacteria may be either rods of approximately 0.5  $\mu\text{m}$  in diameter, and 3-10 $\mu\text{m}$  in length or spherical. They are characterized by red or purple colours. The purple part of the membranes contains only one protein, bacteriorhodopsin, whereas the red part of it contains three types of rhodopsin, namely halorhodopsin (HR) and two types of sensory rhodopsins (Figure 2.2). Halobacteria membranes contain ATP-synthetase/ATPase as well which along with BR



provide chemical energy for the cell. Upon absorption of sunlight BR pumps protons out of the cell. The resulting proton gradient across the cell is utilized by the ATPases to synthesize ATP.

The genome of Halobacterium species has been sequenced and comprises 2,571,010 base pairs (bp) of DNA into three circular strands, one large chromosome with 2,014,239 bp, and two smaller ones with 191,346 and 365,425 bp.

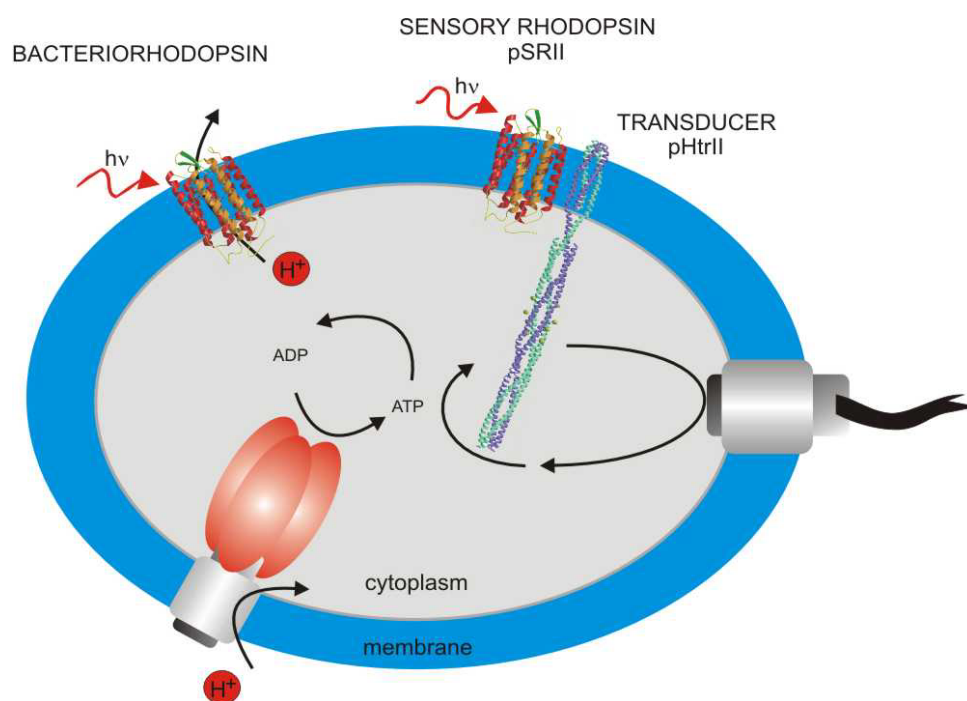


Figure 2.2: Schematic model of a halobacterial cell and its main functional systems for phototaxis and photosynthesis

## 2.1. Structure and function of BR

After its discovery, BR has been intensively studied using methods of spectroscopy, crystallography, and biochemistry. Detailed information are available on its structure[15-17], function, main steps in proton translocation, and conformational changes of the protein during the photocycle[18-25].

BR is isolated from the bacteria in form of purple membranes (PM). PMs are hexagonal crystalline arrays of BR trimers, which lead to extraordinary stability against external conditions. BR does not denature below 80°C (in some cases up to 160°C!), and retains its properties in a pH range from 0-11. PMs consist of 25% lipids and 75% BR molecules by weight, and are 4.5-5 nm thick. A cross-section of PM fragments varies up to 1 μm, and depends on the type of the cell culture and on the conditions of growth.

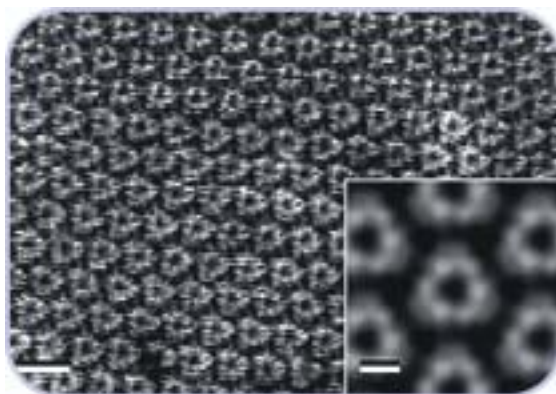


Figure 2.3: The hexagonal crystalline array of BR trimers.

The crystalline structure has been explored by means of electron and neutron diffraction methods. Figure 2.3 shows an electron-density map of the hexagonal packing of BR trimers with a unit cell size of 63Å[26]. Each trimer is stabilized by 12-14 molecules of lipids.

The BR molecule is a retinal-protein complex, which has the weight of 26 kDA, consisting of a protein part and a retinal molecule (Vitamin A aldehyde) bound via a protonated Schiff base to lysine 216(Figure 2.4).

BR is a single polypeptide chain consisting of 248 amino acids, which was first deciphered by Ovchinnikov et al[27] and independently in Khorana's laboratory[28]. Figure 2.5 shows the amino acid sequence of BR proposed in 1979.



Investigations on the 3D protein structure have been going on for approximately 25 years. The first model for the general spatial structure of BR was proposed as early as 1975 by Henderson[30]. Cryo-electron microscopy of 2-dimensional crystals to 3.5Å resolution and especially X-ray diffraction of 3-dimensional crystals grown by the cubic phase method to 1.55Å resolution[31], gave detailed information about the structure of this protein. Figure 2.6 shows the model of the tertiary structure of bacteriorhodopsin. Helices E, F, and G are approximately perpendicular to the plane of the membrane, whereas helices A, B, C, and D cross the membrane at small angles from the normal. All helices together form a proton channel, the pathway of a proton during its transport across the membrane.

The protonated Schiff base of the retinal is located in helix G at 0.6-1.0 nm from the cytoplasmic side of the membrane, whereas the ionic ring is almost in the middle of it. The dipole moment of the retinal builds up an angle of 20-30° with the plane of membrane. The active site consists of the protonated retinal Schiff base, two counter-ions Asp85, Asp212, and a water molecule (402). The binding pocket of the chromophore is responsible for the suppression of retinal isomerizations, different from all-trans-13cis that could occur in free retinal, e.g. isomerizations leading to 7-cis, 9-cis, and 11-cis-retinal.

The Schiff base divides the proton channel into two parts, so-called extracellular and cytoplasmic ones. The first of them involves hydrogen-bonded Arg82, Glu194, Glu204 and at least seven water molecules[31;32]. Mutation of any of these residues results in strong inhibition of the proton release upon protonation of Asp85. Hydrogen bonds between Thr89, Tyr185, Tyr57, and Ser193 give additional stability to the protein.

The cytoplasmic region contains no such polar network, but it does contain a movable structural element. The  $\alpha$ -helical repeat of helix G is interrupted by a  $\pi$ -bulge at Ala-215 and Lys-216[31], caused by hydrogen bonds of the two main-chain C=O groups to water molecules (501) and (502). This features offer the possibility of conformational changes near helix G where the retinal is bound.

Water (501) is further hydrogen bonded to the indole nitrogen of Trp182, a residue that contacts the retinal polyene chain. Water (502), in turn, is hydrogen bonded to Asp96. This forms a chain of covalent and hydrogen bonds, with Trp182, water 501, Ala215, Lys216, water (502), Thr46, and Asp96 as participants. The chain connects helices C, F and G together.

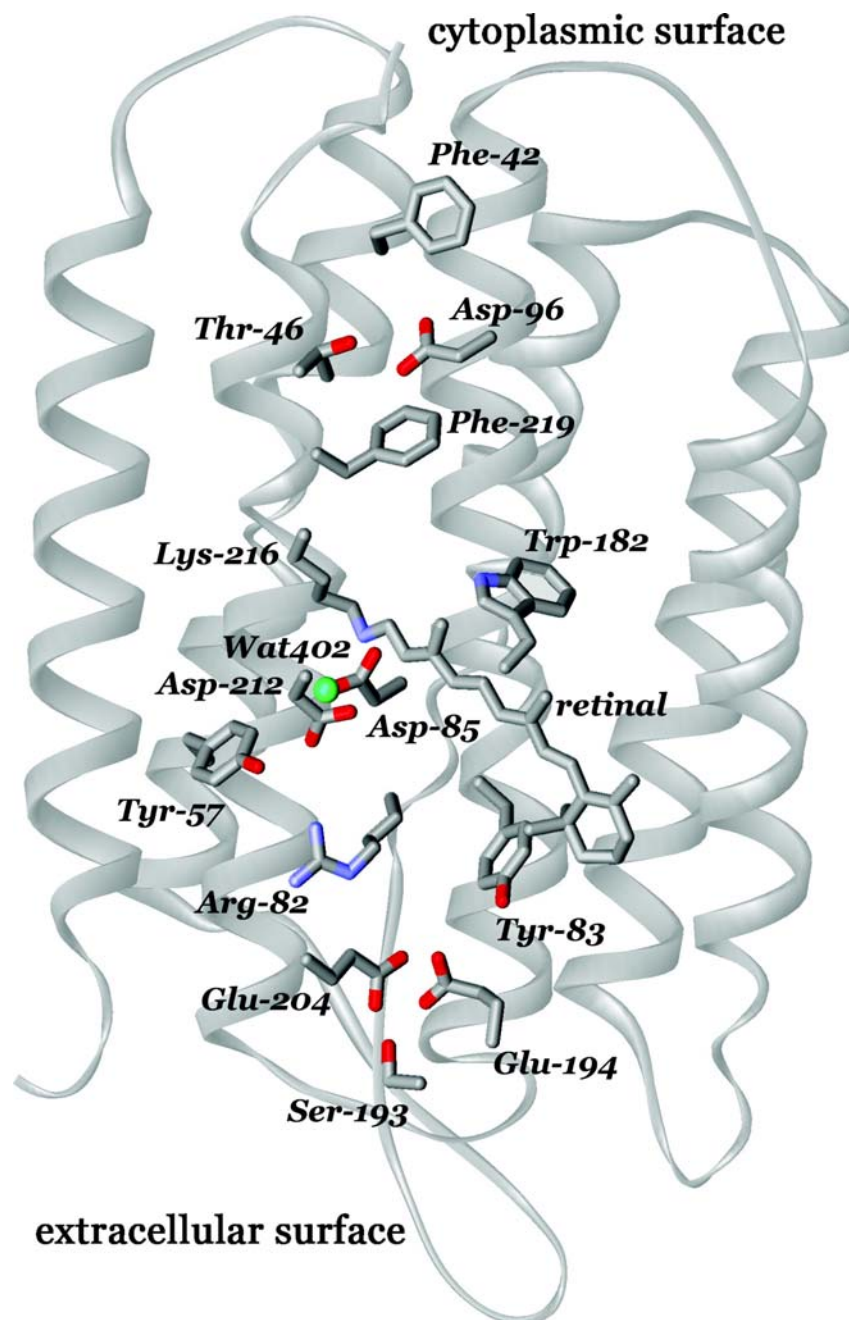


Figure 2.6: The model of tertiary structure of bacteriorhodopsin.

BR can be either in the so-called light-adapted or in the dark-adapted states. These states have different absorption spectra. Whereas BR in the light-adapted state absorbs at 570nm, the absorption maxima of BR in the dark-adapted state is shifted to 560nm. Moreover, BR in the dark-adapted state contains a 50:50 mixture of 13cis/all-trans configuration of retinal, whereas its light-adapted form is predominantly all-trans.

## 2.2. The photocycle of BR

Upon absorption of a photon the retinal undergoes an all-trans/13cis, 15-anti isomerization and BR goes through a photocycle, during which a proton is transported from the cytoplasmatic to the extracellular side. The proton pathway contains at least the following amino-acids E194/E204-R82-D85-Schiff base-D96-D38.

The proton transport is accompanied by a series of spectral changes caused by the appearance and vanishing of spectral different intermediates. A schematic representation of the photocycle is given in figure 2.7.

The absorption maximum of each intermediate under normal conditions is given near its common abbreviation ( $J_{625}$ ,  $K_{590}$ ,  $L_{550}$ ...). The time-constant of the decay are marked near the arrows connecting two spectral intermediates. For some intermediates, the time of decay may fluctuate by orders of magnitude depending on external conditions. The absorption maxima are quite independent of external conditions and their variation does not exceed the range of 10 to 20 nm.

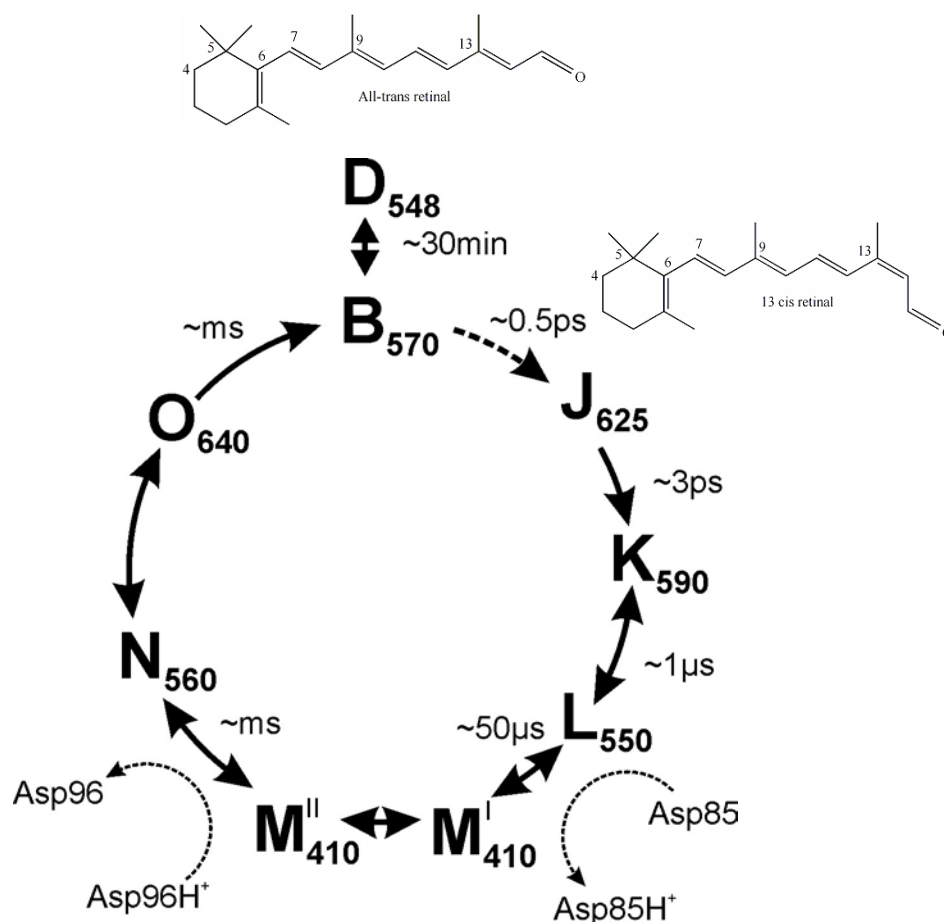


Figure 2.7: Photocycle of BR. The subscripts are the absorption maxima of intermediates.

Only the first step of the cycle requires light, whereas the other transitions represent just processes of a thermal relaxation. Existence of at least two spectrally indistinguishable intermediates M1 and M2 has been showed by many authors[33-36] and was observed in the X-ray structures of M1 and M2[37]. In accordance with a widely accepted model, the formation of M1 is related to the transfer of a proton from the Schiff base to Asp85. The transition from M1 to M2 corresponds to a reorientation of the deprotonated Schiff base from the extracellular to the cytoplasmic part of the proton channel (the so called protonation switch). During the M2 to N transition, the Schiff base is re-protonated from Asp96. Whereas all the conversions between the intermediates are reversible, the transition

from M1 to M2 is considered to be the main irreversible step in the photocycle. During this transition a conformational change of the protein occurs which involves an outward movement of helix F.

The generally accepted model of the primary light-induced events in BR is shown in figure 2.8. Upon absorption of a quantum of light the chromophore undergoes a transition from its ground state to a vibrationally excited state  $S_1$  (200fs). After about 0.2 ps, the vibrationally excited level  $S_1$  relaxes *via* a torsional motion of  $90^\circ$  about the  $C_{13}=C_{14}$  double bond to the second minimum of  $S_1$ . This approach was first suggested for retinal proteins in [38;39] and proved at pump-probe experiments with femtosecond time resolution [40;41]. In another 0.5 ps, the electron-excited state  $S_1$  converts to the J state completing 13-cis (180 $^\circ$ ) isomerization and reserving the energy to vectorial proton transport, or returns to the ground state. The quantum yield value of the photochemical reaction, according to the latest data equals to 0.66 [42] or slightly less, close to 0.5 [43;44].

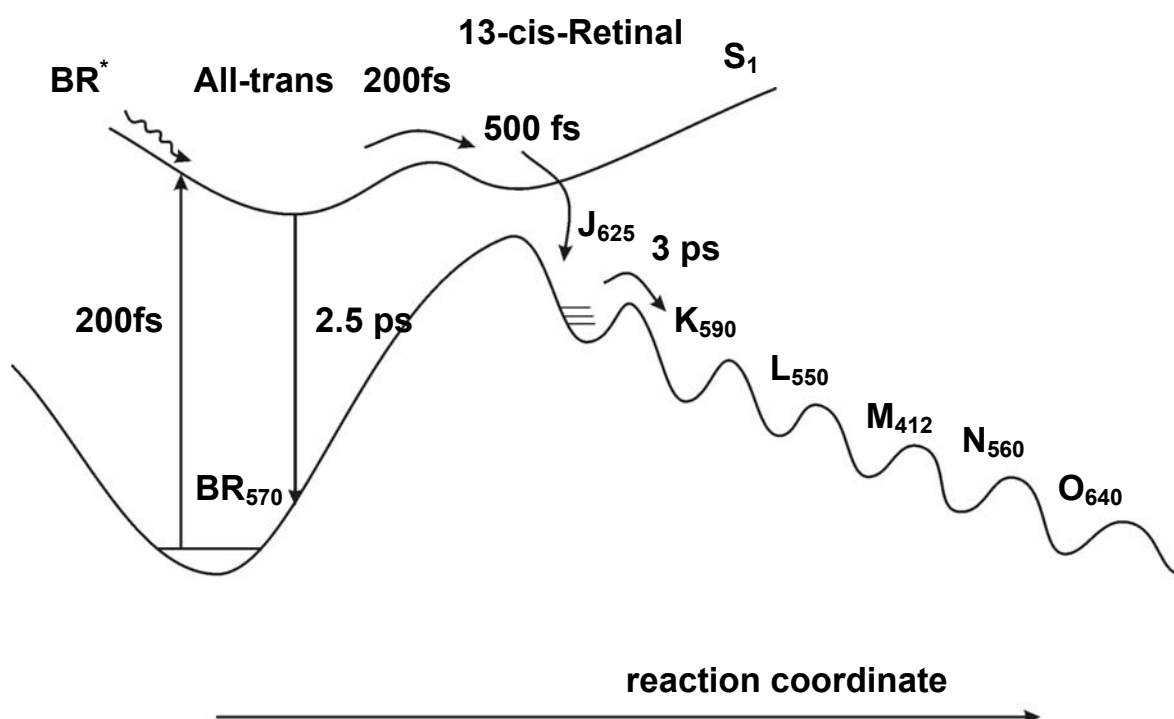


Figure 2.8: Energy diagram describing the trans-cis isomerization of the retinal upon light excitation and following reactions of thermal relaxation to the ground state



Investigations of properties of BR at low temperatures, which were started in the 1970s, gave a lot of supplementary information about the structure of the intermediates and its spectral and photochemical properties. A gradual increasing of the temperature from the liquid helium range allowed to trap almost all photocycle intermediates starting with K as the fastest (having the lowest activation energy). The low temperature method helped to discover more than 20 intermediates appearing during the photochemical transformations of BR. It was shown, that each of the intermediates is photoactive[45;46]. Upon absorption of light it can be transformed back to the BR ground state.

When a PM suspension is cooled down to 94 K, its absorption maximum shifts from 570 to 578 nm. By green light exposure the species converts to the product with absorption band at 600 nm. This product is photoreactive, and red radiation shifts it to the BR ground state. It corresponds to K590 of a normal photocycle and is the first stable product in the temperature range from 4 K to 94 K.

By rising the temperature to 144 K, K590 converts to L550. At temperatures above 184 K, L partially converts to M, another part relaxes to the BR ground state[47]. At temperatures below 224 K, the absorption maximum of M412 shifts to 419 nm. When the sample is warmed up to 250K and then cooled again, about 30% of the pigment can be trapped in the N state[48]. The part of the pigment under these conditions (ca 40%) is converted to the BR ground state, and the rest stays in the M[49]. The absorption spectrum of N was reported in several studies with the maxima in the range 550-562 nm and a maximum extinction coefficient of 0.68-0.78 of BR[49-51]. Up to now, the O-like intermediate has not been trapped in large amounts because it does not accumulate at low temperatures[48].

The main physical properties of the intermediates of bacteriorhodopsin are summarized in Table 2.1

Table 2.1. Physical properties of the intermediates of BR. The data taken from [52].

Name	$\lambda_{\max}$ (nm)	Ext. Coeff. (M cm <sup>-1</sup> )	Retinal configuration	Schiff base conformation	Schiff base protonation	T <sub>freeze</sub> (°C)
BR	570	63000	All-trans	Anti	Yes	-
K	590	52100	13-cis	Anti	Yes	-190
L	550	48900	13-cis	Anti	Yes	-100
M1	410	48800	13-cis	Anti	No	-30
M2	410	48800	13-cis	Anti	No	-10
N	560	46100	13-cis	Anti	Yes	-60
O	640	61900	All-trans	Anti	Yes	-

## 2.3 Methods of bacteriorhodopsin modification

As mentioned before, the wild-type form of BR as found in nature has quite attractive properties. The high stability toward chemical and thermal degradation, switchability and high NLO-properties make it an excellent candidate for optical application. Moreover, there is at least one advantage, namely the broad spectra of methods which can be used to modify bacteriorhodopsin making it more attractive with respect to conventional inorganic and organic materials:

### 1. *Retinal by retinal analog substitution*

The substitution of a retinal molecule by its analog leads to a partial or complete alteration of the absorption spectra of the ground state and intermediates, the degree of light-adaptation, photocycle properties, the proton activity etc. The initial stage for a retinal substitution requires the apoprotein (i.e. bacteriorhodopsin without native retinal). This can be achieved in two different ways: by using the photoinduced hydroxylaminolysis of

bacteriorhodopsin or a microbiological method that artificially creates bacterial cultures not forming retinal.

The first method has been developed by Oesterheld and Schulmann in 1974[53]. This method is based on a reaction of BR under strong light exposure with hydroxylamine ( $\text{NH}_2\text{OH}$ ), during which the cleavage of the Schiff base occurs and the retinal forms with hydroxylamine a retinaloxim (retinal- $\text{HC}=\text{N}-\text{OH}$ ). After removal of the retinal (extraction in organic solvents) the pure apoprotein is obtained.

The creation of retinal-modified bacteriorhodopsin is relative simple. If the analog of an artificial retinal is added to an apoprotein, the spontaneous self-assembly of the new molecule occurs. The effectiveness and speed of this process depends on many factors like temperature, and the nature retinal analog.

Another method for protein synthesis includes the growth of artificial cell cultures in a retinal-deficient environment[54]. The isolated membranes called “white membranes” show no absorptions in the 570 nm region.

To modify the retinal there are several possibilities:

1. Side-chain alteration[55].
2. Side-chain substitution in the 9, 13, and 14 positions of the polyene chain.
3. Modification of the ionic ring. This kind of alteration allows producing a large family of analogs with high stability and photoactivity. The absence of the ring does not lead to a disappearing of the main photochemical properties, but to a decreasing of protein stability[56]
4. Locked configurations, i.e. analogs of retinal of different types where the chain is blocked at position 13 which excludes trans-cis isomerization[57;58].

## 2. *Random mutagenesis*

Random mutagenesis was applied in 1983 by Oesterhelt[59]. During random mutagenesis new strains of bacteria were selected which possess a certain amino acid alteration[60;61]. The main physical properties of the bacteriorhodopsin mutants obtained by random mutagenesis are summarized in Table 2.2.

Table 2.2. Physical properties of some mutants of BR obtained by random mutagenesis

Mutant	Absorption maxima,		Half-time of the		Ref.
	nm		state M, ms		
	DA <sup>a</sup>	LA	Arise	Decay	
Wild type	558	568	$6 \cdot 10^{-2}$	15	[61]
Y57N	555	560	M is not detected		[61]
D85E	610	610	$10^{-2}$		[61]
D96N	560	569		$10^5$	[61]
D96G	557	566		150	[61]
W138R	490	490			[61]
W10C	548	562		150	[61]

<sup>a</sup>DA and LA, dark- and light-adapted forms of the chromophore, respectively.

## 3. *Site-specific (site-directed) mutagenesis*

The method of site-specific mutagenesis was first employed by Khorana and colleagues for the production of BR mutants. It is one of the most important methods to investigate structural and functional properties of proteins where selected amino acids are replaced by means of a chemically synthesized BR gene expressed, e.g. in *E. coli*. This method allows to determine the role of each amino acid of the protein.

Already in the first investigations, Asp85, Asp212, and Arg82 were suggested to be the main counter-ions of the retinal pocket. The simultaneous replacement of Asp85 and Asp96 with Asn shifts the absorption maxima of the ground spectra to 600-610 nm, and the lifetime of the M intermediate is considerably increased.

The main physical properties of the bacteriorhodopsin mutants obtained by site-directed mutagenesis are summarized in Table 2.3.

Table 2.3. Physical properties of some mutants of BR obtained by site-directed mutagenesis

Mutant	Absorption maxima nm		Half-time of the state M, ms		Ref.
	DA <sup>a</sup>	LA	Arise ( $\mu$ s)	Decay (ms)	
Wild type	558	568	60	15	
Ala53Gly	544	548	1.6	15	[62]
Asp36Asn	550	560	-	-	[63;64]
Asp85Asn	589	588	-	-	[65]
Asp85Glu	556	568	2.6	350	[65;66]
Asp85Ala	600	600	2800	230	[66]
Asp96Ala	558	558	39	7000	[66]
Asp96Asn	553	560	200	10000	[63;66]
Asp96Glu	553	561	30	900	[63;66]
Asp104Asn	550	560	-	-	[63;64]
Asp115Ala	543	543	5	130	[66]
Asp115Asn	533	529	70	300	[65;66]
Asp115Glu	536	538	130	250	[65;66]
Asp212Asn	555	548	220	200	[65;66]
Asp212Glu	584	581	2	850	[65;66]
Asp212Ala	540	-	-	-	[63;64]

Arg82Ala	564	566	3	60	[65;66]
Arg82Gln	575	580	7-10	<100	[66;67]
Arg134Gln	551	557	10	5	[67]
Arg227Gln	551	563	10	70	[67]
Gly122Cys	524	524	7	20	[62]
Glu194Gln	541	545	-	-	[63;64]
Leu93Thr	531	531		800	[68;69]
Leu93Val	547	553		10	[68;69]
Leu93Ala	532	532		800	[68;69]
Met20Ala	551	560	1	17	[62]
Met20Glu	550	556	4	16	[62]
Met118Ala	474	478	11	293	[62]
Met118Glu	552	556	97	51	[62]
Met145Ala	475	477	52	159	[62]
Met145Glu	550	560	8	8	[62]
Tyr185Phe	556	573	-	-	[63;64]
Val49Leu	551	556	11	14	[62]
Val49Ala	549	549	167	25	[62]

---

<sup>a</sup>DA and LA, dark- and light-adapted forms of the chromophore, respectively.

#### 4. *Chemical modification*

The amino acid residues can be also altered by ferments or chemical reagents, which remove or replace some fragments of the polypeptide chain. For instance, the proteolysis of the amino acid tail groups (C-, N-terminal tails) of the protein and of the polypeptide chain loops between the helices changes a few characteristics of the photocycle[70;71]

The kinetics of the formation and decay of the M intermediate can be retarded by cyclohexadione, reaching up to 10 minutes in partially dehydrated films and polyacrylamide gels [72].

The cleavage of BR into two unequal parts does not affect the generation of a membrane photopotential by the smaller part containing the chromophore[73].

### 5. *Changing the surrounding medium (viscosity, pH, etc.)*

- *Viscosity*

The first experiments on BR concerning changes in viscosity have been made by Beence *et al.* [74]. The viscosity was altered by addition of glycerine-like components to PM suspension. Photocycle measurements have shown that only during the last two transitions of the photocycle the influence of the viscosity can be seen. As a rule, the lifetimes of M and O intermediates are prolonged by increasing the viscosity[75].

- *Pressure*

Increasing the pressure induces alterations in the equilibrium between intermediates. For instance, at 2.5 kBar a reversible shift in the equilibrium between LA and DA forms of BR toward the 13-cis-retinal can be observed. The results were derived on a PM suspension placed in a 0.01 M imidazole buffer at pH 7.2. For this buffer solution, the pH does not change in the range of 1-6000 Bar. Lowering of the M decay rate by more than one order of magnitude can be achieved by changing the pressure from 1 to 6000 Bar. The dependence of different transitions on the pressure is similar to the viscosity dependence. The fast processes in the BR photocycle are less sensitive to pressure than the slow ones. The slow processes are connected to conformational changes of the protein including changes of the protein volume.

- *Electric and magnetic fields*

The first experiments on the influence of a strong magnetic field on BR properties were made as early as 1977[76]. The orientation of the PM fragments in a magnetic field of 17000 G has been shown by neutron scattering methods and polarization

spectroscopy. This effect occurs due to the diamagnetic properties of  $\alpha$ -helical structures whose movements and rotations within the membrane are restricted.

The first experiments with a pulsed electric field have been pioneered by Shinar *et al*[77]. It was shown that in the first 200 ms the field affects the chromophore, changing its orientation by more than  $20^\circ$ . After that, in the next 100 ms, the reorientation of the whole PM fragments occurs. The strength of field has to be at least 10kV/cm. In comparison with an orientation induced by static magnetic field, this method allows to orient PMs in a uniform fashion. Moreover, the shift of the absorption band can be observed[78]. By placing PM suspensions in a strong electric field a new absorption band at 630 nm appears whereas the old one at 570 nm diminishes. Upon red light exposure the amplitude at 630 nm is reduced. These results were explained by rearrangement of the charges in polar and polarizable groups in the chromophore-protein complex under the influence of a strong electric field.

- *Dehydration*

Dehydration processes exert a strong influence on the photocycle of bacteriorhodopsin. By decreasing the relative humidity, a distortion of the photocycle during the N to O transition was observed. At 88% of relative humidity the photocycle ends at the M intermediate and then goes directly to the BR ground state[79]. Upon dehydration from 94 to 7% the M half-time constant increases from 10 ms to 10 sec both in a PM water suspension[80] and in polymeric layers[81]. When the relative humidity becomes less than 1.0%, a new photoproduct with absorption maximum at 506 nm was detected[82].

- *Solvents*

Detailed studies on the influence of different organic solvent on the BR absorption spectra and photoactivity have been provided by[83;84]. It was found that the most organic solvents do not affect the function of BR.

In the solubilization process of the PM using detergents a decomposition of the crystal structure occurs, leading to the formation of unstable monomeric BR molecules, which are still photochemically active[85;86]. The solubilized BR



molecules retain the main properties of membrane-incorporated molecules confirming the suggestion that the crystalline structure has a protective, rather than functional role. By treatment of PM with non-ionic detergent Triton-100 the maximum of the absorption spectrum shifts from 570 nm to 550 nm. By using sodium dodecylsulfate detergent, the appearance of a species with an absorption maximum at 600 nm at neutral pH was observed. By exposition to red light it irreversibly converts to a product with an absorption maximum at 440 nm[87].

## 2.4 Nonlinear optical properties of bacteriorhodopsin.

### State of the art

A second harmonic generation by wild type bacteriorhodopsin was first reported by Aktsipetrov *et al.* in 1987. Later, the second-order nonlinear properties of purple membrane-poly (vinyl alcohol)(PM-PVA) films and the free retinal and retinal Schiff bases spread at air-water interfaces were investigated by Huang *et al.*[88]. It was established, by comparison of the second harmonic signal from the PM-PVA films and of the photochemistry of bacteriorhodopsin, that the main contribution of the SHG signal comes from the retinal incorporated into the opsin matrix. The magnitudes of the first hyperpolarizability of the BR<sub>570</sub> and M<sub>412</sub> states have been determined to be  $2500 \times 10^{-30}$  esu and  $280 \times 10^{-30}$  at wavelength of 1064nm, respectively. The values for the chromophore systems varied from 130 to  $280 \times 10^{-30}$  esu. From a simple two-level model the normalized (to dipole moment of the protonated Schiff base) dipole moment change was determined to be by a factor of 1.7 larger than that of the free retinal. Moreover, the obtained dipole moment change of the ground state of BR was found to be larger than in the M state.

In 1990, a two-photon double-resonance method was applied to characterize the electronic and dipolar properties of the all-trans retinal in the light-adapted bacteriorhodopsin[89]. The two-photon double resonance spectrum was collected from 820 to 1200 nm, indicating two maxima, an intense band at  $18000 \text{ cm}^{-1}$  which was assigned to a  ${}^1\text{B}_u^+$ -like excited state,

the second one at  $21000\text{ cm}^{-1}$  to a  ${}^1A_g^{*+}$ -like excited state. The change in dipole moments of these transitions was assessed to be  $13.5 \pm 0.8D$  for the ground state to the  ${}^1B_u^{*+}$ -like state transition and  $9.1 \pm 4.8D$  for the  ${}^1A_g^{*+}$ -like excited state transition. The value of the first hyperpolarizability was obtained to be  $2250 \times 10^{-30}$  esu at a fundamental frequency of 1064 nm. It was concluded that a protonated Schiff base chromophore is situated in a very ionic and probable charged binding site in the absence of a charged species nearby the  $\beta$ -ionic ring.

The first Hyper-Rayleigh Scattering (HRS) measurements on bacteriorhodopsin and all-trans retinal in different solvents were performed by Clays *et al* in 1993[90]. The HRS technique was applied to BR, which was solubilized in Triton X-100. The value for  $\beta_{\text{eff}}$  of bacteriorhodopsin was determined to be  $2100 \times 10^{-30}$  esu. It was shown that the highly correlated molecules of BR in membranes enhance the macroscopic susceptibility. The experimental results were then compared to the theoretical ones, calculated at the Hartree-Fock ab initio level. The influence of solvents was taken into account by Onsager's self-consistent reaction field approach. Correlation between theory and experiment was found. It was concluded that the solvents polarity has a major influence on the second-order nonlinear response.

The indicatrix of the hyper-Rayleigh scattered light intensity of a suspension of bacteriorhodopsin was first analyzed by Clays *et al*[91;92]. It was shown that both coherent second harmonic light and incoherent hyper-Rayleigh scattering contribute to the observed signal. Then, the fit of the angular dependence gave values for the refractive indices  $n_o$  and  $n_{2o}$  of 1.5 for the optically linear apo-protein matrix, whereas the refraction index for the retinal itself was previously estimated to be 1.8-2.1. It was concluded that patches of BR molecules are a natural (nonlinear) photonic bandgap material.

Third order nonlinear optical properties of BR-films were investigated through a degenerate four-wave mixing experiment[93;94]. The light-induced changes of the index of refraction are typically in the order of  $n_2=10^{-2}\text{ cm}^2/\text{W}$  for  $\text{BR}_{\text{D96N}}$  and somewhat lower for  $\text{BR}_{\text{WT}}$  for  $\lambda=633\text{nm}$ .

## Chapter 3

### Theoretical Background

#### 3.1 Nonlinear polarization. The Anharmonic Oscillator Model

By applying a static electric field or by propagating an electromagnetic wave, a polarization of the medium occurs. At modest field strengths, the magnitude of oscillation of electrons will be proportional to the applied field and is given by[95]:

$$\vec{P}(\vec{r}, t) = \int_{-\infty}^{\infty} \chi^{(1)}(\vec{r} - \vec{r}', t - t') \cdot E(\vec{r}, t') d\vec{r}' dt', \quad (3.1)$$

where  $\chi^{(1)}$  is a linear medium-depended susceptibility.

If the field is a monochromatic wave:

$$E(\vec{r}, t) = E(\vec{k}, \omega) = \vec{E}(\vec{k}, \omega) \exp(i\vec{k} \cdot \vec{r} - i\omega t), \quad (3.2)$$

then by employing of a Fourier transformation the polarization can be expressed as:

$$\vec{P}(\vec{k}, \omega) = \chi^{(1)}(\vec{k}, \omega) \cdot \vec{E}(\vec{k}, \omega), \quad (3.3)$$

where

$$\chi^{(1)}(\vec{k}, \omega) = \int_{-\infty}^{\infty} \chi^{(1)}(\vec{r}, t) \exp(-i\vec{k} \cdot \vec{r} + i\omega t) d\vec{r} dt$$

In the case of a sufficiently strong field the polarization response is no longer linear and the polarization can be given as a power series expansion in the electric field:

$$\begin{aligned}
\vec{P}(\vec{r}, t) = & \int_{-\infty}^{\infty} \chi^{(1)}(\vec{r} - \vec{r}', t - t') \cdot E(\vec{r}', t') d\vec{r}' dt' + \\
& + \int_{-\infty}^{\infty} \chi^{(2)}(\vec{r} - \vec{r}_1, t - t_1; \vec{r} - \vec{r}_2, t - t_2) : \vec{E}(\vec{r}_1, t_1) \vec{E}(\vec{r}_2, t_2) d\vec{r}_1 dt_1 d\vec{r}_2 dt_2 + \\
& + \int_{-\infty}^{\infty} \chi^{(2)}(\vec{r} - \vec{r}_1, t - t_1; \vec{r} - \vec{r}_2, t - t_2; \vec{r} - \vec{r}_3, t - t_3) : \vec{E}(\vec{r}_1, t_1) \vec{E}(\vec{r}_2, t_2) \vec{E}(\vec{r}_3, t_3) d\vec{r}_1 dt_1 d\vec{r}_2 dt_2 d\vec{r}_3 dt_3 + \dots
\end{aligned} \tag{3.4}$$

where  $\chi^{(n)}$  is the nonlinear susceptibility of the order n.

If the electric field can be represented as a sum of planar monochromatic waves, then as in the linear case, by Fourier transformation the polarization of the medium can be expressed as:

$$\vec{P}(\vec{k}, \omega) = \vec{P}^{(1)}(\vec{k}, \omega) + \vec{P}^{(2)}(\vec{k}, \omega) + \vec{P}^{(3)}(\vec{k}, \omega) + \dots \tag{3.5}$$

where:

$$\vec{P}^{(1)}(\vec{k}, \omega) = \chi^{(1)}(\vec{k}, \omega) \cdot \vec{E}(\vec{k}, \omega),$$

$$\vec{P}^{(2)}(\vec{k}, \omega) = \chi^{(2)}(\vec{k} = \vec{k}_i + \vec{k}_j, \omega = \omega_i + \omega_j) : \vec{E}(\vec{k}_i, \omega_i) \vec{E}(\vec{k}_j, \omega_j), \tag{3.6}$$

$$\vec{P}^{(3)}(\vec{k}, \omega) = \chi^{(3)}(\vec{k} = \vec{k}_i + \vec{k}_j + \vec{k}_l, \omega = \omega_i + \omega_j + \omega_l) : \vec{E}(\vec{k}_i, \omega_i) \vec{E}(\vec{k}_j, \omega_j) \vec{E}(\vec{k}_l, \omega_l)$$

$$\begin{aligned}
& \chi^{(n)}(\vec{k} = \vec{k}_1 + \vec{k}_2 + \dots + \vec{k}_n, \omega = \omega_1 + \omega_2 + \dots + \omega_n) = \\
& = \int_{-\infty}^{\infty} \chi^{(n)}(\vec{r} - \vec{r}_1, t - t_1; \dots; \vec{r} - \vec{r}_n, t - t_n) \cdot \\
& \cdot \exp\left\{-i\left[\vec{k}_1(\vec{r} - \vec{r}_1) - \omega_1(t - t_1) + \dots + \vec{k}_n(\vec{r} - \vec{r}_n) - \omega_n(t - t_n)\right]\right\} d\vec{r}_1 dt_1 \dots d\vec{r}_n dt_n
\end{aligned} \tag{3.7}$$

In contrast to inorganic materials such as semiconductors (GaAs, CdS) or ionic crystals (LiNbO<sub>4</sub>, KDP) the polarization of the most molecular-based ensembles, are closely related to the individual properties of these compounds. The microscopic polarization (dipole moment) analogue to eq. 3.5 can be written:

$$\vec{p} = \alpha \vec{E} + \beta : \vec{E}\vec{E} + \gamma : \vec{E}\vec{E}\vec{E} + \dots, \quad (3.8)$$

where  $\alpha$  is the polarizability,  $\beta$ ,  $\gamma$  etc. are hyperpolarizabilities. They are the tensors of different ranks and, as the susceptibilities, they are frequency dependent. Due to the electronic origin of the nonlinearity, the frequency dispersion of  $\beta$  occurs at optical frequencies, whereas in ionic compounds there are additional large contributions at low frequencies, below the microwave range, due to displacement of ions.

The exact expression for the hyperpolarizability obtained in the framework of perturbation theory (SOS) will be given in section 3.3.3.2. Indeed, the basic properties follow from the simplest model of an anharmonic oscillator, with quadratic force (cubic potential) acting on the system.

In an one-dimensional case, the equation of motion is given by:

$$\ddot{x} + G\dot{x} + \omega_0^2 x - \nu x^2 = -\left(\frac{q}{m}\right)E, \quad (3.9)$$

where  $x$  represents the displacement of the electron,  $\omega_0$  is the resonance frequency,  $E$  is the applied field,  $q$  and  $m$  are the charge and mass of the electron, respectively.

If the applied field can be represented as a sum of plane, monochromatic waves:

$$E = E(\omega_1)e^{-i\omega_1 t} + E(\omega_1)e^{i\omega_1 t} + E(\omega_2)e^{-i\omega_2 t} + \dots = \sum_n E(\omega_n)e^{-i\omega_n t}, \quad (3.10)$$

and  $\nu x^2$  is small compared to the other terms,  $x$  can be approximated as:

$$x = x_1 + x_2 + \dots, x_1 \sim E, x_2 \sim E^2, x_1 \gg x_2 \gg x_3 \dots$$

The initial equation (3.9) is split into:

$$\ddot{x}_1 + G\dot{x}_1 + \omega_0^2 x_1 = -\left(\frac{q}{m}\right)E \quad (3.11)$$

$$\ddot{x}_2 + G\dot{x}_2 + \omega_0^2 x_2 = -vx_1^2, \quad (3.12)$$

The solutions for these two cases are:

$$x_1 = \left(-\frac{q}{m}\right) \sum_n \frac{E(\omega_n) e^{-i\omega_n t}}{\omega_0^2 - i\omega_n G - \omega_n^2}, \quad (3.13)$$

$$x_2 = \left(-\frac{q^2 v}{m}\right) \sum_{n,m} \frac{E(\omega_n) E(\omega_m) e^{-i(\omega_n + \omega_m)t}}{F(\omega_0, \omega_n, \omega_m, G)}, \quad (3.14)$$

where  $F(\omega_0, \omega_n, \omega_m, G)$  is expressed as:

$$F(\omega_0, \omega_n, \omega_m, G) = (\omega_0^2 - i\omega_n G - \omega_n^2) * (\omega_0^2 - i\omega_n G - \omega_n^2) \times \\ \times (\omega_0^2 - i(\omega_n + \omega_m)G - (\omega_n + \omega_m)^2), \quad (3.15)$$

The relationship between  $P$  and  $x$  is:

$$P = \sum P_i, P_i = -Nqx_i, \quad (3.16)$$

In the case of linear polarization:

$$P^{(1)} = \sum_n \chi^{(1)}(\omega_n) E(\omega_n) e^{-i\omega_n t}, \quad (3.17)$$

the linear susceptibility is given by:

$$\chi^{(1)}(\omega_n) = N\left(\frac{q^2}{m}\right)(\omega_0^2 - i\omega_n G - \omega_n^2)^{-1} = N\left(\frac{q^2}{m}\right)[D(\omega_n)]^{-1}, \quad (3.18)$$

And in the case that the polarization quadratic-dependent on the field:

$$P^{(2)} = \sum_n \chi^{(2)}(\omega_n, \omega_m) E(\omega_n) E(\omega_m) e^{-i(\omega_n + \omega_m)t}, \quad (3.19)$$

the susceptibility of the second order is given by:

$$\chi^{(2)}(\omega_n, \omega_m) = \frac{-m\nu}{N^2 q^2} [\chi^{(1)}(\omega_n)] [\chi^{(1)}(\omega_m)] [\chi^{(1)}(\omega_n + \omega_m)] = \left(\frac{Nq^3\nu}{m^2}\right) [D(\omega_n)]^{-1} [D(\omega_m)]^{-1} [D(\omega_n + \omega_m)]^{-1}, \quad (3.20)$$

Hence, the susceptibility of second order at frequencies  $\omega_n, \omega_m$  is proportional to the linear susceptibilities at corresponding frequencies.

### 3.2 Local field correction factors

The macroscopic susceptibilities are related to the corresponding molecular polarizabilities by local field correction factors and the molecular number density  $N$ [96]:

$$\chi_{IJ}^{(1)} = N \sum_{ij} f_I \langle \cos \theta_{Ii} \rangle f_J \langle \cos \theta_{Jj} \rangle \alpha_{ij}, \quad (3.21)$$

$$\chi_{IJK}^{(2)} = N \sum_{ijk} f_I \langle \cos \theta_{Ii} \rangle f_J \langle \cos \theta_{Jj} \rangle f_K \langle \cos \theta_{Kk} \rangle \beta_{ijk}, \quad (3.22)$$

$$\chi_{IJKL}^{(3)} = N \sum_{ijkl} f_I \langle \cos \theta_{Ii} \rangle f_J \langle \cos \theta_{Jj} \rangle f_K \langle \cos \theta_{Kk} \rangle f_L \langle \cos \theta_{Ll} \rangle \gamma_{ijkl}, \quad (3.23)$$

where the variables denote the molecular axes,  $\theta_{li}$  is the angle between the macroscopic axis I and microscopic i. The local field factors have been introduced to account for the difference between the applied field and the field acting in a matter, due to the interactions between molecules.

In the case of the dipole approximation for the interaction among molecules, which is reasonable in liquids or cubic crystals due to reduction of higher-multipole fields by symmetry cancellation, and the uniformity of polarization in matter, the local field is written as[95]:

$$\vec{\xi}(\omega) = \vec{E}(\omega) + 4\pi L \vec{P}(\omega), \quad (3.24)$$

where L is a dimensionless rank-two tensor, which has been derived by conventional electrostatic methods. It depends only on the shape of the cavity, but not on its size. In general the form of the cavity is ellipsoidal, and the components of L are expressed by:

$$L_i = \frac{a_1 a_2 a_3}{2} \int_0^\infty \frac{ds}{(s + a_i^2) [(s + a_1^2)(s + a_2^2)(s + a_3^2)]^{1/2}}, \quad (3.25)$$

where  $a_1, a_2,$  and  $a_3$  are the axis of the ellipsoid and the sum of  $L_1, L_2, L_3$  is equal to 1.

For a spherical cavity  $L_1=L_2=L_3=1/3$ . The local field is given by:

$$\vec{\xi}(\omega) = \vec{E}(\omega) + \frac{4\pi}{3} \vec{P}(\omega), \quad (3.26)$$

The relation between the macroscopic susceptibilities and microscopic nonlinearities in this case can be expressed as:

$$\chi^{(1)}(\omega) = N \left[ \frac{\varepsilon^{(1)}(\omega) + 2}{3} \right] \alpha^{(1)}(\omega), \quad (3.27)$$



$$\chi_{ijk}^{(2)}(\omega = \omega_1 + \omega_2) = N \left[ \frac{\varepsilon^{(1)}(\omega) + 2}{3} \right] \left[ \frac{\varepsilon^{(1)}(\omega_1) + 2}{3} \right] \left[ \frac{\varepsilon^{(1)}(\omega_2) + 2}{3} \right] \alpha_{ijk}^{(2)}(\omega = \omega_1 + \omega_2), \quad (3.28)$$

...

$$\chi^{(n)}(\omega = \omega_1 + \omega_2 + \dots + \omega_n) = N \left[ \frac{\varepsilon^{(1)}(\omega) + 2}{3} \right] \left[ \frac{\varepsilon^{(1)}(\omega_1) + 2}{3} \right] \dots \left[ \frac{\varepsilon^{(1)}(\omega_n) + 2}{3} \right] \alpha^{(n)}(\omega = \omega_1 + \omega_2 + \dots + \omega_n), \quad (3.29)$$

where  $\left[ \frac{\varepsilon^{(1)}(\omega_n) + 2}{3} \right]$  is the well-know Lorentz correction factor.

In the case of polar liquids we must consider not only polarization, but orientations of the permanent dipoles. The appearing local factors are known as the Onsager correction factors, and given by:

$$f(0) = \frac{\varepsilon_0(\varepsilon_\omega + 2)}{2\varepsilon_0 + \varepsilon_\omega}, \quad (3.30)$$

### 3.3 Theory of Hyper-Raleigh-scattering

The possibility of coherent double-quantum scattering was first analyzed in detail by Amstrong *et al*[97]. It was found that such effects can occur in certain crystals at certain orientations but not in fluids. It follows from the expression for the macroscopic electric polarization of the medium:

$$\vec{P} = \chi^{(1)} \vec{E} + \chi^{(2)} : \vec{E} \vec{E} + \dots, \quad (3.31)$$

In a system possessing a centre of symmetry the polarization vector must change its sign as the electric vector does. Consequently,  $\chi^{(2)}$  must be vanishing. However, low intensities of second-order light scattering in isotropic samples have later been observed by Tehune,

Maker, and Savage[98]. Second-order light scattering from centrosymmetric molecules in liquids has also been reported[99]. Such second-order processes owe to the high lability of the molecules in the liquid phase that may break temporarily the centrosymmetry of the medium during the incoming laser radiation. However, in contrast to the linear light scattering appearing due to translational (density) fluctuations, the orientational fluctuations are the main cause of the scattering process here[100].

The exact expression for the HRS intensity may be obtained in the frame of quantum electrodynamics. For a system of noninteracting molecules, the rate of frequency doubling can be expressed by applying the Fermi-rule[101]:

$$\Gamma = \frac{2\pi}{\hbar} \langle |M_{FI}|^2 \rangle_{\tau} \rho_F, \quad (3.32)$$

where  $\rho_F$  is the density of an excited state,  $M_{FI}$  is the matrix element averaged for the ensemble of molecules. If the photon interchange between molecules is neglected,  $M_{FI}$  can be written as:

$$M_{FI} = \sum_{\eta} m_{FI}(\eta), \quad (3.33)$$

where  $m_{FI}$  are the matrix elements for individual molecules. The averaged value of  $M_{FI}$  can be separated into one- and two-centre contributions as follows:

$$\begin{aligned} \langle |M_{FI}|^2 \rangle_{\tau} &= \sum_{\eta} \langle |m_{FI}(\eta)|^2 \rangle_{\tau} + \sum_{\eta} \sum_{\eta'} \langle m_{FI}(\eta) \rangle_{\tau} \langle m_{FI}(\eta') \rangle_{\tau}^* =, \quad (3.34) \\ &= N \langle |m_{FI}|^2 \rangle_{\tau} + N(N-1) \langle m_{FI} \rangle_{\tau}^2 \end{aligned}$$

where the second term describes the coherent frequency doubling, which disappears in isotropic media. The expressions for the transition matrix elements and the state densities are given by[102]:

$$m_{FI}(\eta) = -i \left[ \frac{\hbar c^{2\omega}}{2\varepsilon_0 V} \right]^{3/2} \sqrt{n(n-1)} k^\omega (k^{2\omega})^2 \frac{1}{2} \bar{\beta}(\eta) \dots \bar{e}^{2\omega} \bar{e}^\omega \bar{e}^\omega, \quad (3.35)$$

$$\rho_F = \frac{V(k^{2\omega})^2}{8\pi^3 \hbar c^{2\omega}} d\Omega, \quad (3.36)$$

Taking into account the above equations, the intensity of incoherent scattered light can be expressed as:

$$I(k^{2\omega}, \lambda^{2\omega}) = \hbar(c^{2\omega})(k^{2\omega}) \frac{d\Gamma}{d\Omega} = \frac{(k^{2\omega})^4 (k^\omega)^2 \hbar^2 (c^{2\omega})^3}{128\varepsilon_0^3 \pi^2 V^2} [n(n-1)] N \langle \bar{\beta}^2 \rangle, \quad (3.37)$$

With the fundamental radiation:

$$I^\omega = \frac{n(c^\omega)}{V} \hbar(c^\omega)(k^\omega), \quad (3.38)$$

(3.37) can be, finally, written as:

$$I(k^{2\omega}, \lambda^{2\omega}) = \frac{(k^{2\omega})^4 (I^\omega)^2}{128c\varepsilon_0^3 \pi^2} N \langle \bar{\beta}^2 \rangle = C_{HRS} N (I^\omega)^2 \langle \bar{\beta}^2 \rangle, \quad (3.39)$$

As in the linear case, the intensity of the scattered harmonic light is inversely proportional to the fourth power of the fundamental wavelength. As a second-order process, it is also proportional to the square of the incident intensity. The brackets denote the average over all orientations.

The application of the hyper-Raleigh-scattering technique for the determination of the first-order hyperpolarizability was introduced by the group of Persoons in the early nineties[100;103]. The HRS technique has advantages over the conventional methods. It is not as time-consuming as SHG of Langmuir-Blodgett films. In contrast to electric-field-induced second-harmonic generation, the HRS technique does not require a strong electric

field to break the centrosymmetry. Therefore, the HRS technique is not limited to molecules that have a permanent dipole. Both ionic species and the molecules possessing octopolar charge distribution can be probed by the HRS technique. Moreover the EFISHG technique complicates the data analysis by measurement of value that is coupled to the dipole moment and the second-order hyperpolarizability[100].

## 3.4 Calculation of the electronic structure of molecules. Methods of modern quantum physics

The consideration of atomic and molecular electronic properties demands the employment of quantum mechanics methods. The analytical solution of the Schrödinger equation can be derived only for a few (one-electron) quantum systems, like a hydrogen atom and a  $H_2^+$  molecule. Therefore, a variety of transformation and approximations must be applied to find the fundamental solutions. The following section provides an overview of methods underlying the theoretical calculations.

### 3.4.1. The adiabatic and Born-Oppenheimer approximations

The adiabatic or Born-Oppenheimer approximations are the first of several approximations used to simplify the solution of the Schrödinger equation, by separation of nuclear and electronic motion, owing to the significant difference of the electron and proton mass.

The total Hamilton operator of system can be written as[104]:

$$H_{tot} = T_n + T_e + V_{ne} + V_{ee} + V_{nn}, \quad (3.40)$$

where  $T_n$ ,  $T_e$  are the kinetic energies,  $V_{ne}$ ,  $V_{ee}$ , and  $V_{nn}$  are the potential energies of the nuclei and electrons.

Or:

$$H_{tot} = T_n + H_e, \quad (3.41)$$

where  $H_e$  is the electronic Hamilton operator:

$$H_e = T_e + V_{ne} + V_{ee} + V_{nn}, \quad (3.42)$$

We assume that the full set of solutions for the electronic Schrödinger equation is available:

$$H_e(\vec{R})\Psi_i(\vec{R}, \vec{r}) = E_i(\vec{R})\Psi_i(\vec{R}, \vec{r}), i = 1, 2, \dots, \infty, \quad (3.43)$$

The electronic wave functions can be chosen to be orthogonal and normalized, due to hermiticity of the Hamilton operator, i.e.:

$$\int \Psi_i^*(\vec{R}, \vec{r})\Psi_j(\vec{R}, \vec{r})d\vec{r} = \delta_{ij}, \quad (3.44)$$

$$\delta_{ij} = 1, i = j$$

$$\delta_{ij} = 0, i \neq j$$

The total wave function of the system can be written as an expansion in the set of electronic functions:

$$\Psi_{tot}(\vec{R}, \vec{r}) = \sum_i \Psi_{ni}(\vec{R})\Psi_i(\vec{R}, \vec{r}), \quad (3.45)$$

By substitution of (3.45) into (3.42), (3.42) can be given as:

$$\sum_{i=1}^{\infty} (T_n + H_e)\Psi_{ni}(\vec{R})\Psi_i(\vec{R}, \vec{r}) = E_{tot} \sum_{i=1}^{\infty} \Psi_{ni}(\vec{R})\Psi_i(\vec{R}, \vec{r}) \quad (3.46)$$

$$\sum_{i=1}^{\infty} \left\{ \Psi_i (\nabla_n^2 \Psi_{ni}) + 2(\nabla_n \Psi_i)(\nabla_n \Psi_{ni}) + \Psi_{ni} (\nabla_n^2 \Psi_i) + \Psi_{ni} E_i \Psi_i \right\} = E_{tot} \sum_{i=1}^{\infty} \Psi_{ni}(\vec{R}) \Psi_i(\vec{R}, \vec{r}), \quad (3.47)$$

By multiplying of eq. (3.47) from the left side by  $\Psi_j^*$  and integration over the electron coordinates:

$$\nabla_n^2 \Psi_{nj} + E_j \Psi_{nj} + \sum_{i=1}^{\infty} \left\{ 2 \langle \Psi_j^* | \nabla_n | \Psi_i \rangle (\nabla_n \Psi_{ni}) + \langle \Psi_j^* | \nabla_n^2 | \Psi_i \rangle \Psi_{ni} \right\} = E_{tot} \Psi_{nj}, \quad (3.48)$$

The sum contains terms which couple different electronic states. These are the *first- and second non-adiabatic coupling elements*, respectively. In the case of the *adiabatic approximation* all coupling element are neglected, excepting the terms with  $i=j$ :

$$(\nabla_n^2 + E_j + \langle \Psi_j^* | \nabla_n^2 | \Psi_j \rangle) \Psi_{nj} = E_{tot} \Psi_{nj}, \quad (3.49)$$

This can be expressed as follows:

$$(T_n + E_j(\vec{R}) + U(\vec{R})) \Psi_{nj}(\vec{R}) = E_{tot} \Psi_{nj}(\vec{R}), \quad (3.50)$$

where  $U(\vec{R})$  is the so-called *diagonal correction*. Normally, it is a slowly varying function. In the Born-Oppenheimer approximation the *diagonal correction* term is neglected, too:

$$(T_n + E_j(\vec{R})) \Psi_{nj}(\vec{R}) = E_{tot} \Psi_{nj}(\vec{R}), \quad (3.51)$$

That is, the nuclei move in a potential, which is given by the solution of the electronic Schrödinger equation. The solution of (3.51) gives the vibration and rotation energy levels of quantum systems. The Born-Oppenheimer approximation gives usually good results, failing only for systems possessing closely laying energy levels.

## 3.4.2. Hartree-Fock Theory

### 3.4.2.1. Molecular orbitals

Since the electrons are fermions with spins  $\frac{1}{2}$  the total electronic function of a quantum system has to be antisymmetric with respect to interchange of any two electron coordinates, i.e.:

$$\Psi(\vec{r}_1, \dots, \vec{r}_i, \dots, \vec{r}_j, \dots, \vec{r}_n) = -\Psi(\vec{r}_1, \dots, \vec{r}_j, \dots, \vec{r}_i, \dots, \vec{r}_n), \quad (3.52)$$

Molecular orbital theory decomposes  $\Psi$  into a combination of single electron molecular orbitals:  $\phi_1, \phi_2, \dots$ . The simplest antisymmetric function of them can be built up from the Slater Determinants:

$$\Psi = \frac{1}{\sqrt{N!}} \begin{vmatrix} \phi_1(1) & \phi_2(1) & \dots & \phi_N(1) \\ \phi_1(2) & \phi_2(2) & \dots & \phi_N(2) \\ \dots & \dots & \dots & \dots \\ \phi_1(N) & \phi_2(N) & \dots & \phi_N(N) \end{vmatrix}, \langle \phi_i | \phi_j \rangle = \delta_{ij}, \quad (3.53)$$

A one-electron molecular orbital represents a so-called spin-orbital, i.e. a product of a spatial orbital and a spin function. In the presence of an external magnetic field there are two possible states with the spin oriented along and opposite to the field. The corresponding spin functions are denoted  $\alpha$  and  $\beta$ . They obey the following orthonormality conditions:

$$\langle \alpha | \alpha \rangle = \langle \beta | \beta \rangle = 1 \quad (3.54)$$

$$\langle \alpha | \beta \rangle = \langle \beta | \alpha \rangle = 0$$

Consideration of a single determinant means that electron correlation is neglected.

### 3.4.2.2. The Variation Principle. The Roothaan-Hall Equation

The objective is now to derive the solution of the electronic Schrödinger equation starting from a trial wave function, which is taken in the form of a Slater determinant. For this purpose the variation principle can be used leading to the Roothaan-Hall equation[104]. The starting point of this principle is that the expectation value of the energy of any antisymmetric normalized wave function is always greater than the energy for the exact wave function. First, we will evaluate the energy for a Slater determinant. The determinant wave function is convenient to express as:

$$\Psi = A[\phi_1(1)\phi_2(2)\dots\phi_N(N)] = A\Pi, \quad (3.55)$$

where  $\Pi$  is the diagonal product,  $A$  is the operator of permutations over the diagonal of the determinant:

$$A = \frac{1}{\sqrt{N!}} \sum_{p=0}^{N-1} (-1)^p P = \frac{1}{\sqrt{N!}} \left[ 1 - \sum_{ij} P_{ij} + \sum_{ijk} P_{ijk} - \dots \right], \quad (3.56)$$

where 1 is the identity operator,  $P_{ij}$  is the operator of all possible permutations of two electron coordinates and so on.

The permutation operator obeys the following equations:

$$AH = HA \quad (3.57)$$

$$AA = \sqrt{N!}A$$

Considering the electronic Hamiltonian:

$$H_e = T_e + V_{ne} + V_{ee} + V_{nn}, \quad (3.58)$$



where only the electron-electron repulsion term depends on two electron coordinates:

$$T_e = -\sum_{i=1}^N \frac{1}{2} \nabla_i^2, \quad (3.59)$$

$$V_{ne} = -\sum_{i=1}^N \sum_a \frac{Z_a}{|\vec{R}_a - \vec{r}_i|}, \quad (3.60)$$

$$V_{ee} = \sum_{i=1}^N \sum_{j>i} \frac{1}{|\vec{r}_i - \vec{r}_j|}, \quad (3.61)$$

$$V_{nn} = \sum_a \sum_{b>a} \frac{Z_a Z_b}{|\vec{R}_a - \vec{R}_b|}, \quad (3.62)$$

The above equations can be rewritten according to the electron indices as:

$$h_i = -\frac{1}{2} \nabla_i^2 - \sum_a \frac{Z_a}{|\vec{R}_a - \vec{r}_i|}, \quad (3.63)$$

$$g_{ij} = \frac{1}{|\vec{r}_i - \vec{r}_j|}$$

$$H_e = \sum_{i=1}^N h_i + \sum_{i=1}^N \sum_{j>i} g_{ij} + V_{nn}, \quad (3.64)$$

where  $h_i$  is the energy of electron  $i$  in the field of all nuclei,  $g_{ij}$  is a two electron operator.

The energy of a system in that case can be expressed as:

$$\begin{aligned} E &= \langle \Psi | H_e | \Psi \rangle = \langle A\Pi | H_e | A\Pi \rangle = \\ &= \sqrt{N!} \langle \Pi | H_e | A\Pi \rangle = \sum_p (-1)^p \langle \Pi | H | P\Pi \rangle, \end{aligned} \quad (3.65)$$

Since  $V_{mn}$  does not depend explicitly on the electron coordinates, it can be integrated immediately:

$$\langle \Psi | V_{mn} | \Psi \rangle = V_{mn} \langle \Psi | \Psi \rangle = V_{mn}, \quad (3.66)$$

Taking into account that for the one-electron operator only the identity operator, for the two electron operator only the identity and  $P_{ij}$  operator can give non-zero contribution, the energy of the system thus can be written as:

$$E = \sum_{i=1}^N h_i + \sum_{i=1}^N \sum_{j>i}^N (J_{ij} - K_{ij}) + V_{mn}, \quad (3.67)$$

Or more explicitly:

$$E = \sum_{i=1}^N \langle \phi_i | h_i | \phi_i \rangle + \frac{1}{2} \sum_{ij}^N (\langle \phi_j | J_i | \phi_j \rangle - \langle \phi_j | K_i | \phi_j \rangle) + V_{mn}, \quad (3.68)$$

where

$$\begin{aligned} J_i | \phi_j(2) \rangle &= \langle \phi_i(1) | g_{12} | \phi_i(1) \rangle | \phi_j(2) \rangle \\ K_i | \phi_j(2) \rangle &= \langle \phi_i(1) | g_{12} | \phi_j(1) \rangle | \phi_i(2) \rangle, \end{aligned} \quad (3.69)$$

$J_{ij}$  is called a *Coulomb* integral. It represents the classical repulsion between charge distributions.  $K$  is called an *exchange* integral.

In order to derive the wave function that minimizes the energy (3.68) the variation principle can be utilized. However, the wave functions must remain orthogonal and normalized. Such a constrained optimization can be performed by means of *Lagrange multipliers*, keeping in mind that a small change in the orbitals should not change the Lagrange function, i.e.:

$$L = E - \sum_{ij}^N \lambda_{ij} (\langle \phi_i | \phi_j \rangle - \delta_{ij}), \quad (3.70)$$

$$\delta L = \delta E - \sum_{ij}^N \lambda_{ij} (\langle \delta \phi_i | \phi_j \rangle + \langle \phi_i | \delta \phi_j \rangle) = 0, \quad (3.71)$$

The variation of the energy is expressed as:

$$\begin{aligned} \delta E &= \sum_{i=1}^N (\langle \delta \phi_i | h_i | \phi_i \rangle + \langle \phi_i | h_i | \delta \phi_i \rangle) + \\ &+ \frac{1}{2} \sum_{ij}^N (\langle \delta \phi_i | J_i - K_j | \phi_i \rangle + \langle \phi_i | J_i - K_j | \delta \phi_i \rangle) +, \quad (3.72) \\ &+ \langle \delta \phi_j | J_i - K_i | \phi_j \rangle + \langle \phi_j | J_i - K_i | \delta \phi_j \rangle \end{aligned}$$

$$\begin{aligned} \delta E &= \sum_{i=1}^N (\langle \delta \phi_i | h_i | \phi_i \rangle + \langle \phi_i | h_i | \delta \phi_i \rangle) + \\ &+ \sum_{ij}^N (\langle \delta \phi_i | J_j - K_j | \phi_i \rangle + \langle \phi_i | J_j - K_j | \delta \phi_i \rangle) \end{aligned}, \quad (3.73)$$

Equation (3.73) can be rewritten as:

$$\delta E = \sum_{i=1}^N (\langle \delta \phi_i | F_i | \phi_i \rangle + \langle \phi_i | F_i | \delta \phi_i \rangle), \quad (3.74)$$

where  $F_i$  is a Fock operator:

$$F_i = h_i + \sum_{j=1}^N (J_j - K_j), \quad (3.75)$$

Thus, the variation of the Lagrange function can be given by:

$$\delta L = \sum_{i=1}^N \langle \delta \phi_i | F_i | \phi_i \rangle + \langle \phi_i | F_i | \delta \phi_i \rangle - \sum_{ij}^N \lambda_{ij} (\langle \delta \phi_i | \phi_j \rangle + \langle \phi_i | \delta \phi_j \rangle), \quad (3.76)$$

The wave functions, which are looked for, make (3.76) to:

$$\delta L = 0, \quad (3.77)$$

Using:

$$\begin{aligned} \langle \phi | \delta \phi \rangle &= \langle \delta \phi | \phi \rangle^* \\ \langle \phi | F | \delta \phi \rangle &= \langle \delta \phi | F | \phi \rangle^*, \quad (3.78) \end{aligned}$$

Equation (3.76) can be rewritten as:

$$\begin{aligned} \delta L &= \sum_{i=1}^N \langle \delta \phi_i | F_i | \phi_i \rangle - \sum_{ij} \lambda_{ij} \langle \delta \phi_i | \phi_j \rangle + \\ &+ \sum_{i=1}^N \langle \delta \phi_i | F_i | \phi_i \rangle^* - \sum_{ij} \lambda_{ij}^* \langle \delta \phi_i | \phi_j \rangle^* = 0 \end{aligned}, \quad (3.79)$$

$$\sum_{ij} (\lambda_{ij} - \lambda_{ji}^*) \langle \delta \phi_i | \phi_j \rangle = 0, \quad (3.80)$$

$$\lambda_{ij} = \lambda_{ji}^*$$

The first two terms give us the final set of Hartree-Fock equations:

$$F_i \phi_i = \sum_j \lambda_{ij} \phi_j, \quad (3.81)$$

By choosing of the so-called *canonical* orbitals the matrix of Lagrange multipliers becomes diagonal i.e.:

$$\lambda_{ij} \rightarrow 0 \quad \lambda_{ii} \rightarrow \varepsilon_i, \quad (3.82)$$

$$F_i \phi_i' = \varepsilon_i \phi_i'$$

And the energy of a system can be written either in such a form:

$$E = \sum_{i=1}^N \varepsilon_i - \frac{1}{2} \sum_{ij}^N (J_{ij} - K_{ij}) + V_{nn}, \quad (3.83)$$

or using the definition of  $F_i$  (3.75):

$$\varepsilon_i = \langle \phi_i | F_i | \phi_i \rangle = h_i + \sum_{j=1}^N (J_{ij} - K_{ij}), \quad (3.84)$$

It must be noted at this point that in the Hartree-Fock theory electron-electron repulsion is considered in an average fashion and the Hartree-Fock method is referred to as a *Mean Field* approximation.

The Hartree-Fock equation can be solved numerically. Usually each MO is represented as a linear combination of basis functions. These basis functions are centred on the atomic nuclei and conventionally called *atomic orbitals*, although any set of appropriate functions can be used:

$$\Psi_i = \sum_{\alpha}^M c_{\alpha i} \chi_{\alpha}$$

The Hartree-Fock equation (3.81) can be written as:

$$F_i \sum_{\alpha}^M c_{\alpha i} \chi_{\alpha} = \varepsilon_i \sum_{\alpha}^M c_{\alpha i} \chi_{\alpha}, \quad (3.85)$$

By multiplying of (3.85) from the left by a basis function and integration the following equations can be derived:

$$FC = SC\varepsilon, \quad (3.86)$$

These are the *Roothan-Hall* equations, i.e. the Fock equations in the atomic basis set, here:

$$F_{\alpha\beta} = \langle \chi_{\alpha} | F | \chi_{\beta} \rangle, \quad (3.87)$$

$$S_{\alpha\beta} = \langle \chi_\alpha | \chi_\beta \rangle$$

### 3.4.2.3 Electron correlation effects. Configuration interaction method

It has to be noted that the Hartree-Fock theory does not provide an adequate treatment of the correlation between the motions of the electrons within a molecular system. Whereas the major correlation effects of the electrons with the same spin are included automatically, the motion of the electrons with the opposite spins remains uncorrelated under Hartree-Fock theory. One of the approaches solving this problem is the configuration interaction method. Since the exact wave function  $\Psi$  cannot be expressed by a single determinant, as Hartree-Fock theory assumes, Configuration Interaction (CI) method constructs the other determinants by replacing one or more occupied orbitals with virtual ones. This is equivalent to exciting electrons to higher energy levels. The full CI method represents the wave function  $\Psi$  as a linear combination of the Hartree-Fock determinant and all possible substituted determinants:

$$\Psi = b_0\Psi_0 + \sum_{s>0} b_s\Psi_s, \quad (3.88)$$

where the first term represents Hartree-Fock level, and  $s$  runs over all possible substitution, i.e. the above equation denotes a mixing of all of the possible electronic states of the molecule.

### 3.4.2.4 The semiempirical INDO/S method

It can be shown that the computation cost for performing HF computation rises as the forth power of the number of basis functions[104]. Semiempirical methods reduce the computation time. First of all, only valence electrons are taken into account. This means

that for carbon, e.g., only  $2s$ ,  $2p_x$ ,  $2p_y$ ,  $2p_z$  are used for the construction of the basis set. All calculations are performed in the *Zero Differential Overlap* approximation that neglects all products of basis functions which are located at different atoms. That is,

- (1) the overlap matrix  $S$  is reduced to a unity matrix;
- (2) one-electron integrals involving three centres are set to zero;
- (3) all three- and four-centres integrals are neglected;

For the theoretical calculation, we will use the semiempirical INDO/S method. This method belongs to the group of methods that use the *Intermediate Neglect of Differential Overlap* (INDO) approximation, which neglects all two-centre two-electron integrals of non-Coulomb type, as well. The repulsion energies for the electrons to the orbitals on an atom are explicitly evaluated by using an empirical formula because the analytical approach does not reproduce the experimentally obtained results for the absorption spectra[105]. The empirical formula used to evaluate electron repulsion integrals in the MOPAC program are the Pariser-Parr formula for triplet states and the Nishimoto-Mataga-Weiss formula for singlet states. The parameterization scheme, which has been developed by Zener may be found elsewhere[106;107].

### 3.4.3. Calculation of the hyperpolarizabilities

Once the approximation level for the Hamiltonian is defined, there are, generally, two methods for the calculation of the molecular hyperpolarizabilities[96]. They are briefly described in the following sections.

#### 3.4.3.1. The coupled method

The first one is the so-called *coupled procedure* (broadly labeled as *finite-field*). By this method, the electronic structure of the molecule is calculated in the presence of an external

uniform static field, i.e., the molecular Hamiltonian explicitly contains a term describing the interaction between a finite perturbing electric field and the electronic structure:

$$H(\vec{F}) = H_0 - e\vec{r}\vec{F}, \quad (3.89)$$

where  $H_0$  is the Hamiltonian of an unperturbed system,  $\vec{F}$  is an applied electric field. The new wave functions of the system, the energies, and the dipole moment, as a function of the field strength, can be consequently found:

$$E(\vec{F}) = \langle \psi(\vec{F}) | H(\vec{F}) | \psi(\vec{F}) \rangle, \quad (3.90)$$

$$\mu(\vec{F}) = \langle \psi(\vec{F}) | \sum_i q_i(F) \cdot \vec{r}_i(\vec{F}) | \psi(\vec{F}) \rangle, \quad (3.91)$$

where  $q_i$  and  $\vec{r}_i$  are the charges and positions of all nuclei and electrons, respectively. Since the dipole moment is expressed as:

$$\mu_i(F) = \mu_i^0 + \sum_j \alpha_{ij} F_j + \frac{1}{2} \sum_{j,k} \beta_{ijk} F_j F_k + \frac{1}{6} \sum_{j,k,l} \gamma_{ijkl} F_j F_k F_l + \dots, \quad (3.92)$$

where  $\mu_i^0$  is the permanent dipole moment, the (hyper)polarizabilities can be elementary derived by differentiating  $\mu(F)$  with respect to  $F$ :

$$\alpha_{ij} = \left. \frac{\partial \mu_i}{\partial F_j} \right|_{F=0}, \quad (3.93)$$

$$\beta_{ijk} = \left. \frac{\partial^2 \mu_i}{\partial F_j \partial F_k} \right|_{F=0}, \quad (3.94)$$



$$\gamma_{ijkl} = \frac{\partial^3 \mu_i}{\partial F_j \partial F_k \partial F_l} \Big|_{F=0}, \quad (3.95)$$

Equivalently, they can be evaluated via the Hellman-Feynman theorem, by differentiating the energy, i.e.:

$$\alpha_{ij} = \frac{\partial \mu_i}{\partial F_j} = \frac{\partial}{\partial F_j} \left( -\frac{\partial E}{\partial F_i} \right) = -\frac{\partial^2 E}{\partial F_i \partial F_j} \Big|_{F=0}, \quad (3.96)$$

$$\beta_{ijk} = -\frac{\partial^3 E}{\partial F_i \partial F_j \partial F_k} \Big|_{F=0}, \quad (3.97)$$

$$\gamma_{ijkl} = -\frac{\partial^4 E}{\partial F_i \partial F_j \partial F_k \partial F_l} \Big|_{F=0}, \quad (3.98)$$

However, the above equations are limited to the static field. In fact, the applied fields must be oscillatory:

$$\vec{F}(\omega) = \vec{F} + F_\omega \cos(\omega t), \quad (3.99)$$

where  $\omega$  is the frequency of the applied field. It can be shown, that the frequency-dependent response can be derived, as a higher derivative of the so-called “pseudo-energy” with respect to the applied field. The pseudo-energy is the eigenvalue of the operator  $H - i\hbar \partial / \partial t$ . There are also some other time-dependent methods, like random phase approximation (RPA) [108] and multiconfiguration response function, which has been used for frequency-dependent hyperpolarizabilities calculations[109].

### 3.4.3.2 The Sum Over States method

The second method utilizes the standard time-dependent perturbation theory, using the fact that the wave function of the perturbed system can be expanded over a complete set of functions of the same system in the absence of perturbation.

Using a semiclassical approach, where the electromagnetic field is described classically and the molecules by quantum mechanics, the time-dependent Schrödinger equation is written as:

$$H\Psi = i\hbar \frac{\partial\Psi}{\partial t}, \quad (3.100)$$

with the Hamiltonian

$$H = H_0 - e\vec{E} \cdot \vec{r}, \quad (3.101)$$

If a complete set of unperturbed eigenfunctions are known:

$$\Psi_n(\vec{r}) = e^{-i\omega_n t} \psi_n, \quad (3.102)$$

where  $\psi_n$  are the time-independent eigenfunctions of  $H_0$ , the wave function of the perturbed system is expressed as follows:

$$\Psi = \sum_{n,s} a_n^{(s)} \Psi_n, \quad (3.103)$$

Here, the coefficients  $a_n^{(s)}$  are determined using the Schrödinger equation:

$$\dot{a}_n^{(s+1)}(t) = (i\hbar)^{-1} \sum_{n'} H'_{nn'} e^{i\omega_{nn'} t} a_{n'}^{(s)}, \quad (3.104)$$

where  $s$  refers to the order of perturbation,

$$H'_{nn'} = \langle n | H' | n' \rangle, \quad (3.105)$$

$$\omega_{nn'} = \omega_n - \omega_{n'}$$

and

$$a_n^{(0)}(t=0) = \delta_{ng}, \quad (3.106)$$

Then, the total polarization can be written as:

$$P = \langle \Psi | e\vec{r} | \Psi \rangle = \left\langle \sum_n (\delta_{ng} + a_n^{(1)} + a_n^{(2)}) | n \rangle \left| e\vec{r} \right| \sum_m (\delta_{mg} + a_m^{(1)} + a_m^{(2)}) | m \rangle \right\rangle, \quad (3.107)$$

Keeping the terms, depending quadratically on the field the following equation for  $p^{(2)}$  can be derived:

$$p^{(2)} = \sum_n \sum_{n'} a_n^{(1)*} a_{n'}^{(1)} \langle n | e\vec{r} | n' \rangle + \sum_n (a_n^{(2)*} \langle n | e\vec{r} | g \rangle + a_n^{(2)} \langle g | e\vec{r} | n \rangle), \quad (3.108)$$

Explicit substitution of coefficients  $a_n^{(1)}$ ,  $a_n^{(2)}$ , that has been done by [110], leads to:

$$\begin{aligned} \beta_{ijk} = & -\frac{e^3}{8\hbar^2} \sum_n \sum_{n'} \{ (r_{gn'}^j r_{n'n}^i r_{gn}^k + r_{gn'}^k r_{n'n}^i r_{gn}^j) \left( \frac{1}{(\omega_{n'g} - \omega)(\omega_{ng} + \omega)} + \frac{1}{(\omega_{n'g} + \omega)(\omega_{ng} - \omega)} \right) + \\ & + (r_{gn'}^i r_{n'n}^j r_{gn}^k + r_{gn'}^i r_{n'n}^k r_{gn}^j) \left( \frac{1}{(\omega_{n'g} + 2\omega)(\omega_{ng} + \omega)} + \frac{1}{(\omega_{n'g} - 2\omega)(\omega_{ng} - \omega)} \right) + \\ & + (r_{gn'}^i r_{n'n}^k r_{gn}^j + r_{gn'}^k r_{n'n}^j r_{gn}^i) \left( \frac{1}{(\omega_{n'g} - \omega)(\omega_{ng} - 2\omega)} + \frac{1}{(\omega_{n'g} + \omega)(\omega_{ng} + 2\omega)} \right) \} \end{aligned} \quad (3.109)$$

where  $r_{nn}^i = \langle \psi_n | r^i | \psi_n \rangle$  is the matrix element of the displacement operator  $r^{(i)}$  along the  $i$ th molecular axis. As is described by Morley and all[111], the above equation can be rewritten in the more convenient form by transforming to a charge-centroid coordinate system:

$$\begin{aligned} \beta_{ijk} = & -\frac{e^3}{8\hbar^2} \sum_{n \neq g} \sum_{\substack{n' \neq g \\ n' \neq n}} \{ (r_{gn}^j r_{n'n}^i r_{gn}^k + r_{gn}^k r_{n'n}^i r_{gn}^j) \left( \frac{1}{(\omega_{n'g} - \omega)(\omega_{ng} + \omega)} + \frac{1}{(\omega_{n'g} + \omega)(\omega_{ng} - \omega)} \right) + \\ & + (r_{gn}^i r_{n'n}^j r_{gn}^k + r_{gn}^i r_{n'n}^k r_{gn}^j) \left( \frac{1}{(\omega_{n'g} + 2\omega)(\omega_{ng} + \omega)} + \frac{1}{(\omega_{n'g} - 2\omega)(\omega_{ng} - \omega)} \right) + \\ & + (r_{gn}^i r_{n'n}^k r_{gn}^j + r_{gn}^k r_{n'n}^j r_{gn}^i) \left( \frac{1}{(\omega_{n'g} - \omega)(\omega_{ng} - 2\omega)} + \frac{1}{(\omega_{n'g} + \omega)(\omega_{ng} + 2\omega)} \right) \} + \\ & + 4 \sum_{n \neq g} \{ r_{gn}^j r_{gn}^k \Delta r_n^i (\omega_{ng}^2 - 4\omega^2) + r_{gn}^i (r_{gn}^k \Delta r_n^j + r_{gn}^j \Delta r_n^k) (\omega_{ng}^2 + 2\omega^2) \} \times \frac{1}{(\omega_{ng}^2 - \omega^2)(\omega_{ng}^2 - 4\omega^2)} \} \end{aligned} \quad , (3.110)$$

where  $\Delta r_n^i = r_{nn}^i - r_{gg}^i$  is the difference in the dipole moment per electron charge between excited and ground states. As follows from the perturbation theory, energetically similar levels mix most effectively leading to substantial modification of the ground state resulting in appearance of high polarizabilities. It has to be noted, that for this formalism the frequency of the incident light is an input parameter. Therefore, dispersive curve calculations are trivial task for this method in comparison with the *finite-field* treatment.

## Two level model

In general, the sum-over-states expansion is indefinite, taking into account many excited states. By restriction of the summation to one lowest lying excited state, the so-called two-level model can be derived:

$$\beta_{iii} = \frac{(\hbar\omega_{gn})^2 (r_{gn}^i)^2 \Delta\mu_{gn}^i}{[(\hbar\omega_{gn})^2 - (2\hbar\omega)^2][(\hbar\omega_{gn})^2 - (\hbar\omega)^2]}, \quad (3.111)$$

or

$$\beta_{iii} \propto \frac{(\hbar\omega_{gn})f_{gn}\Delta\mu_{gn}^i}{[(\hbar\omega_{gn})^2 - (2\hbar\omega)^2][(\hbar\omega_{gn})^2 - (\hbar\omega)^2]}, \quad (3.112)$$

where  $f_{gn}$  is the oscillator strength related to the extinction coefficient  $\varepsilon$ . In the static case the following relations can be found:

$$\beta \propto \frac{r_{gn}^2 \Delta\mu_{gn}}{E_{gn}^2}, \quad (3.113)$$

$$\beta \propto \frac{f_{gn} \Delta\mu_{gn}}{E_{gn}^3}, \quad (3.114)$$

That is, the large hyperpolarizabilities are observed for systems, which exhibit low-lying charge-transfer levels.

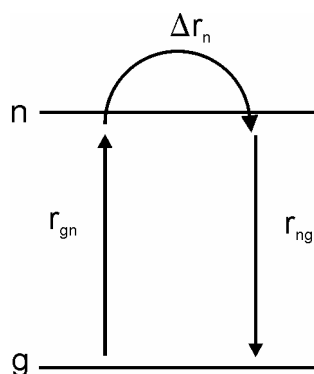


Figure 3.3: Two level model

### 3.4.4. Solvation models

Strictly speaking, all the equations presented so far are valid for the vacuum. Therefore, they are inadequate for describing molecular optical and nonlinear optical properties in solution. Generally, all methods characterizing the effect of solvent can be divided into two types: those which describe the solvent as continuum medium and those which account for the individual properties of the solvent molecules.

#### 3.4.4.1. Continuum solvation models

The continuum solvation methods consider a solvent as a uniform polarizable medium with a dielectric constant  $\epsilon$ . The solute is placed into an appropriate cavity within the solvent. Normally, the solvation process is treated in a self-consistent way, which means that the electronic properties of a solute are calculated iteratively, taking into account the polarization of the medium during each step of the calculations.

The simplest model is the *Born*[112] reaction field model, where the cavity is spherical and only the charge of the molecule is considered. The energy difference between the vacuum and the medium is given by:

$$\Delta E = -\left(1 - \frac{1}{\epsilon}\right) \frac{q^2}{2a}, \quad (3.115)$$

In the *Onsager*[113] reaction field model, the shape of the cavity is spherical as well, but the permanent dipole moment of the molecule is taken into account. The energy difference in that case is expressed as:

$$\Delta E = -\frac{\epsilon - 1}{2\epsilon + 1} \frac{\mu^2}{a^3}, \quad (3.116)$$

In a self-consistent way the back-polarization changes the dipole moment of the molecule. The molecular Hamilton operator is expressed as:

$$H = H_0 + V_\sigma, \quad (3.117)$$

where  $V_\sigma$  for an arbitrary shape of the cavity is given by:

$$V_\sigma(\vec{r}) = \int \frac{\sigma(\vec{r}_s)}{|\vec{r} - \vec{r}_s|} d\vec{r}_s, \quad (3.118)$$

where  $\sigma(\vec{r}_s)$  is the charge density on the surface of the hole, which can be derived numerically. For a spherical cavity it can be solved analytically:

$$V_\sigma = -\frac{2(\varepsilon - 1)}{(2\varepsilon + 1)a^3} \vec{r} \cdot \vec{\mu}, \quad (3.119)$$

In terms of the Hartree-Fock theory the operator  $V_\sigma$  corresponds to addition of an extra term to the Fock matrix elements:

$$F_{\alpha\beta} = \langle \chi_\alpha | \vec{F}_i | \chi_\beta \rangle - \frac{\varepsilon - 1}{(2\varepsilon + 1)a^3} \vec{\mu} \langle \chi_\alpha | \vec{r} | \chi_\beta \rangle, \quad (3.120)$$

The Tomasi's *Polarizable Continuum Model* (PCM) [114] defines the cavity as series of interlocking atomic spheres. The solvent is considered as continuum medium with a dielectric constant  $\varepsilon$ , too. The isodensity PCM (IPCM) and Self-consistent Isodensity Polarized Continuum Models (SCI-PCM) defines the cavity as an isodensity surface of the molecule. The later one, however, includes the effects of polarized charges on the isodensity surface.

The *Conductor Screening Models*[115] also employ molecular shaped cavities, and represent the electrostatic potential by partial atomic charges.

### 3.4.4.2 The hybrid QM/MM method

The above described solvation methods consider the medium as continuous and homogeneous. Consequently, these methods are not capable of appreciating the contribution of individual residues. Moreover, systems like the membrane protein bacteriorhodopsin contain thousands of atoms. However, even SCF calculations of the whole protein are such time consuming that they are limited to about 500-1000 atoms using a supercomputer, so far. Calculations of the excitation energies, which need CI methods, are even much more computational expensive. Obviously, such calculations are out of reach, too. Nevertheless, since the retinal chromophore can be assumed to be solely responsible for the optical properties of the protein, this problem may be solved by means of the so-called hybrid QM/MM methods[116;117]. In those methods, the region of interest is calculated quantum mechanically, and the rest is treated by classical mechanics. In our calculations we use the QM/MM method implemented in the Mopac package[118;119].

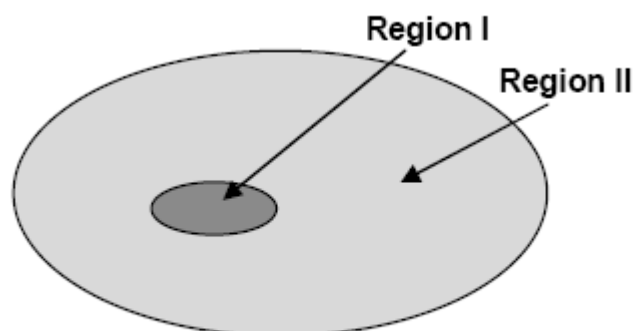


Figure 3.4: General solvation model of the QM/MM method

For such systems the Hamiltonian has the form:

$$H = H^I + H^{II} + V, (3.121)$$



where  $H^I$  and  $H^{II}$  are the Hamiltonian operators for the regions I and II, respectively.  $V$  describes the interactions between the regions. The Schrödinger equation for the whole system is given by:

$$H|\Psi_n\rangle = E_n|\Psi_n\rangle, \quad (3.122)$$

where  $\Psi_n$  is the wave function of the system. If the electron exchange is negligible, the total wave function can be represented as:

$$\Psi_n = \Psi_n^I \Psi_n^{II}, \quad (3.123)$$

where  $\Psi_n^I, \Psi_n^{II}$  are the wave functions for the regions I and II, respectively. The energy of the whole system is then given by:

$$E_n = \langle \Psi_n^I | H^I + V[\Psi_n^{II}] | \Psi_n^I \rangle + \langle \Psi_n^{II} | H^{II} | \Psi_n^{II} \rangle, \quad (3.124)$$

where

$$V[\Psi_n^{II}] = \langle \Psi_n^{II}(\vec{r}') | \frac{1}{|\vec{r} - \vec{r}'|} | \Psi_n^{II}(\vec{r}') \rangle, \quad (3.125)$$

is the coulomb potential per unit charge of the charge distribution of region II. The energy of the ground state is:

$$\begin{aligned} E_0 &= \langle \Psi_0^I | H^I + V[\Psi_0^{II}] | \Psi_0^I \rangle + \langle \Psi_0^{II} | H^{II} | \Psi_0^{II} \rangle \\ &= \langle \Psi_0^I | H^I | \Psi_0^I \rangle + \langle \Psi_0^I | V[\Psi_0^{II}] | \Psi_0^I \rangle + \langle \Psi_0^{II} | H^{II} | \Psi_0^{II} \rangle, \quad (3.126) \\ &= E_0^I + \langle \Psi_0^I | V[\Psi_0^{II}] | \Psi_0^I \rangle + E_0^{II} \end{aligned}$$

The energy of the  $i$ -th excited state is:

$$E_i = E_i^I + \langle \Psi_i^I | V[\Psi_i^{II}] | \Psi_i^I \rangle + E_i^{II}, \quad (3.127)$$

Hence, the excitation energy can be represented as follows:

$$\Delta E_i = E_i^I - \Delta E_0^I + \langle \Psi_i^I | V[\Psi_i^{II}] | \Psi_i^I \rangle - \langle \Psi_0^I | V[\Psi_0^{II}] | \Psi_0^I \rangle + E_i^{II} - E_0^{II}, \quad (3.128)$$

In the QM/MM method the interactions between regions I and II as well as the interactions inside of region II are treated by classical electrostatics. Herein we define:

- $Q^I$ : Atomic charges of the ground state in the region I.
- $Q^{II}$ : Atomic charges of the ground state in the region II.
- $Q^I + q^{I,i}$ : Atomic charges of  $i$ -th excited state in the region I.
- $Q^{II} + q^{II,i}$ : Atomic charges of  $i$ -th excited state in the region II.

In order to describe the interaction between the atoms  $a$  and  $m$  ( $a$  and  $m$  belong to different regions) the following matrix is introduced:

$$G_{am} = \frac{1}{|\vec{r}_a - \vec{r}_m|}, \quad (3.129)$$

In these terms the interaction can be rewritten as:

$$\langle \Psi_0^I | V[\Psi_0^{II}] | \Psi_0^I \rangle = Q^I G Q^{II}, \quad (3.130)$$

$$\langle \Psi_i^I | V[\Psi_i^{II}] | \Psi_i^I \rangle = (Q^I + q^I) G (Q^{II} + q^{II}), \quad (3.131)$$

In analogy to (3.129) for the interactions between regions I and II, for the interactions inside the region II the matrix  $R_{mn}$  is introduced:

$$R_{mn} = \frac{1}{|\vec{r}_m - \vec{r}_n|} \quad (m \neq n), \quad (3.132)$$

$$R_{mm} = 0$$

Using R the electrostatic energies in the region II are:

$$E_0'' = \frac{1}{2} Q' G Q'' , (3.133)$$

$$E_i' = \frac{1}{2} (Q' + q') G (Q'' + q'') , (3.134)$$

Finally, the excitation energies can be formulated as follows:

$$\Delta E_i = E_i' - E_0' + (Q' + q') G q'' + q' G Q'' + \frac{1}{2} q'' R q'' + q'' R Q'' , (3.135)$$

It can be shown by solving the Schrödinger equation,

$$(H' + V[\Psi_0'']) |\Psi_n'\rangle = E_n' |\Psi_n'\rangle , (3.136)$$

that the simple CI treatment does not yield the correct excitation energy. Indeed, the Fock matrix in this case can be modified as:

$$F_{\mu\mu} = F_{\mu\mu}^0 + (G Q'')_l \quad (\phi_\mu \in \text{atom l}), (3.137)$$

The SCF calculations give the ground state energy:

$$E_0' = E_0' + Q' G Q'' , (3.138)$$

and the excitation energies:

$$\Delta E_i' = E_i' - E_0' + q^{l,i} G Q'' , (3.139)$$

which are different from (3.135). Therefore, the absent terms must be added to (3.139) in the following way:

$$\Delta E_i = \Delta E'_i + (Q^I + q^{I,i})Gq^{II,i} + \frac{1}{2}q^{II,i}Rq^{II,i} + q^{II,i}RQ^{II}, \quad (3.140)$$

### ***Polarizable Mosaic Model***

Whereas the charges  $Q$  are determined by the LMSO methods, the charges  $q^{II,i}$ , i.e. the atomic charge redistribution, have to be calculated in a different way. For these purposes the so-called *polarizable mosaic model* (PMM) [120] is used to appreciate explicitly the electronic polarization of a protein matrix. In PMM, each covalent bond in region II is replaced by a dielectric cylindrical stick, whose polarizability is determined by the nature of the original bond. For the PMM model,  $q^{II,i}$  is given by [120]:

$$q^{II} = (I - AR)^{-1} AG^t q^I, \quad (3.141)$$

where  $I$  is a unit matrix. The components of matrix  $A$  are defined as:

$$A_{mn} = \frac{\alpha_{mn}}{d_{mn}^2} \quad (m \neq n), \quad (3.142)$$

$$A_{mm} = -\sum_n \frac{\alpha_{mn}}{d_{mn}^2}, \quad (3.143)$$

where  $d_{mn}$  is the distance between atoms  $m$  and  $n$ , and  $\alpha_{mn}$  is the polarizability along the bond, which is calculated by *molar bond refraction* (see below). In this equation,  $AR$  represents dipole-dipole interactions within region II, whereas  $AG^t$  are the charge-dipole interactions between regions I and II.

If the interactions within the region II are fairly weak:

$$(I - AR)^{-1} \approx I, (3.144)$$

Accordingly, equation (3.141) can be simplified to:

$$q^{II} = AG^t q^I, (3.145)$$

Neglecting the interactions inside of region II causes overestimation of the interactions between regions I and II and consequently lead to an overestimation of the wavelength shift[119].

### ***Parametrization of Bond Polarizability***

As mentioned above, the polarizability of the bonds between atoms in the QM/MM method is estimated by *molar bond refraction* using an empirical rule for the description of the refractive indices in the medium. The polarizability and the refractive index are connected via the Lorentz-Lorentz equation:

$$\frac{n^2 - 1}{n^2 + 1} \frac{M}{\rho} = \frac{4\pi N_a \alpha_{iso}}{3} = P_M, (3.146)$$

where  $M$  is molecular weight,  $\rho$  is density of the medium,  $N_a$  is Avogadro's number, and  $P_M$  is the molar refraction, which can be represented as:

$$P_M = \sum_n P_n, (3.147)$$

where  $P_n$  is the contribution of the  $n$ th atom. In MOS-F's QM/MM method, the new parameter *molar bond refraction* is introduced as follows:

$$P_{m-n} = \frac{P_m}{\nu_m} + \frac{P_n}{\nu_n} + P_\pi, \quad (3.148)$$

where  $\nu_m$  is the valence number counted only for  $\sigma$ -bonds of the atom  $m$ . The  $P_\pi$  term is only introduced when the atomic pair exhibits a  $\pi$ -bond. For a cylindrical shape the isotropic polarizability is expressed as:

$$\alpha_{iso} = \frac{\alpha_{||} + 2\alpha_{\perp}}{3} \quad (3.149)$$

where  $\alpha_{||}$  and  $\alpha_{\perp}$  are the polarizabilities along and perpendicular to the bond, respectively. By assuming that  $\alpha_{\perp}$  equals to 0, the following expression is obtained:

$$\alpha_{mn,iso} = \frac{9P_{m-n}}{4\pi N_a} \quad (3.150)$$

Values for the molar bond refractions for proteins are implemented in MOS-F V.7.0.

## **Chapter 4**

# **Calculation of Linear and Nonlinear Optical Properties of Modified Bacteriorhodopsins**

### **4.1 The origin of the nonlinear optical properties of bacteriorhodopsin**

BR consists of the protein matrix and all-trans retinal, a chromophore which is responsible for its (non)linear optical properties. Indeed, there is no absorption at 568 nm and the corresponding frequency doubling in white membranes that contain no retinal. Upon reconstitution of the apoprotein with the retinal its optical properties change drastically and the absorption maximum shifts to the red by 130nm. Several mechanisms of this shift have been proposed: (1) elongation of the  $\pi$ -conjugated system due to the ring/chain coplanarization[121], (2)  $\pi$ -electron delocalization due to weakening of the interaction between protonated Schiff base and its counterion[122], and (3) interaction of the chromophore with polar and polarizable residues in the protein[123]. All mechanisms mentioned above are directly related to the degree of delocalization of  $\pi$ -electrons of the polyene chain. On the other hand, the first hyperpolarizability  $\beta$  is very sensitive to  $\pi$ -electron delocalization[124].

In order to examine the influence of these mechanisms on the first hyperpolarizability some theoretical calculations have been performed. The first theoretical calculation has been done on model systems like retinal derivatives. After that, we have calculated the polarizabilities and dipole moments of protein side chains residues to establish their probable contribution to the polarizability of the hydrophobic interior of the protein. For

this purpose we used the semiempirical *intermediate neglect of differential overlap for spectroscopy/configuration interaction/sum-over-states* (INDO/S/CI/SOS) method. Finally, the first hyperpolarizabilities for BR mutants and for BR analogue as well as for the photoreceptor NpSRII have been calculated by means of a quantum mechanical/molecular mechanical-configuration interaction (QM/MM-CI) method.

### **Chromophore part**

The retinal is a conjugated polyene chromophore that possesses an extended  $\pi$ -electron system coupled with a low-lying strongly allowed excited state. Moreover, the first electronic transition has a charge transfer character. Upon light excitation the negative charges at the  $\beta$ -ionic ring are shifted towards to the Schiff base making the C<sub>14</sub>C<sub>15</sub>H=NH-Lys linkage more negative as it is shown in figure 4.1.

To investigate the dependence of the (non)linear optical properties on the polyene length several retinal analoga have been chosen (1-4). As clearly seen from Table 4.1., the number of double bonds has a strong effect on the first hyperpolarizability of the polyene chain. An exponential increase of  $\beta$  with the number of double bonds in the polyene chain is observable. The absorption maxima of such derivatives shift to red with an increase of the number of double bonds, pointing out the enhancement of the delocalization of  $\pi$ -electrons along the molecular chain. Our results are in good agreement with those for the corresponding retinal derivatives measured experimentally by the HRS technique[125].



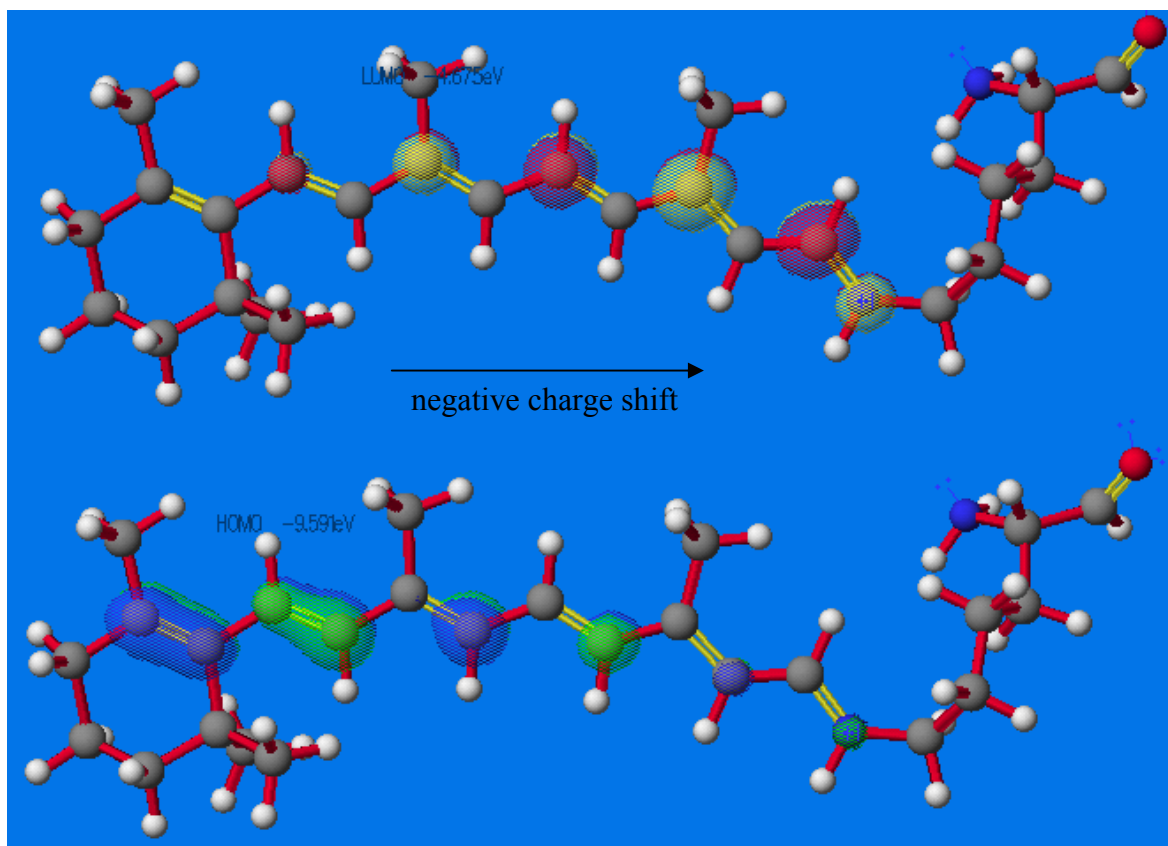
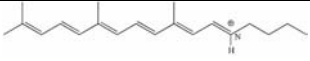
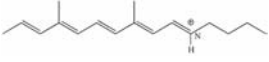
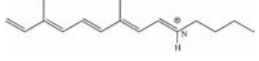
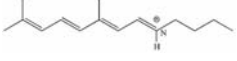
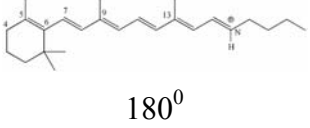
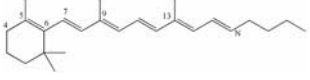


Figure 4.1 The direction of the charge transition upon excitation into the lowest-lying strongly allowed excited state (HOMO-LUMO)

However, it is known that the effective conjugation length reaches a limiting value that reduces the effectiveness of additional double bonds. One of the methods to overcome this limitation could be to use charged species on one or both sides of the polyene chain[126]. This method is similar to those that use effective donor-acceptor groups at the end of the polyene chain. In order to analyze the influence of charges, analogue (5-6) have been calculated. Their structures were obtained from the Protein data base (2PDB). Structure (5) is protonated, whereas (6) is in its deprotonated form. As can be seen from the table 4.1, protonation of the Schiff base results in a more than ten-fold enhancement of the first hyperpolarizability shifting the absorption maximum from 369 nm to 499 nm. It is interesting to note that the experimental value for the absorption maximum of the protonated Schiff base in solution is 440nm, whereas its deprotonated form appears at 370

nm, indicating that the effect of protonation there is partially compensated by the anions of the buffer solution.

Table 4.1: Calculated optical properties of retinal analogue.  $\Delta_{\text{calc}}$ : the difference of the dipole moment from the excited state to the ground state;  $\beta_{\text{calc}}^{\text{stat}}$ : calculated static hyperpolarizability

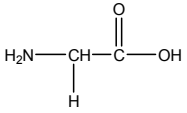
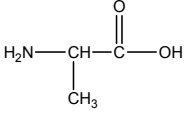
	Retinal analogue (dihedral angle $\gamma$ for the C6-C7 single bond)	$\lambda_{\text{max}}^{\text{calc}}$ of retinal analogue, nm	Oscillator strength, a.u.	$\Delta_{\text{calc}}$ , D	$\beta_{\text{calc}}^{\text{stat}}$ , $10^{-30}$ cm <sup>5</sup> /esu
1		457	2.12	13.28	181
2		449	1.97	9.24	83
3		434	1.94	8.83	66
4		405	1.72	6.78	34
5	 180 <sup>0</sup>	499	2.06	14.86	203
6		369	2.58	4.49	19
7	165 <sup>0</sup>	494	2.04	14.88	196
8	150 <sup>0</sup>	490	1.95	15.41	184
9	120 <sup>0</sup>	463	1.78	15.28	140
10	90 <sup>0</sup>	435	1.90	11.62	109
11	60 <sup>0</sup>	457	1.79	14.22	129
12	30 <sup>0</sup>	489	1.77	14.8	161
13	0 <sup>0</sup>	497	1.80	14.33	168

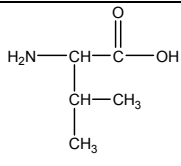
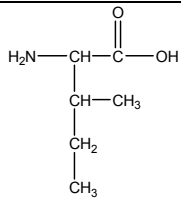
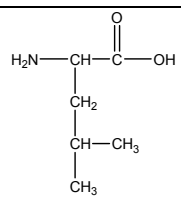
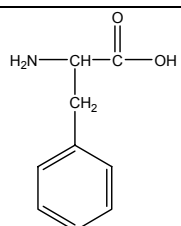
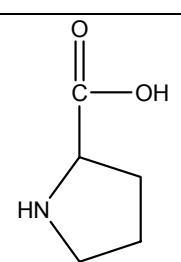
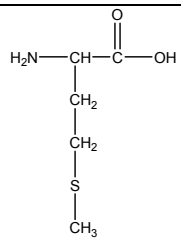
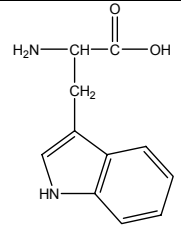
The influence of the planarity of the retinylidene chromophore on the first hyperpolarizability can be evaluated by comparison of the retinal analoga (5) and (7)-(12). The analogue 13(dihedral angle  $\gamma=0^\circ$ ) is in the ring-chain twisted *s cis* conformation, whereas 5 is in the *s trans* conformation as in BR (dihedral angle  $\gamma=180^\circ$ ). Analoga (7-11) represent intermediate states characterized by different dihedral angles  $\gamma$  for the C6-C7 single bond. An increase of 21% is obtained in the first hyperpolarizability on going from the twisted *s cis* to *s trans* conformation, whereas the absorption maximum is shifted to red by 2 nm.

### Protein part

Extensive studies on the wild type BR have shown that the nonlinear optical properties of the chromophore are significantly enhanced by the surrounding protein. Polarizable amino acids can stabilize the excited state of the chromophore. It was found that the induced dipole is at least 1.5 times larger in BR than for all-trans retinal with a protonated Schiff base in solution. The factors that can contribute are the environmental polarizability and polarity. To clarify the contributions of individual groups, the polarizabilities and dipole moments of the side chains of the amino acids have been calculated. The obtained results are summarized in Table 4.2.

Table 4.2. Properties of the amino acids

Amino acid	Structure	Permanent dipole, D	Static polarizability, $10^{-24}\text{cm}^3$	Dynamic polarizability at 1064 nm, $10^{-24}\text{cm}^3$	Dynamic polarizability at 532 nm, $10^{-24}\text{cm}^3$
Gly		3.45	0.16	0.16	0.18
Ala		3.00	0.49	0.50	0.56

Val		2.51	0.18	0.19	0.21
Ile		2.50	0.19	0.19	0.21
Leu		5.47	0.07	0.08	0.08
Phe		2.76	3.20	3.80	4.97
Pro		5.19	0.19	0.2	0.22
Met		2.79	0.2	0.21	0.26
Trp		3.13	5.91	6.28	7.72

Cys	$\begin{array}{c} \text{O} \\ \parallel \\ \text{H}_2\text{N}-\text{CH}-\text{C}-\text{OH} \\   \\ \text{CH}_2 \\   \\ \text{SH} \end{array}$	6.57	0.09	0.1	0.11
Ser	$\begin{array}{c} \text{O} \\ \parallel \\ \text{H}_2\text{N}-\text{CH}-\text{C}-\text{OH} \\   \\ \text{CH}_2 \\   \\ \text{OH} \end{array}$	1.32	0.21	0.24	0.67
Thr	$\begin{array}{c} \text{O} \\ \parallel \\ \text{H}_2\text{N}-\text{CH}-\text{C}-\text{OH} \\   \\ \text{CH}-\text{OH} \\   \\ \text{CH}_3 \end{array}$	3.80	0.33	0.35	0.39
Asn	$\begin{array}{c} \text{O} \\ \parallel \\ \text{H}_2\text{N}-\text{CH}-\text{C}-\text{OH} \\   \\ \text{CH}_2 \\   \\ \text{C}=\text{O} \\   \\ \text{NH}_2 \end{array}$	3.14	0.22	0.23	0.26
Gln	$\begin{array}{c} \text{O} \\ \parallel \\ \text{H}_2\text{N}-\text{CH}-\text{C}-\text{OH} \\   \\ \text{CH}_2 \\   \\ \text{CH}_2 \\   \\ \text{C}=\text{O} \\   \\ \text{NH}_2 \end{array}$	6.74	0.06	0.06	0.08
Arg	$\begin{array}{c} \text{O} \\ \parallel \\ \text{H}_2\text{N}-\text{CH}-\text{C}-\text{OH} \\   \\ \text{CH}_2 \\   \\ \text{CH}_2 \\   \\ \text{CH}_2 \\   \\ \text{NH} \\   \\ \text{C}=\text{NH} \\   \\ \text{NH}_2 \end{array}$	14.15	0.13	0.13	0.15
Tyr	$\begin{array}{c} \text{O} \\ \parallel \\ \text{H}_2\text{N}-\text{CH}-\text{C}-\text{OH} \\   \\ \text{CH}_2 \\   \\ \text{C}_6\text{H}_4 \\   \\ \text{OH} \end{array}$	3.99	3.40	3.92	12.45
His	$\begin{array}{c} \text{O} \\ \parallel \\ \text{H}_2\text{N}-\text{CH}-\text{C}-\text{OH} \\   \\ \text{CH}_2 \\   \\ \text{C}_4\text{H}_3\text{N} \end{array}$	6.94	2.04	2.14	2.51

Asp	$  \begin{array}{c}  \text{O} \\  \parallel \\  \text{H}_2\text{N}-\text{CH}-\text{C}-\text{OH} \\    \\  \text{CH}_2 \\    \\  \text{C}=\text{O} \\    \\  \text{OH}  \end{array}  $	8.82	0.78	0.79	0.85
Glu	$  \begin{array}{c}  \text{O} \\  \parallel \\  \text{H}_2\text{N}-\text{CH}-\text{C}-\text{OH} \\    \\  \text{CH}_2 \\    \\  \text{CH}_2 \\    \\  \text{C}=\text{O} \\    \\  \text{OH}  \end{array}  $	15.04	0.08	0.09	0.10
Lys	$  \begin{array}{c}  \text{O} \\  \parallel \\  \text{H}_2\text{N}-\text{CH}-\text{C}-\text{OH} \\    \\  \text{CH}_2 \\    \\  \text{CH}_2 \\    \\  \text{CH}_2 \\    \\  \text{CH}_2 \\    \\  \text{NH}_2  \end{array}  $	18.76	0.03	0.04	0.04

As can be seen, the aromatic residues (phenylalanine, tyrosine, and tryptophan) possess significant polarizabilities, one order of magnitude higher than the other ones. The calculated results are in the good agreement with those showing a shift of the absorption maximum of the protonated retinal Schiff base in ethanol by addition of phenol or indole[127;128].

## 4.2 Calculations for bacteriorhodopsin mutants and variants

To investigate effect of electronic polarization of the whole hydrophobic interior on the first hyperpolarizability of retinal as well as a relative contribution to that of certain amino residues on the position of mutation, a hybrid quantum mechanical/molecular mechanical-configuration interaction (QM/MM-CI) method of the MOPAC program has been used. In this method the chromophore region is calculated quantum mechanically, whereas the protein part is treated using molecular mechanics. The polarization of the protein part is

taken into account by the “polarizable mosaic model” approximation. The validity of such treatment for the electronic structure calculations was shown previously by investigation of several alanine mutants of BR[120]. In particular, it was shown that the polarization of amino acid residues W86, W182, Y185 play a predominant role in the bathochromic shift of the absorption maxima of BR.

The calculation procedure was as follows. The calculated structures are the ground state and M1 state of wild type BR, the ground state of BR mutants W86F, W189F, W182F, W138C, Y185F, Y83F, and of the light receptor NpSRII. The positions of mutations in the chromophore-binding pocket for BR are shown in figure 4.2. The structures of wild type BR, the M1 intermediate, and SRII were derived from the files 2PDB, 1P8H, and 1H68 of the protein data bank, respectively. The structures of the BR mutants were derived from the structure of wild-type by replacing of the side chain at the position of mutation BR using the program INSIGHT II (Biosym). Hydrogen atoms were added to the initial structures using the MOPAC program. The carboxyl group of Asp96 of all mutants was protonated. First, the atomic charges of the ground state of the whole protein were evaluated by the MOZYME function of MOPAC utilizing the AM1 Hamiltonian (which is most suitable for the charge distribution calculation) and a cutoff distance of 7.0 Å for short-range interactions. The coordinates of the protein were then divided into *all-trans*-retinal+Lys 216 as chromophore part (region I) and the remainder (region II).

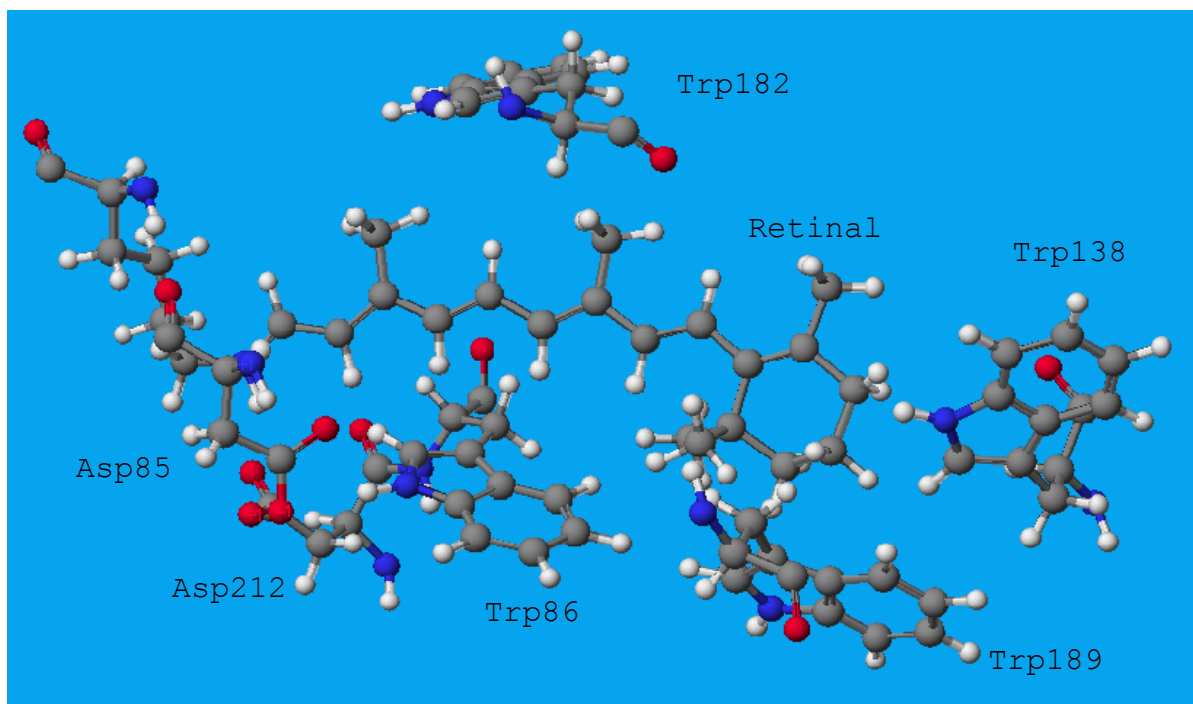


Figure 4.2. The residues located in the chromophore-binding pocket

The obtained static hyperpolarizabilities as well as other optical properties (experimental and calculated values) are summarized in Table 4.2. It has to be noted that the calculated absolute value of absorption maxima of the ground state of BR is different to that reported in [120], but in excellent agreement with experiment (probably due to the consideration of the side chain of Lys216 in region I). The calculated absorption maxima of the other variants are also in good agreement with the experimental results except for the mutants W189F and Y83F, which exhibit a shift in an opposite direction compared to the experiment. Their hyperpolarizabilities, therefore, have not been calculated. The change in dipole moments upon excitation is also in good agreement with that measured by two-photon absorption for wild type BR ( $13.5 \pm 0.8D$ ) [89]. As can be seen, there is an increase of 40% in the static hyperpolarizability for the BR molecule with respect to the protonated Schiff base (Table 4.1, structure 5). Thus, our theoretical results indicate that the high polarizable aromatic residues determine the magnitude of  $\beta$  significantly. They are in good agreement with those determined experimentally for the model retinal chromophores [5]. For the other mutants the dependence of the second-order nonlinear optical response on the



polarizability of the surrounding residues can be seen clearly, by comparison of wild-type BR and mutants W86F and W182F. In these mutants the tryptophan residues are replaced by phenylalanine whose polarizability is smaller. As a consequence, their absorption spectra exhibit a blue shift and the values of the static hyperpolarizability decrease. The difference in the dipole moments also shows a decrease. In the case of the Y185F mutant, the first hyperpolarizability is increased relative to wild-type BR accompanied by a red shift in the absorption spectrum, despite the fact that the polarizability of phenylalanine is somewhat lower than that of tyrosine (see Table 4.2). This red shift could originate from a lowering of the permanent dipole of the phenylalanine with respect to a tyrosine residue which destabilizes the excited state of the retinal to a weaker extent. As a result, its absorption spectrum is shifted to the red enhancing the second-order nonlinearity of the Y185F mutant. As in the case of retinal in vacuum, the protonation of the Schiff base exerts the major influence on the first hyperpolarizability. A 5.3-fold enhancement may be found by going from its deprotonated to the protonated form neglecting the frequency dispersion effect which has a strong influence, too.

Moreover, we calculated linear and nonlinear optical properties of the photoreceptor sensory rhodopsin, NpSRII. This protein possesses a high degree of similarity in its three-dimensional structure to BR. However, despite of this fact its absorption spectrum has its maximum at 497 nm. The calculated value for the absorption maximum agrees with the experimental one within 15 nm and its calculated static hyperpolarizability is slightly lower than for BR.

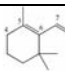
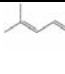
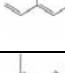
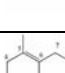
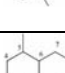
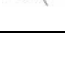
Table 4.3. Measured and calculated optical properties of BR mutants and NpSRII. DA: dark-adapted; LA: light-adapted;  $f_{\text{calc}}$ : calculated oscillator strength;  $\Delta_{\text{calc}}$ : the difference in dipole moment between excited state and ground state;  $\beta_{\text{calc}}^{\text{stat}}$ : calculated static hyperpolarizability  $\beta(0;0,0)$

Mutant	$\lambda_{\text{max}}^{\text{exp}}$ of BR (mutant), nm		$\epsilon_{\text{max}}$ of BR (mutant), $\text{M}^{-1} \text{cm}^{-1}$	$\lambda_{\text{max}}^{\text{calc}}$ of BR (mutant), nm	$f_{\text{calc}}$ , a.u.	$\Delta_{\text{calc}}$ , D	$\beta_{\text{calc}}^{\text{stat}}$ , $10^{-30}$ $\text{cm}^5/\text{esu}$
	LA	DA					
BR	568	558	63000	566	1.76	13.26	224
W86F	547	534	47000	556	1.74	13.57	211
W189F	521	513	-	561	-	-	-
W182F	491	477	-	511	1.95	12.88	172
W138C	547	543	-	533	1.70	14.56	246
Y185F	573	556	-	589	1.69	13.41	250
Y83F	540	533	-	573	-	-	-
NpSRII	497		48000	513	1.65	18.00	191
M1	410		34000	416	1.44	3.38	42
D85_protonated	605		-	602	1.74	13.7	287

There has been a tremendous number of retinal analogues studied with respect to their photochromic properties[58]. However, up to now, their nonlinear optical properties have never been determined. We calculated the first hyperpolarizabilities for several BR analogues which lack the six-membered ring and which differ in length of the conjugated chain (BR analogues (2)-(4)) as well as those with the ring and different number of double bonds (BR analogues (5) and (6)). The structures of the BR analogues were derived from the files 2PDB of the protein data bank by means of a truncation of the unnecessary parts of the retinal. The obtained structures were not optimized. The first hyperpolarizabilities as well as the other calculated optical properties of the above BR analogues are given in Table 4.4. The calculated absorption maxima agree with the experimental results. This indicates that the difference in colour of the pigments is caused by the differences in the

chromophore rather than by the differences in the BR structures. As can be seen, by comparison of the BR analogues (1)-(3) there is a strong dependence on the number of double bonds. This is similar to those results obtained for the retinal analogues in vacuum (Table 4.1). An exponential increase of  $\beta_{\text{stat}}$  with the number of double bonds in the polyene chain is also observable. Moreover, as in the case of wild type BR, reconstitution of the retinal analogue with the high polarizable opsin-matrix gives at least an enhancement of 40% to the static hyperpolarizability. From this table, it is obvious that  $\beta_{\text{stat}}$  of the BR analogue (2) is larger than that of wild type BR (1) indicating that the electron-donating properties of the  $\beta$ -ionone ring is quite weak.

Table 4.4. Measured and calculated optical properties of BR and BR variants. DA: dark-adapted; LA: light-adapted; SBH<sup>+</sup>: the protonated *n*-butyl Schiff-base;  $f_{\text{calc}}$ : calculated oscillator strength;  $\Delta_{\text{calc}}$ : the difference in dipole moment between excited state to ground state;  $\beta_{\text{calc}}^{\text{stat}}$ : calculated static hyperpolarizability  $\beta(0;0,0)$

	BR (analogue)	$\lambda_{\text{max}}$ of the retinal, nm	$\lambda_{\text{max}}$ of SBH <sup>+</sup> , nm	$\lambda_{\text{max}}$ of BR, nm LA DA	$\lambda_{\text{max}}^{\text{calc}}$ of BR (variants), nm	$f_{\text{calc}}$ , a.u.	$\Delta_{\text{calc}}$ , D	$\beta_{\text{calc}}^{\text{stat}}$ , $10^{-30}$ $\text{cm}^5/\text{esu}$
1		380	440	568 558	566	1.76	13.2	224
2		393	465	538 528	549	1.63	13.5	251
3		364	422	472	481	1.66	10.5	126
4		335	385	430	445	1.54	8.0	48
5		-	390	442 440	453	1.35	11.4	71
6		-	382	438 336	450	1.32	12.5	72

## Chapter 5

### Experimental Part

#### 5.1 Time-resolved optical spectroscopy setup

##### 5.1.1 Sample preparation

Purple membranes were isolated from *Halobacterium salinarium* (strain S9) according to the method of Oesterhelt and Stoeckenius (1974). Site-specific mutants of bacteriorhodopsin T46C, D85C, D96C, R225C, D227C were prepared according to the method of Ferrando et al[129]. The purple membranes were suspended in an acetate buffer (0.01 M) containing 0.1 M NaCl. The pH of the buffer was adjusted by the addition of dilute HCl or NaOH solutions as required. Optical density measurements were performed with a spectrophotometer (UVICON).

##### 5.1.2. Optical Part

The experimental setup for the transient absorption measurements is shown in figure 5.1. A Nd-YAG laser with 8 ns pulse length and 3.5 mJ per pulse at 532 nm was used as an excitation source. The light of a halogen lamp filtered with an IR-cutoff filter was passed through an interference filter and focussed on the sample cuvette. After passing the thermostated cuvette and a grating monochromator it was measured by a photomultiplier. The signal detected in the time range from 10  $\mu$ s to several ms was then recorded with a

digital oscilloscope (Infinium 500 MHz). After transferring to a PC the transient absorption data were reduced to 250 points per trace on a logarithmic time scale for further analysis.

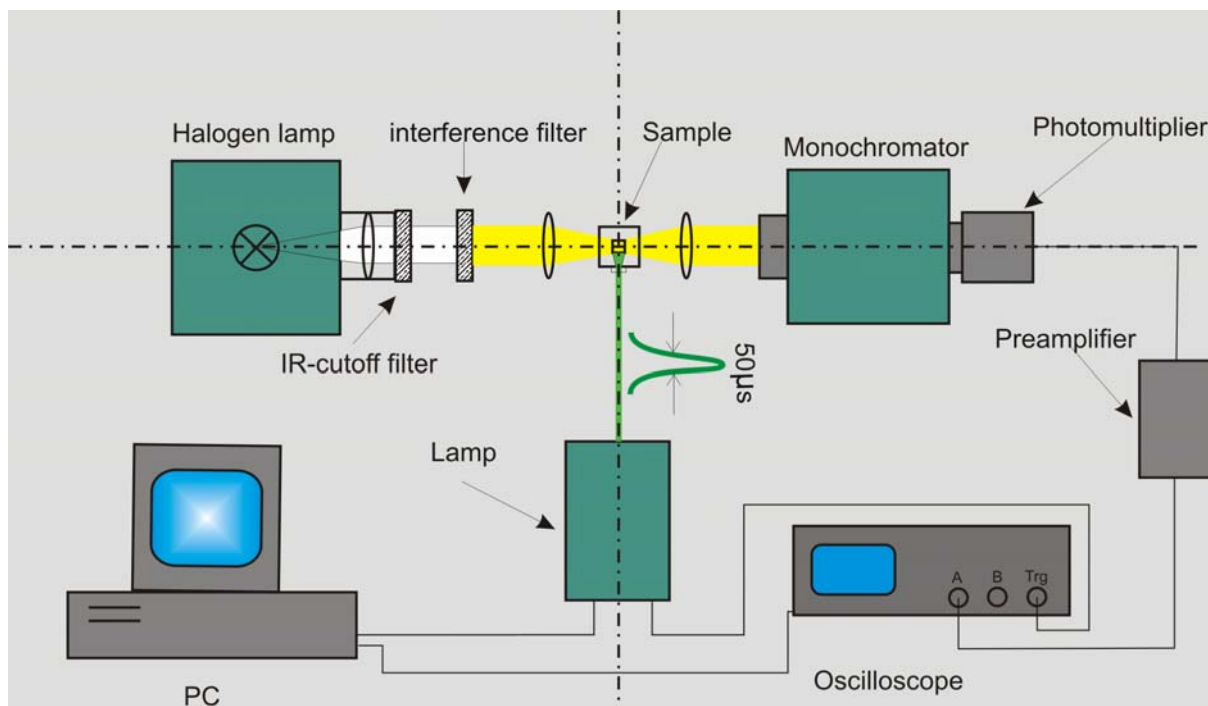


Figure 5.1 The schematic experimental setup for transient absorption measurement

Transient absorbance changes were measured at 11 wavelengths (405, 415, 450, 480, 500, 520, 546, 576, 605, 640, and 650 nm). To improve the S/N ratio 100 single traces were averaged. The temperature of the sample could be varied from 0<sup>0</sup> to 40<sup>0</sup>C with an accuracy of 0.1<sup>0</sup>C. The repetition rate was adjusted between 1s<sup>-1</sup> and 0.1s<sup>-1</sup> depending on the duration of the photocycle of the mutants.

### 5.2.1. Data evaluation. Global fit procedure

The photocycle is regarded as a sequence of first-order reaction. A sequence of any number of first-order reactions can be described by a system of differential equations as follows:

$$\frac{dC_1(t)}{dt} = k_{11}C_1(t) + \dots + k_{1n}C_n(t), \quad (5.1)$$

...

$$\frac{dC_n(t)}{dt} = k_{n1}C_1(t) + \dots + k_{nn}C_n(t)$$

where  $n$  is the total number of intermediates. In the non-degenerate case the general solution of this set of equations can be written as a sum of exponentials:

$$C_i(t) = \sum_{j=1}^n a_{ij} \exp(-k_j^* t), \quad (5.2)$$

where  $k_j^*$  are the apparent rates being dependent on the intrinsic rate constant representing the negative eigenvalues of the matrix  $[k_{ij}]$ . In the case of a sequence of irreversible transitions the number of exponents (5.2) necessary for describing the time evolution of the populations equals the number of intermediates.

The related alterations in the optical density for the different wave lengths measured by transient absorption spectroscopy can be, then, expressed as:

$$\Delta OD(\lambda, t) = d \sum_{i=1}^n \varepsilon_i(\lambda) C_i(t) - d\varepsilon_0(\lambda) \sum_{i=1}^n C_i(t), \quad (5.3)$$

where  $d$  is the thickness of the cuvette,  $\varepsilon_i(\lambda)$  is molar extinction coefficient of the intermediate  $i$ , and  $\varepsilon_0(\lambda)$  is the molar extinction coefficient of the ground state. The substitution of (5.2) in (5.3) yields:

$$\Delta OD(\lambda, t) = \sum_{i=1}^n \bar{A}_i(\lambda) \exp(-k_i^* t), \quad (5.4)$$

where

$$\bar{A}_i(\lambda) = d \sum_{j=1}^n a_{ji} [\varepsilon_j(\lambda) - \varepsilon_0(\lambda)], \quad (5.5)$$

In order to derive the amplitude spectra  $\bar{A}_i(\lambda)$  and the apparent rate constants  $k_i^*$  the fitting program “MultiFit” has been written. This program utilizes the *Levenberg-Marquardt method* as a nonlinear least-squares fitting algorithm. The program works in an iterative way minimizing,  $\chi^2$ , the merit function:

$$\chi^2 = \frac{\sum_{i=1}^L \sum_{j=1}^{n_p} [y(\lambda_i, t_j) - \sum_{m=1}^n \bar{A}_m(\lambda) \exp(-k_m^* t_j)]^2}{n_f}$$

where  $n_p$  is the number of points for the certain wavelength,  $L$  is the number of wavelength, and  $n_f$  is the number of degrees of freedom, which is related to the number of fitting parameters. The program “MultiFit” (written in the Delphi environment) as well as data acquisition software (written in the C++ environment) can be found on a CD-ROM enclosed with this dissertation. The program has some advantages over conventional programs like ORIGIN. Since the number of fitting parameters (amplitudes) is high, it is convenient to set their trial values automatically to unit. Then, the trial set of rate constants has to be set. After that, the amplitudes are evaluated during the first ten iterations keeping the rate constants the same. This procedure allows to derive the appropriate amplitudes

lying in the region of convergence. Finally, the whole set of parameters are automatically evaluated.

## **5.2 Hyper-Raleigh-scattering setup**

### **5.2.1 Sample preparation**

Samples as described in 5.1.1 were used.

### **5.2.2 Optical part**

The general setup for the HRS and time-resolved HRS measurements is shown in figure 5.2. A Q-switched Nd-YAG laser at a fundamental wave length of 1064nm was used as the light source. The laser generates pulses with duration of 8 ns and a nearly Gaussian beam profile with horizontal polarization. Since the HRS represents a second-order nonlinear process, any intensity fluctuations in the fundamental are reflected quadratically in the detected signal. Therefore, a very stable laser source must be used to derive the best results. In order to improve the stability of the laser, the optimal Q-switch delay has been determined to be 160 $\mu$ s, corresponding to the maximum of the output power. The repetition rate could be adjusted under the experimental conditions (especially during the time-resolved measurements of BR mutants) in the range from 0.01 to 10 Hz. Since the beam profile is also dependent on the repetition rate, all relative measurements (first hyperpolarizabilities determination of W86F and D85C mutants) were performed at the same rate. The neutral density filter placed behind the laser is used to keep the HRS signal within the linear range of the photomultiplier. Once this range is chosen, the incident fundamental light intensity is varied by rotation of a half-wave plate between crossed polarizers. A small fraction of the pump intensity is directed onto a fast photodiode (PD). Two RG filters were placed in front of the cuvette holder to eliminate the visible light coming from the flash lamp of the laser. Harmonic light that is generated in a thermostatted



cuvet is collected by a condenser system and focussed on the photomultiplier. In order to select the frequency-doubled radiation, an interference filter with a FWHM of 10nm at 532nm was placed between the lenses of condenser. For the polarization measurements, the numerical aperture was reduced to 0.1 as required to avoid signal averaging over directions different from the perpendicular.

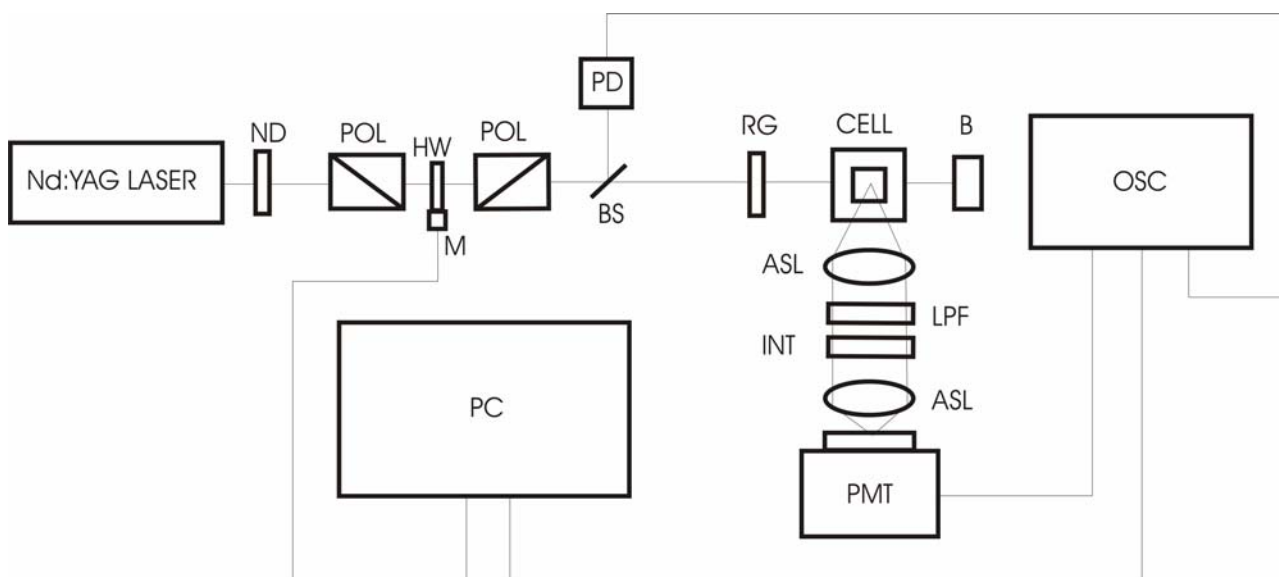


Figure 5.2 Schematic representation of the experimental setup for HRS: ASL, aspheric lens condenser; B, beam stop; BS, beam splitter; HW, half-wave plate; INT, 532 nm interference filter; LFP, short-pass filter; M, stepping motor; ND, neutral density filter; OSC, oscilloscope; PC, personal computer; PD, photodiode; PMT, photomultiplier tube; POL, polarizer; RG, long-pass filter.

Although most of the HRS measurements have been performed with a long cylindrical cell with a quite high intrinsic volume (in order to get the best signal to noise ratio, at modest pump intensities to prevent high order nonlinear processes), for our investigations normal spectroscopic cuvettes were used. It permits to work with a fairly small sample volume, optical elements and applicable in the case of BR due to its arrangement into a membrane molecular ensemble. In this case, the HRS signal is proportional to the square of the number molecules belonging to a membrane patch, whereas, for instance, the two-photonic

luminescence (which contributes as an artefact to HRS signal) grows linearly with their number. The average size of the PM sheets is 500 nm, containing approximately 10000 BR molecules. Obviously, that leads to an increase in the HRS signal by a factor of 10000 compared to not correlated BR molecules at the same pump intensity, lowering the contribution of the luminescence intensity to at least 0.0001 of the total signal.

For the time-resolved HRS measurements an addition light source, a flash lamp with a pulse duration of 20 $\mu$ s, was used for excitation of the sample. Moreover, a band-pass filter was used after the flash lamp to protect the photomultiplier.

### 5.2.3. Electronic part

The electronic part of experimental setup consists of a fast photodiode, a photomultiplier operated in analog mode, and a digital oscilloscope (Infinium 500 MHz). The electronic circuit of the photomultiplier is shown in figure 5.3. In order to improve the linear response of the photomultiplier, chiefly depending on the peak anode current several capacitors have been connected to the last few stages. These capacitors supply the photomultiplier tube with an electric charge during the pulse duration and restrain the voltage drop between the last dynode and the anode. This method makes it possible to derive an output current up to saturation level which is caused by space charge effects in the photomultiplier tube dynodes, attaining several mA. Since the frequency-doubled light pulse to be detected has a fairly short, comparable to the pulse length of the laser, it is also important that the associated circuit is optimized for a wide frequency bandwidth. For these purpose a load resistor  $R_L$  of 50 $\Omega$  is used, serving as a current to voltage converter. Moreover, it is necessary to insert the damping resistors  $R_9$  and  $R_{10}$  of 50 $\Omega$  in the last dynodes, as shown in figure 5.3. They effectively reduce ringing of the output signal, yielding, in our case, the very high contribution to the noise. Both, the fast photodiode and the photomultiplier outputs, are fed directly into the digital oscilloscope (Infinium 500MGz).

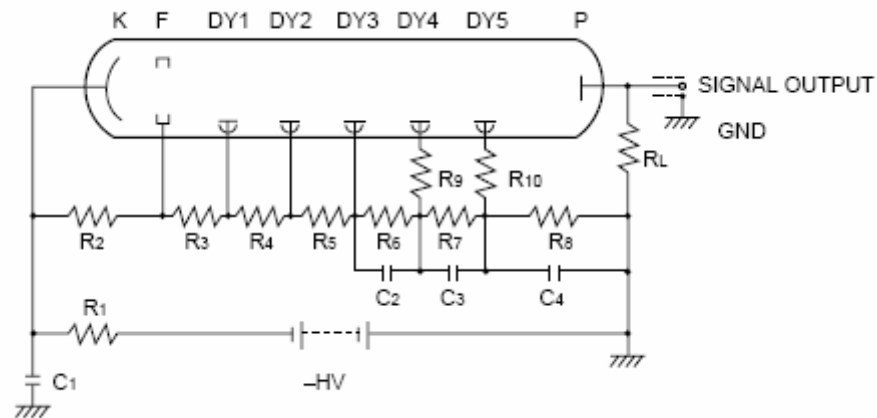


Figure 5.3. The electronic circuit of the photomultiplier

The fast photodiode was used to monitor the incident light intensity, the shape, and stability of the pulses. Moreover, the signal from it serves as a trigger for the oscilloscope. Due to the flight time of electrons in the photomultiplier, the HRS pulse can be monitored 20 ns after the trigger signal. The signal, averaged over 100 pulses, is transferred to a PC. Then, the whole signal is integrated in a time window from 10 to 30 ns after the trigger signal to give the measure which is proportional to the scattering light.

## Chapter 6

# Experimental Results and Discussion

### 6.1 pH dependence of the first hyperpolarizability of bacteriorhodopsin

By conventional site-directed mutagenesis or usage of retinal analogs, as was mentioned before, the optical and nonlinear properties are changed in a step-wise manner. But, for some application their continuous retuning may be of interest. One of the possibilities is to utilize physical and chemical methods. Whereas changing the temperature or the solvents has no significant effect on the optical properties of BR, it is known that the absorption spectrum of BR is sensitive to changes in pH. By lowering the pH, its absorption maximum is shifted from 570nm to 605nm as shown in figure 6.1, forming the so-called blue membrane[130]. The blue form of bacteriorhodopsin does not form the M state and is not capable to translocate protons[131]. It has been shown that Asp85 becomes protonated at low pH, resulting in a weakening of the interaction of the Schiff base with its primary counter ions[132].

The titration experiments were carried out in the pH range from 1.7 to 11. The pH dependence of the first hyperpolarizability is shown in figure 6.2. As can be seen, the first hyperpolarizability shows a complex titration curve with two pKs. Whereas the major part of Asp85 undergoes a transition around pH 3.5, there is another transition near pH 8. The obtained pH dependence is very similar to that measured by absorption spectroscopy[133]. The complex titration behaviour can be described by a D85/X model that supposes that the pK of Asp85 depends on the state of another residue X[134]. Deprotonation of X causes a pK shift of D85 from 3 to 7 elucidating the pH dependence at high pH. Several suggestions

have been made concerning a candidate for the group X. One speculation is that it is a component of the proton release complex which includes residues R82 and Y57[135;136].

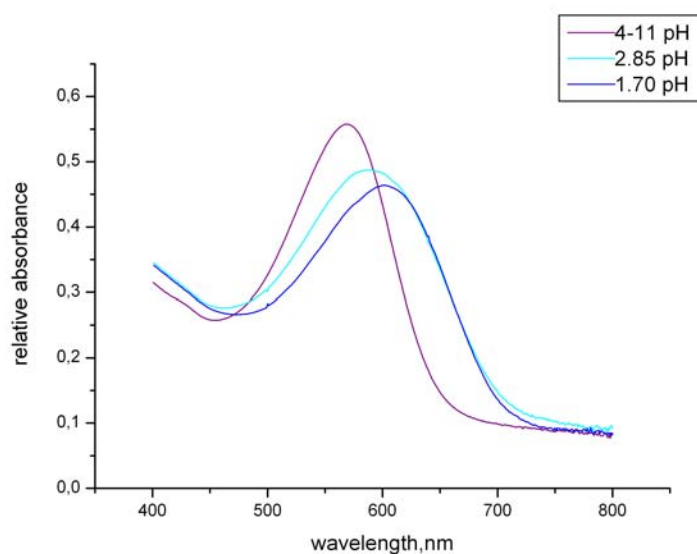


Figure 6.1: Absorption spectra of BR at different pH

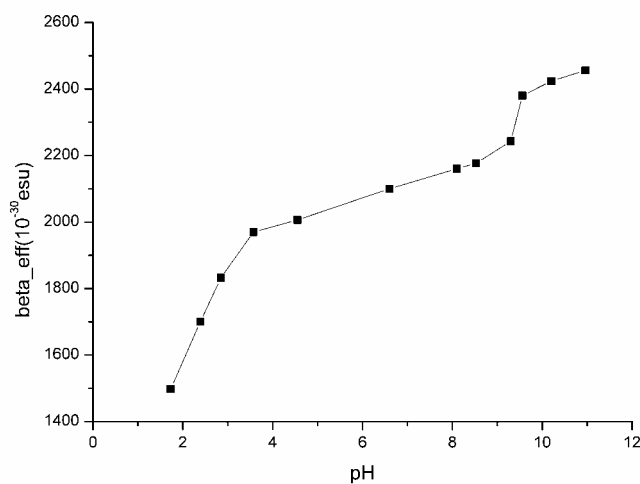


Figure 6.2: pH dependence of the first hyperpolarizability of BR

It has to be noted that the determination of the first hyperpolarizability of wild type BR has been done at neutral pH. However, from the above dependence it can be clearly seen that the value of  $\beta$  at pH 7 (neutral pH) is different to that at pH 11 where the ensemble of BR molecules is completely deprotonated. This is an important point for the quantitative comparison of the experimental and theoretical results.

Table 6.1 summarizes the experimentally determined and calculated linear and nonlinear properties of BR at different pH values. The main component of the first hyperpolarizability was normalized to the value of BR at pH 7. The experimental values of the dipole moment was estimated from the two state model including the damping constants that in the first approximation were assumed to be the same for different pH values and equal to  $1200 \text{ cm}^{-1}$  obtained from the femtosecond hole-burning experiments[137]. For the theoretical calculation, the structure 2BRD of BR taken from the protein data bank was used. BR at pH 2 was modelled by adding a hydrogen atom to the carboxyl group of Asp85 in this structure. The calculated absorption maximum of BR at pH 2 of 602 nm indicates that there is no significant alteration in the structure relative to BR at normal pH i.e. the 37nm red shift is mostly caused by neutralization of the negative charge of Asp85.

Table 6.1 : Linear and nonlinear optical properties of bacteriorhodopsin at different pH

Molecule	Oscillator strength		Absorption maxima, nm		$\frac{\beta_{zzz}^{\text{exp}}}{\beta_{zzz}^{\text{exp}}(bR_{\text{pH}7})}$		$\frac{\beta_{zzz}^{\text{calc}}}{\beta_{zzz}^{\text{calc}}(bR_{\text{pH}7})}$		$\frac{\Delta\mu_{\text{exp}}}{\Delta\mu_{\text{exp}}(bR_{\text{pH}7})}$		$\frac{\Delta\mu_{\text{calc}}}{\Delta\mu_{\text{calc}}(bR_{\text{pH}7})}$	
	$f_{\text{exp}}$	$f_{\text{calc}}$	$\lambda_{\text{exp}}$	$\lambda_{\text{calc}}$								
BR <sub>pH7</sub>	1.02	1.75	568	566	1	1	1	1	1	1	1	1
BR <sub>pH2</sub>	1.03	1.74	603	602	0.68	0.87	1.15	1.04	1.15	1.04	1.15	1.04
BR <sub>pH11</sub>	1.02	-	568	-	1.17	-	0.85	-	0.85	-	0.85	-

<sup>a</sup>DA and LA, dark- and light-adapted forms of the chromophore, respectively. The standard deviations of  $\beta_{zzz}^{\text{exp}}$  are about 10%

## 6.2 Determination of the first hyperpolarizabilities of the BR mutants W86F, D85C

In order to evaluate experimentally the influence of change of the retinal pocket on the first hyperpolarizability of the retinal the BR single mutants W86F and D85C were available. The positions of mutation are shown in figure 6.3. These mutants have different optical properties compared to wild-type BR. The spectrum of W86F is blue-shifted to 547 nm due to the decrease in the polarizability of benzene in comparison to indole. The D85C mutant, where one of the counterions is neutralized, shows an absorption maximum around 590nm. For the evaluation of first order hyperpolarizabilities of these mutants some supplementary information is needed, namely the extinction coefficients for the determination of the concentration and the size distribution of the membrane patches constituting the protein.

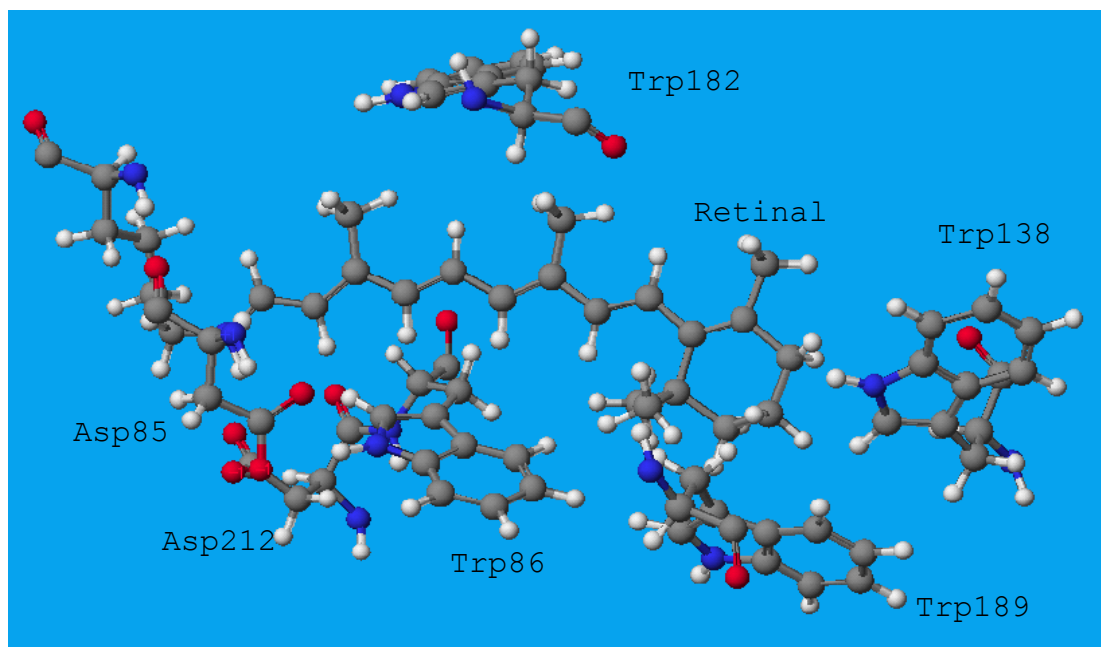


Figure 6.3. The residues located in the chromophore-binding pocket

### 6.2.1. Extinction coefficient determination

For determination of the extinction coefficients, the reaction of photoinduced hydroxylaminolysis has been used[53;138]. All experiments were carried out at room temperature. The concentration of hydroxylamine was adjusted to 0.5M. After addition of hydroxylamine, the BR suspension (in 10mM phosphate buffer, pH7.5) was illuminated with a 200-watt halogen and a high pressure lamp. The light was filtered by two 500-nm-long pass and a 10 cm-length water filter. Under these conditions, retinal oxim is formed and a new absorption band appears with the maximum at 362nm, whose extinction has to be determined for further analysis. The retinal oxim extinction coefficient was estimated from hydroxylaminolysis of wild-type BR (figures 6.4, 6.5) with a known extinction coefficient of  $63000 \text{ mol}^{-1}\text{cm}^{-1}\text{dm}^3$  at 568 nm to be  $30800 \text{ mol}^{-1}\text{cm}^{-1}\text{dm}^3$  at 362nm. The extinction coefficients of the W86F and D85C mutants were then calculated from the ratio between the hydroxylamine and the mutant's absorption amplitudes as shown in figures 6.7, 6.9. In Table 6.2, the extinction coefficients of the mutants are presented. It is remarkable, that the blue-shifted mutants generally show a lower absorbance than the red-shifted ones.

Moreover, we find that the W86F mutant possesses a substantially higher reactivity to hydroxylamine than wild type BR, what is in agreement with results for BR mutants examined in the dark, in a lipid/detergent micelles environment[139]. The reactivity of the W85C mutant was comparable to that of wild-type BR.



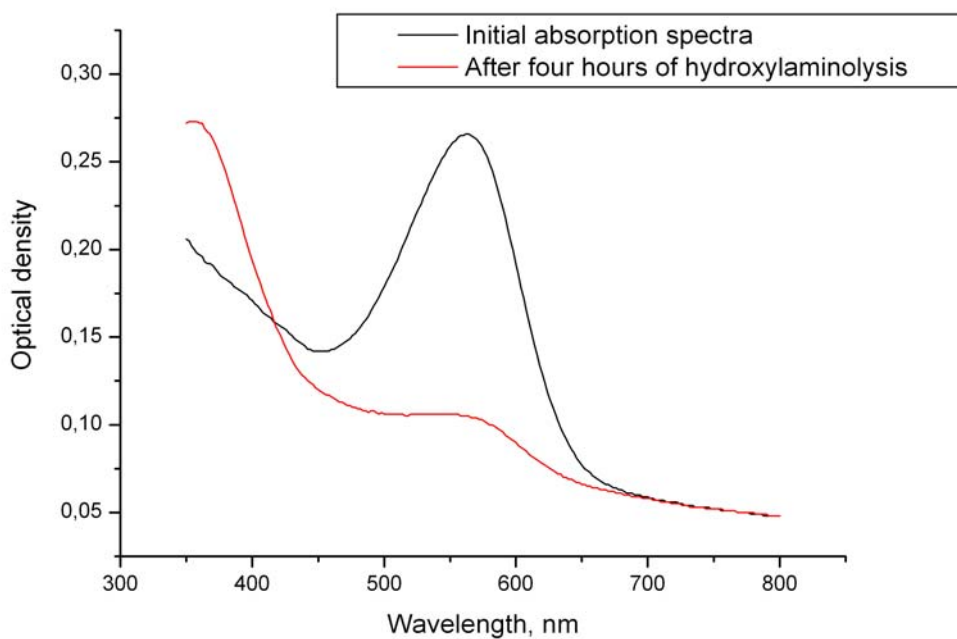


Figure 6.4 Absorption spectra of D85C before and after 4 hours of hydroxylamine treatment

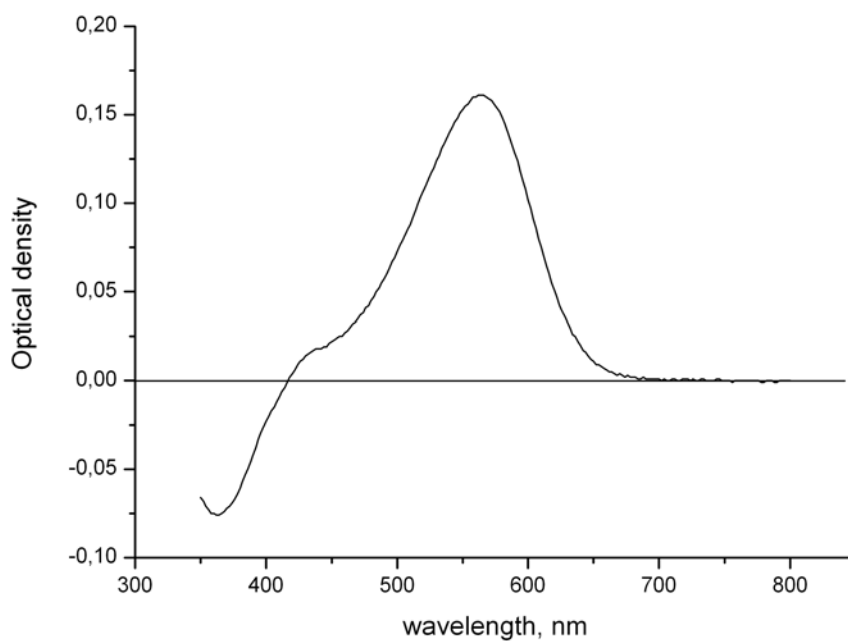


Figure 6.5 Difference spectrum bR minus bR after 4 hours of hydroxylamine treatment

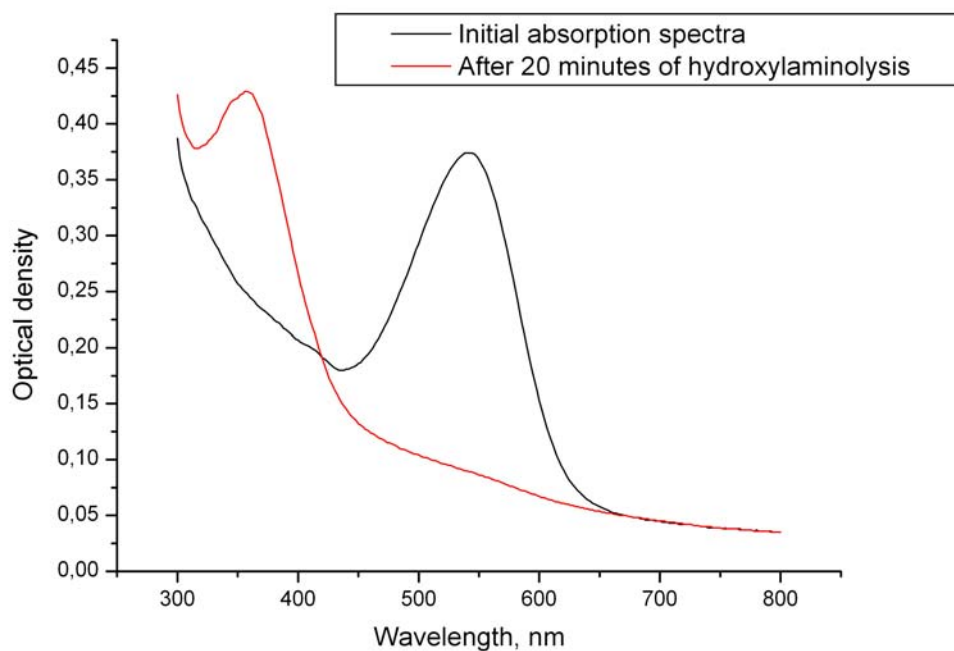


Figure 6.6 Absorption spectra of W86F before and after 20 minutes of hydroxylamine treatment

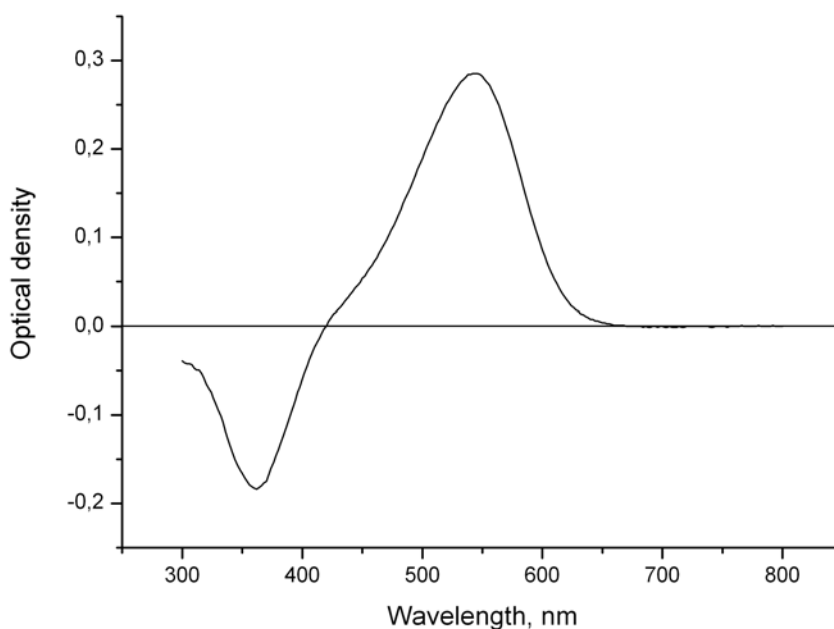


Figure 6.7 Difference spectrum W86F minus W86F after 20 minutes of hydroxylamine treatment

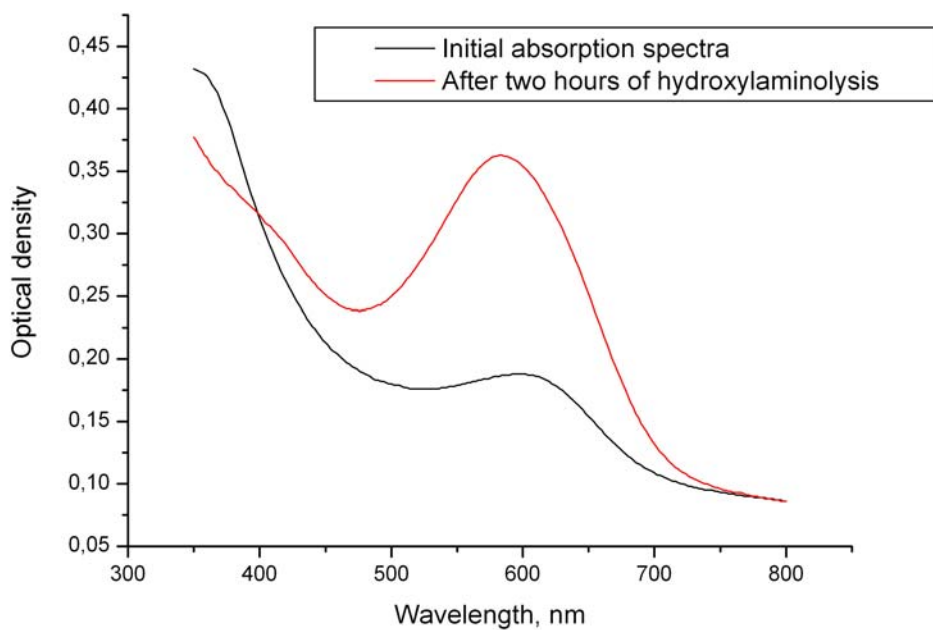


Figure 6.8 Absorption spectra of D85C before and after 2 hours of hydroxylamine treatment

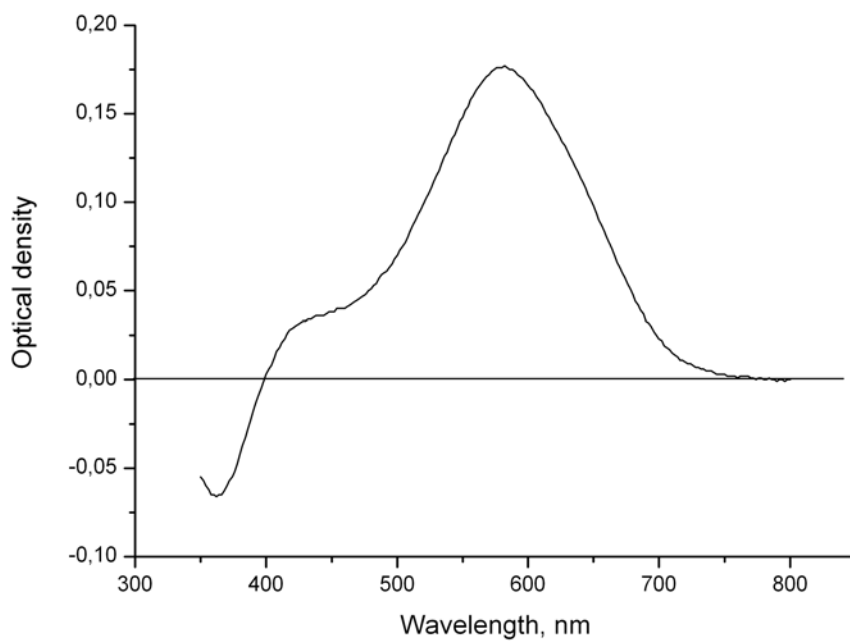


Figure 6.9 Difference spectrum D85C minus D85C after 2 hours of hydroxylamine treatment

Table 6.2 Experimental extinction coefficients, and absorption maxima of BR, mutants W86F and D85C

Mutant	Absorption maxima, nm		Extinction coefficient, $\text{mol}^{-1}\text{cm}^{-1}$
	DA <sup>a</sup>	LA	
Wild type	558	568	63000 (568nm)
W86F	534	547	47000 (547nm)
D85C	-	584	80000 (584nm)

<sup>a</sup>DA and LA, dark- and light-adapted forms of the chromophore, respectively. The standard deviations of extinction coefficient is less than 10%

### 6.2.2. Size distribution measurements

Dynamic light scattering is a useful tool for size distribution measurements. This technique has been applied to study the structure and dynamics of such diverse systems as solids, liquid crystals, gels and biological macromolecules[140]. Here we used the dynamic light scattering to determine the size distribution of purple membrane sheets containing wild type BR and mutants D85C, W86F for further analysis. Since BR was used as a standard with known hyperpolarizability, its size distribution and that of the respective mutants were determined each time prior to the HRS measurements. The observed distribution of the purple membrane sizes of D85C and W86F compared to BR are shown in figures 6.10, 6.11. It can be seen that in both cases the patches of BR were larger than for the mutant. Moreover, in the experiments with D85C and wild type BR there was a small fraction of the wild type purple membranes with a size around  $5\mu\text{m}$ . This small fraction makes the distribution asymmetrical and causes a deviation of the average particle size from the median of the distribution, since the contribution of the small fraction of large membranes is greater.

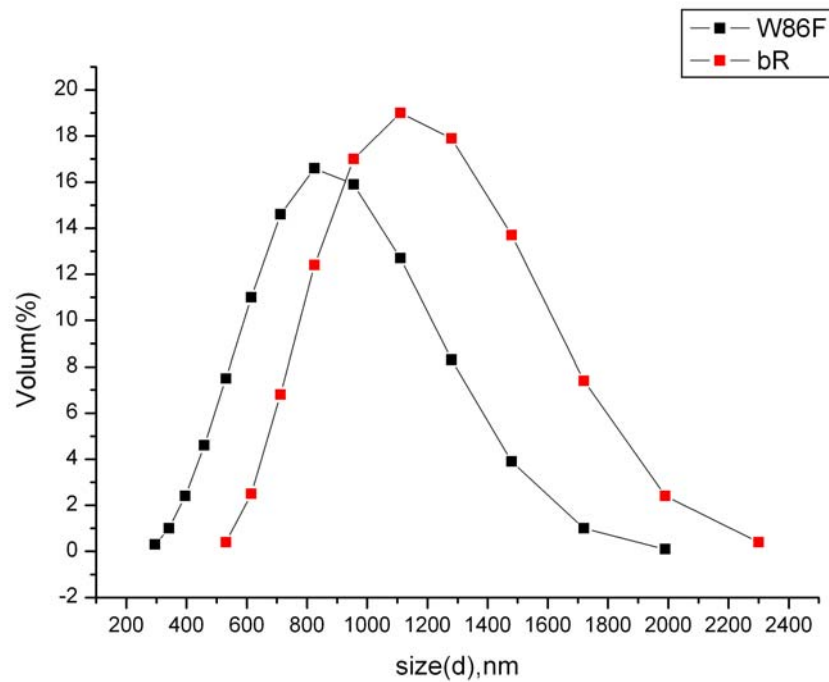


Figure 6.10 Membranes size distribution of wild type bR and W86F mutant

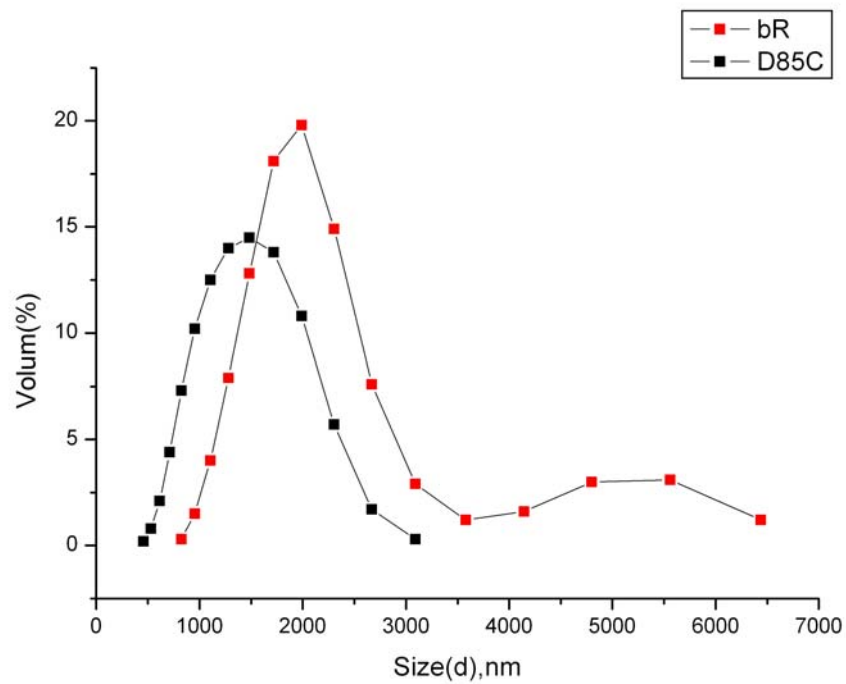


Figure 6.11 Membranes size distribution of wild type bR and D85C mutant

### 6.2.3. HRS measurements of the mutants W86F and D85C

The Hyper-Raleigh scattering measurements were performed on suspension of purple membrane in buffer. In this case, the molecules belonging to the same patch scatter the light in the same phase, whereas there are no fixed phase relations between the fields emitted by different patches. Since the hyperpolarizability of the solvent molecules is much less than that of the membrane patches, their contribution to the signal can be neglected. That is, the total scattered intensity can be written as:

$$I \propto g(\omega)^4 g(2\omega)^2 N \int_{R_{\min}}^{R_{\max}} f(R)(n(R))^2 dR \times \beta_{zzz}^2 I_0^2, \quad (6.1)$$

where  $g(\omega)$  and  $g(2\omega)$  are the local field factors,  $N$  is a total number of membrane patches,  $f(R)$  is a distribution function of purple membrane sizes, and  $n(R)$  is the number of BR molecules per membrane of the size  $R$ . The square of  $n(R)$  takes into account the correlation of the molecules within the membrane patches. On the other hand, the total number of membrane patches  $N$  is related to the measured concentration via the following expression:

$$C = \frac{1}{V} N \int_{R_{\min}}^{R_{\max}} f(R)n(R)dR, \quad (6.2)$$

Thus, expression (6.1) can be rewritten as:

$$I \propto C \cdot \frac{\int_{R_{\min}}^{R_{\max}} f(R) \cdot R^4 dR}{\int_{R_{\min}}^{R_{\max}} f(R) \cdot R^2 dR} \times \beta_{zzz}^2 I_0^2, \quad (6.3)$$

As an external reference with a known hyperpolarizability, the wild type BR has been used. The dependencies of the observed signal on the incident intensity  $I_0$  for wild type BR and the mutants W86F, D85C are shown in figures 6.12 and 6.13. The quadratic fit yields “slopes” of 0.57 and 0.43 for W86F and BR, respectively, in the first case, and of 0.64 and 1.04 for D85C and BR, in the second case. The concentrations of the samples were  $C_{BR} = 2.81 \cdot 10^{-6}$ ,  $C_{W86F} = 6.62 \cdot 10^{-6}$  by determining the hyperpolarizability for W86F and  $C_{BR} = 2.29 \cdot 10^{-6}$ ,  $C_{D85C} = 2.25 \cdot 10^{-6}$  by determining hyperpolarizability D85C. The optical densities of the probes at 532 nm were  $OD_{BR} = 0.21$  and  $OD_{W86F} = 0.4$  in the first case, and  $OD_{BR} = 0.17$  and  $OD_{W85C} = 0.19$ . It can be seen that for the mutant W86F the self-absorption has to be taken into account at the second harmonic wavelength to obtain the correct result. Using expression (6.3) the following relation between the hyperpolarizabilities of BR and that of the mutant W86F can be written:

$$\frac{0.57 \cdot 1.25}{0.43 \cdot 1.15} = \frac{6.62 \cdot 10^{-6}}{2.81 \cdot 10^{-6}} \cdot (0.62) \cdot \frac{\beta_{W86F}^2}{\beta_{BR}^2}, \quad (6.4)$$

where the factor of 0.62 takes into account the discrepancy in the size distribution of BR

and W86F membranes, that was derived by integration of  $\frac{\int_{R_{min}}^{R_{max}} f(R) \cdot R^4 dR}{\int_{R_{min}}^{R_{max}} f(R) \cdot R^2 dR}$  using the size

distributions obtained in the previous section as a function  $f(R)$ . Analogues, for BR and the D85C mutant:

$$\frac{0.64}{1.04} = \frac{2.25 \cdot 10^{-6}}{2.29 \cdot 10^{-6}} \cdot (0.22) \cdot \frac{\beta_{D85C}^2}{\beta_{BR}^2}, \quad (6.4)$$

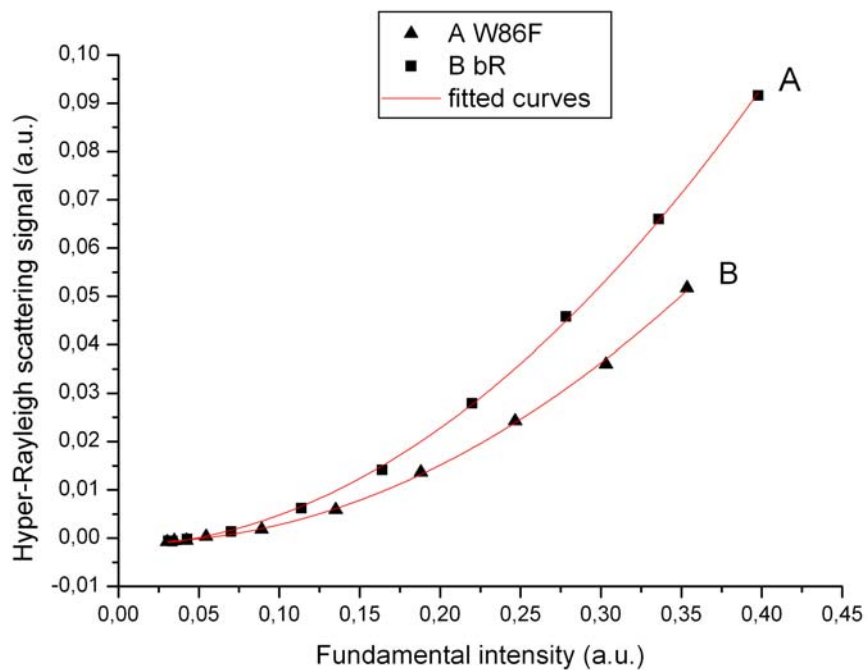


Figure 6.12 Hyper-Rayleigh scattering signal of wild type bR and W86F mutant. Solid curves are the quadratic fit.

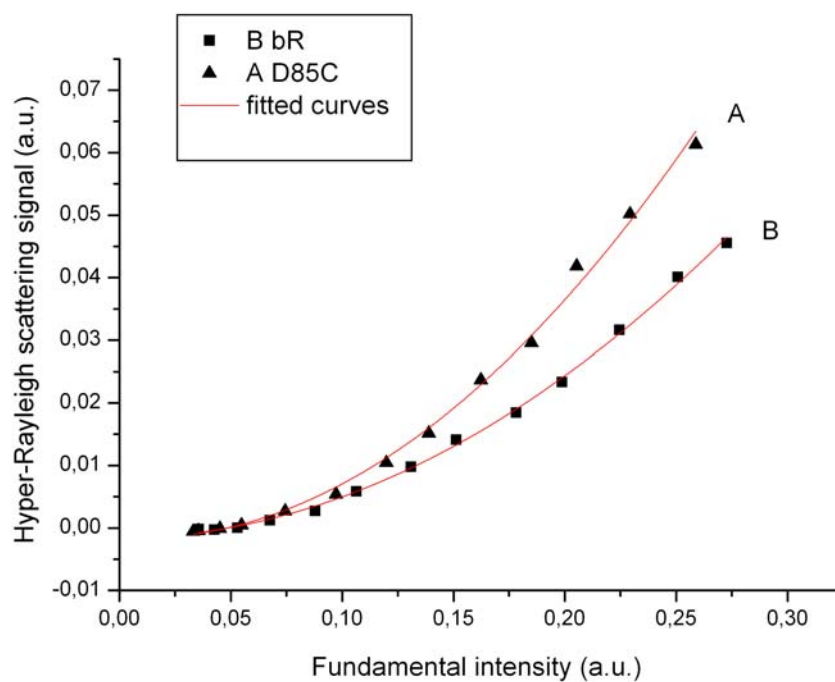


Figure 6.13 Hyper-Rayleigh scattering signal of wild type bR and W86F mutant. Solid curves are the quadratic fit.



Table 6.3 summarizes the experimentally determined and calculated linear and nonlinear properties of native BR and the genetically modified mutants W86F and D85C. The main component of first hyperpolarizability was normalized to the value of wild type BR.

Table 6.3 : Linear and nonlinear optical properties of modified bacteriorhodopsins

Molecule	Absorption maxima, nm		$\frac{\beta_{zzz}^{\text{exp}}}{\beta_{zzz}^{\text{exp}}(bR)}$	$\frac{\beta_{stat}^{\text{calc}}}{\beta_{stat}^{\text{calc}}(bR)}$	$\frac{\Delta\mu_{\text{calc}}}{\Delta\mu_{\text{calc}}(bR)}$
	$\lambda_{\text{exp}}$	$\lambda_{\text{calc}}$			
BR	568	566	1	1	1
BR <sub>D85C</sub>	584	-	1.69	-	-
BR <sub>W86F</sub>	547	550	0.97	0.94	1.02

<sup>a</sup>DA and LA, dark- and light-adapted forms of the chromophore, respectively. The standard deviations of  $\beta_{zzz}^{\text{exp}}$  is about 10%

### 6.3 Examination of the photocycles of BR mutants by means of absorption spectroscopy and HRS techniques

As shown above, the first hyperpolarizability of the retinal moiety is strongly dependent on the presence of charges in the vicinity of the Schiff base changing its electron acceptor property. In other words, the HRS technique could be sensitive to any proton movements taking place in the proton pump bacteriorhodopsin during the photocycle, providing supplementary information about the intrinsic protein dynamics. Indeed, as was recently shown, conformational alterations are correlated with the charge redistribution in the protein[141]. In the present work we compared the kinetics of the reaction measured by means of the time-resolved HRS technique with those obtained by time-resolved optical spectroscopy. For these measurements wild-type BR and its mutants T46C, R225C, R227C, D96C, D85C have been chosen. Residues D85 and D96 are located in helix C.

Site-directed mutagenesis has shown that these residues are involved in the proton transport. While D85 mediates the release of a proton from the Schiff base to the extracellular side, D96 is its primary proton donor. Position T46 is located in the interior of the protein between the proton donor D96 and the Schiff base. The residues R225 and R227 are located in helix G on the extracellular side of the membrane.

### 6.3.1. Time-resolved absorption spectroscopy measurements

Absorbance changes after photoexcitation were recorded from 30 $\mu$ s to the completion of the photocycle. The experimental data have been analyzed by a global fit procedure for 11 wavelengths as defined in chapter 5.1.2. The time courses of the absorbance changes at 405 nm, 520 nm, 570 nm, and 640 nm are shown in figures 6.14, 6.16, 6.18, 6.20, 6.22, and 6.24. The determined time constants describing the photocycle of wild-type BR and BR mutants are summarized in Table 6.4. In the case of BR and the mutants T46V, R225C, R227C, D96C the photocycle kinetics can be satisfactorily approximated by four time constants, whereas the photocycle of the mutant D85C is satisfactorily fitted by three exponents. From the amplitude spectra (figures 6.15, 6.17, 6.19, 6.21, 6.23, and 6.25) it can be seen, that the time constant  $\tau_1$  describes the rise of M because the amplitude of this time constant is negative at the absorption maximum of M (410 nm) and the decay of L (the amplitude at 550 nm is positive), whereas the M intermediate decays with  $\tau_2$ ,  $\tau_3$ , and  $\tau_4$  (the spectral amplitudes at the absorbance maxima of N(550 nm), BR(570 nm), O(640 nm) are negative). The time constant  $\tau_2$  describes the decay of M and the rise of the intermediates N, O, and the BR ground state. It can be seen that  $\tau_3$  characterizes the decay of the O (positive amplitude at 640 nm) and M intermediates to the BR ground state, whereas the slowest component  $\tau_4$  was identified to belong to the photocycle of the 13-*cis* retinal[142]. In the case of the mutants R225C, R227C, and D96C, one additional time constant  $\tau_{10}$  is needed to describe the biphasic rise of the M intermediate. With the exception of T46C and R225C, the values of  $\tau_1$  are the same for wild-type BR and all mutants. The value of  $\tau_1$  is higher by a factor of 1.4 for mutant T46C compared to wild-type BR, whereas the value of  $\tau_1$  for R225C is lower by a factor of 1.5. The values of  $\tau_2$  were found to be the same within

a factor of 2 for all mutants with the exception of mutant D96C, where the time constant  $\tau_2$  is not required to describe its photocycle. The component  $\tau_3$  of the photocycles is similar for wild-type BR and mutants T46C, R225C. A significant increase in  $\tau_3$  was found for mutants D85C and D96C due to the fact that these mutated residues are tightly coupled to the proton transport. For the mutant R227C, the time constant  $\tau_3$  becomes slower by a factor of 2.6 with respect to wild-type BR. The observed alterations in the time constants may be due to the charge distribution changes on the cytoplasmic surface of the membrane patches, or in the case of mutants T46C, D85C, and D96C, to changes in the hydrogen network in the interior of the protein. Taking into account the slightly different experimental conditions and experimental error, the time constants determined in this work agree with the data published by Rink et al[143;144]. The fraction of the intermediate O is significantly higher found for wild-type BR, R225C, and D85C with respect to the remainder mutants.

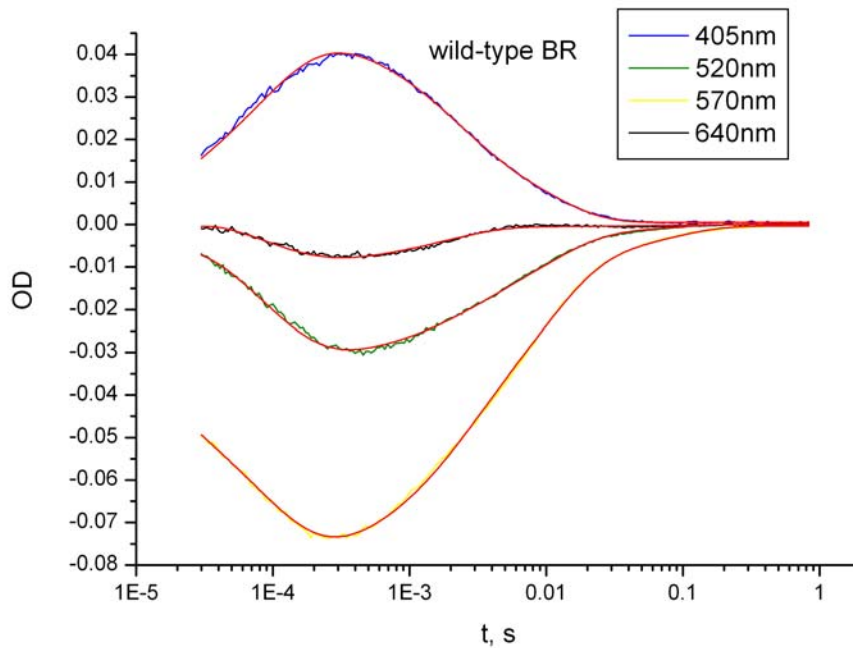


Figure 6.14. Absorbance changes of wild-type bR at different wavelength during the photocycle

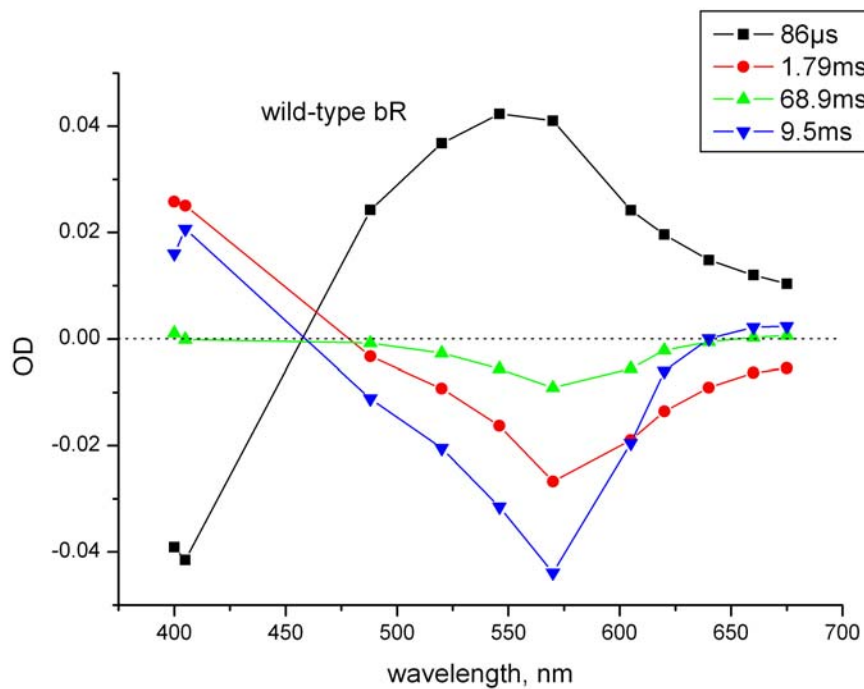


Figure 6.15. Amplitude spectra of the apparent time constants of wild-type BR

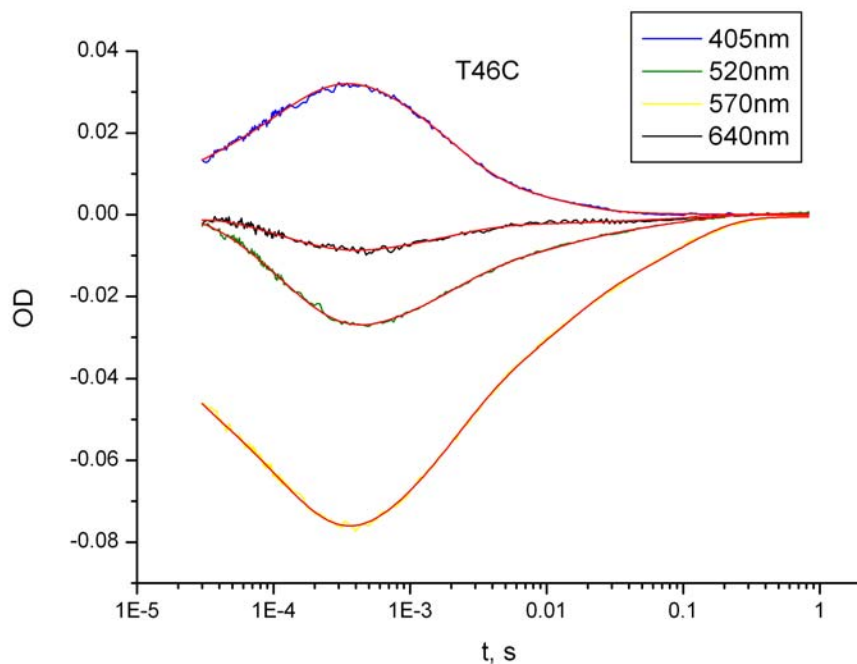


Figure 6.16. Absorbance changes of T46C mutant at different wavelengths during the photocycle

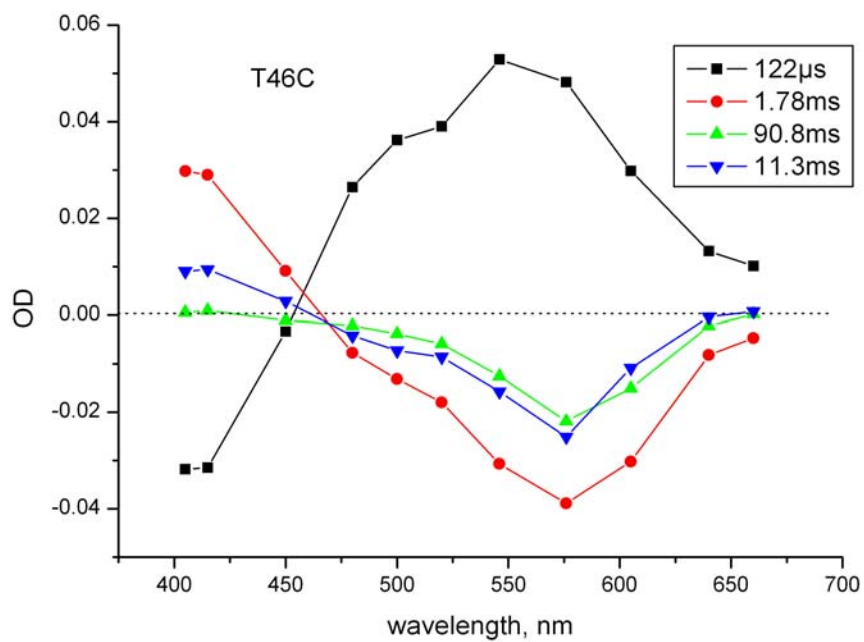


Figure 6.17. Amplitude spectra of the apparent time constants of T46C mutant

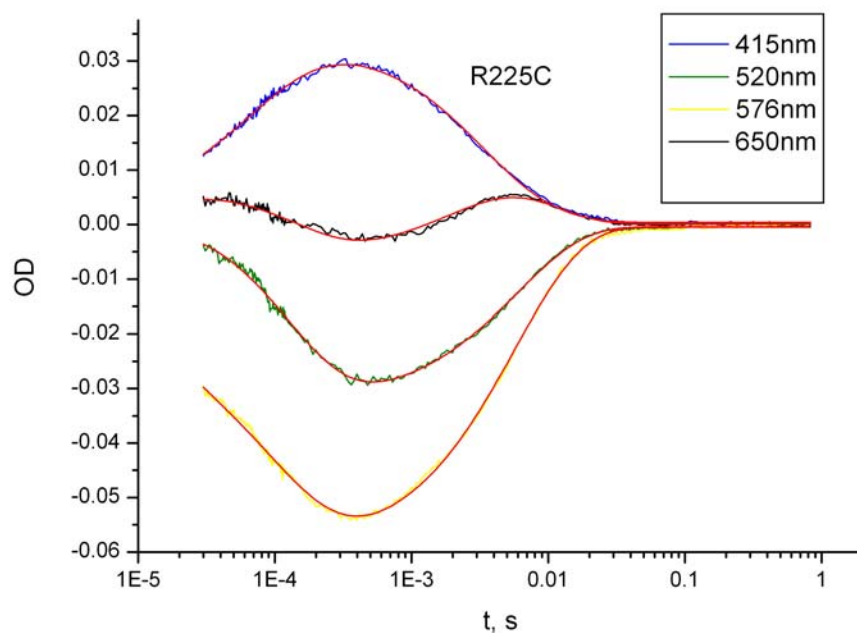


Figure 6.18. Absorbance changes of R225C mutant at different wavelengths during the photocycle

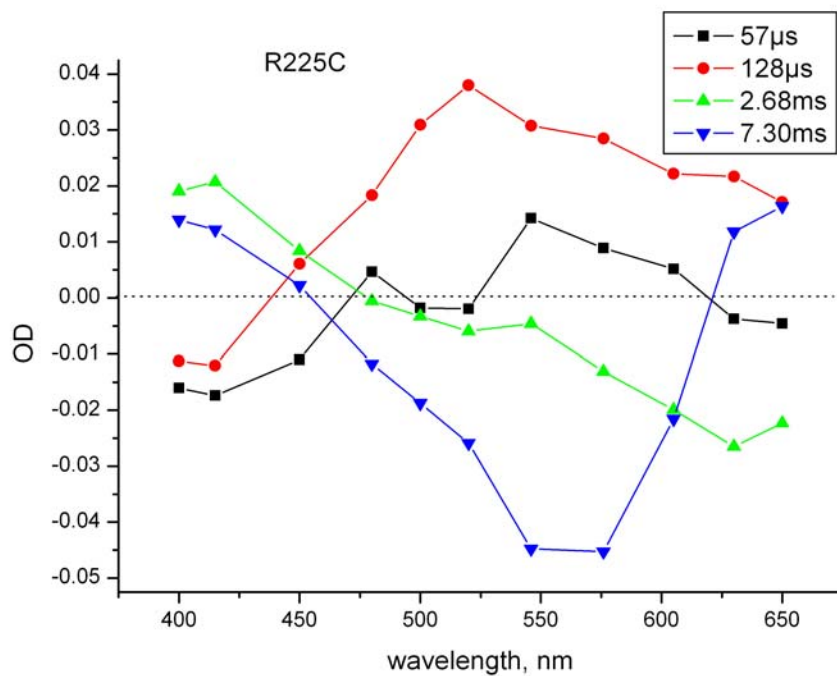


Figure 6.19. Amplitude spectra of the apparent time constants of R225C mutant

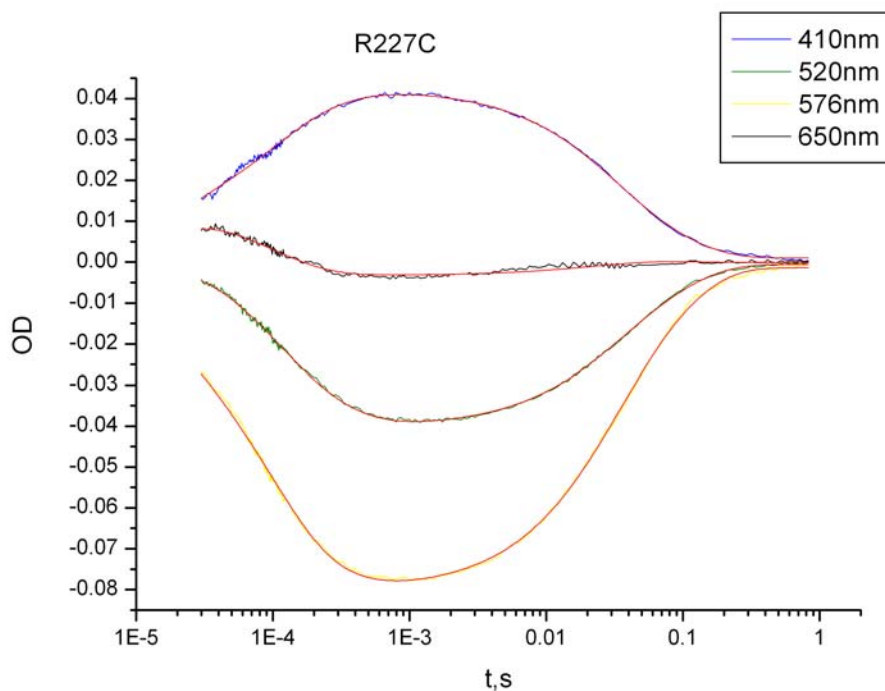


Figure 6.20. Absorbance changes of R227C mutant at different wavelengths during the photocycle

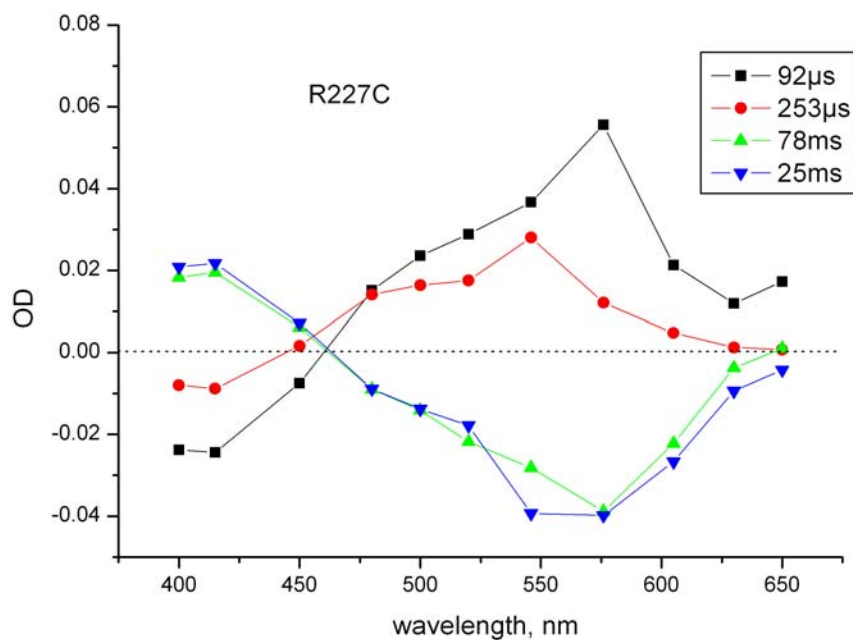


Figure 6.21. Amplitude spectra of the apparent time constants of R227C mutant

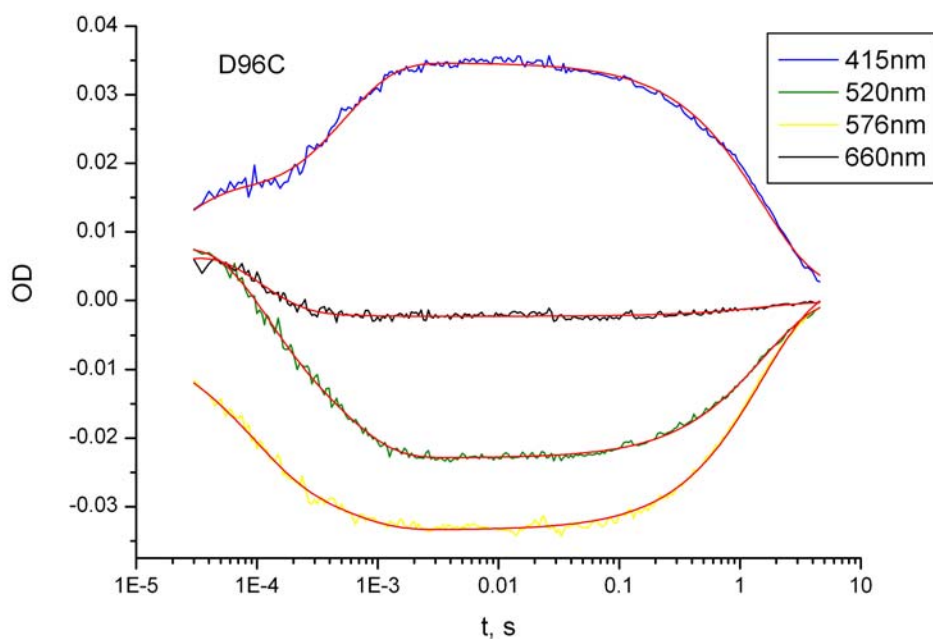


Figure 6.22. Absorbance changes of D96C mutant at different wavelengths during the photocycle

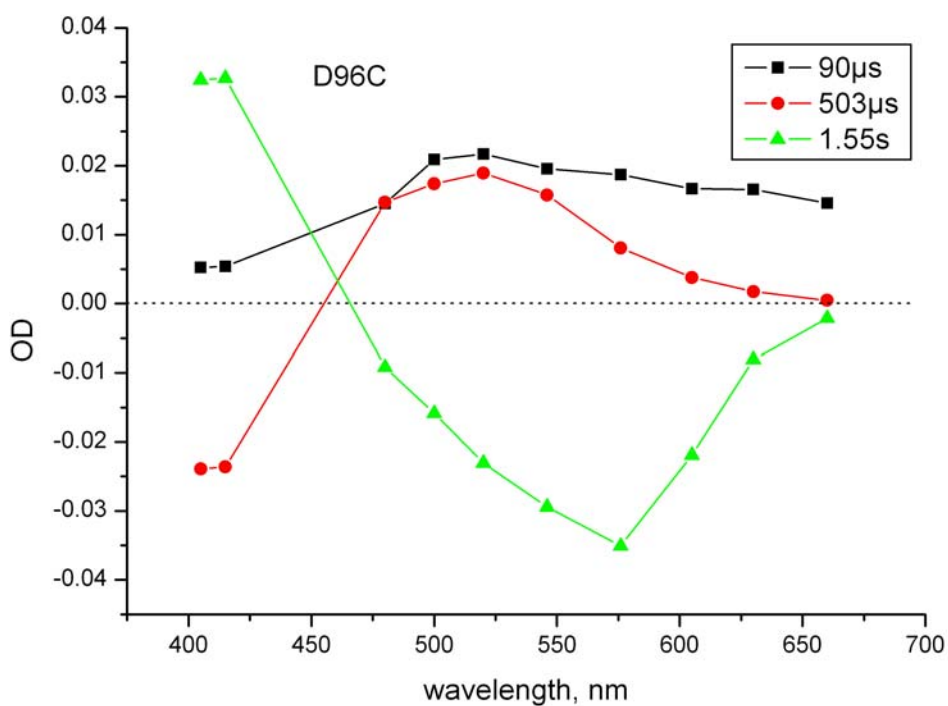


Figure 6.23. Amplitude spectra of the apparent time constants of D96C mutant



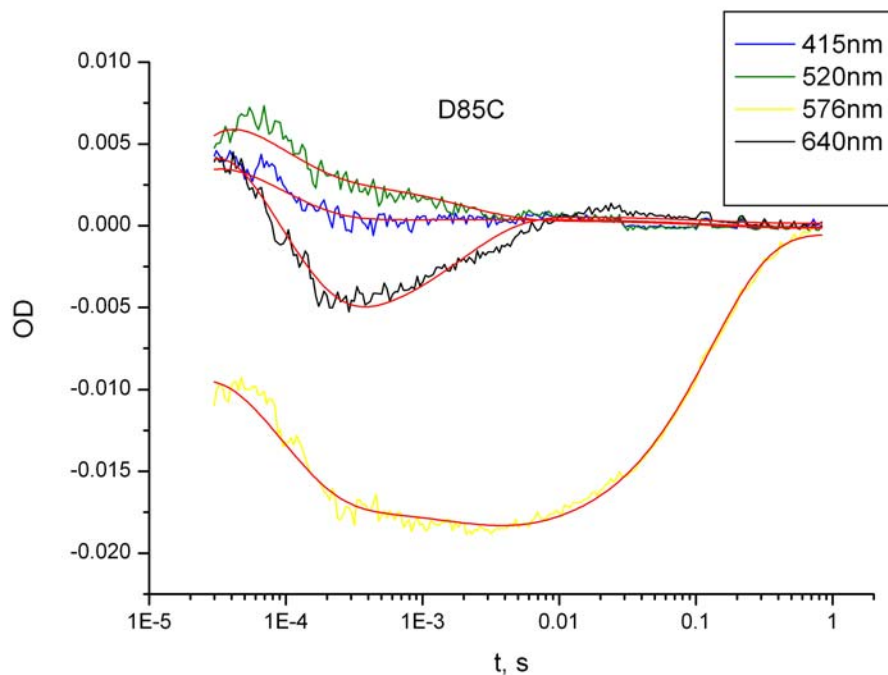


Figure 6.24. Absorbance changes of D85C mutant at different wavelengths during the photocycle

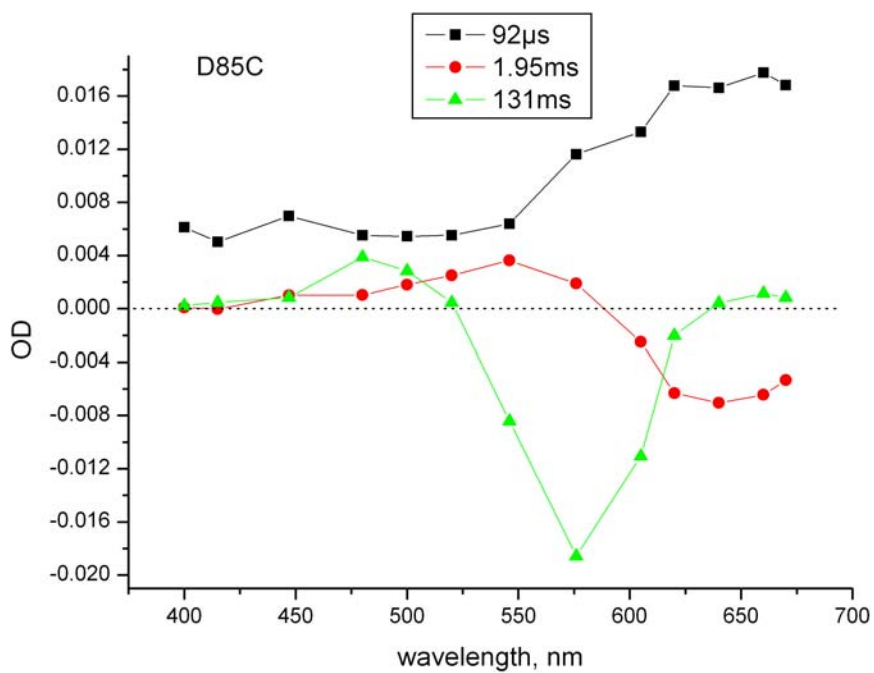


Figure 6.25. Amplitude spectra of the apparent time constants of D85C mutant

Table 6.4. Time constants determined by global fit analysis of the absorbance changes in the visible spectrum, and from the HRS signal changes

Mutant		$\tau_1, \mu\text{s}$	$\tau_{10}, \mu\text{s}$	$\tau_2, \text{ms}$	$\tau_3, \text{ms}$	$\tau_4, \text{ms}$
WT	VIS	86	-	1.8	9.5	69
	HRS	-	-	$0.45 \pm 0.05$	$9.7 \pm 0.6$	-
T46C	VIS	122	-	1.8	11	91
	HRS	-	-	$1.0 \pm 0.7$	$38 \pm 14$	-
R225C	VIS	5	128	2.7	7	-
	HRS	-	-	$1.6 \pm 1.3$	$9.8 \pm 0.4$	-
R227C	VIS	92	253	-	25	78
	HRS	-	-	$2.2 \pm 0.3$	-	$86 \pm 22$
D96C	VIS	90	503	-	1600	-
	HRS	-	$640 \pm 240$	-	$4800 \pm 2500$	-
D85C	VIS	92	-	2.0	130	-
	HRS	-	-	$3.4 \pm 1.4$	$380 \pm 150$	-

The standard deviations of the time constants determined in the visible spectrum are less than 10%; those obtained by means of the HRS technique were determined from the fitting of the transient traces.

### 6.3.2. Time-resolved HRS measurements

Simultaneously with the time-resolved absorption spectroscopy measurements, the time-dependent HRS measurements were performed for wild-type BR and the investigated mutants. Changes in the HRS signal during the photocycle were detected. The time courses of the HRS signal are shown in figures on a logarithmic time scale from 30 $\mu\text{s}$  to the completion of the photocycle (each point is an average over 200 to 1000 photocycles depending on the measured mutant to improve the signal-to-noise ratio). The obtained traces were then approximated by a sum of exponential functions. Starting from 200 $\mu\text{s}$

after excitation, a sum of two exponentials is sufficient to fit the HRS intensity changes for wild-type BR and all measured mutants. One additional time constant,  $\tau$ , is used by the fitting, to account for the transient within the first 100 $\mu$ s. This transient is due to a convolution of the HRS signal with a strong artefact from the flash-lamp, which has a decay time of some dozens microseconds. The evaluated time constants are summarized in Table 6.4.

The corresponding kinetic constants are comparable within the experimental error with the time constants  $\tau_2$ ,  $\tau_3$ , and  $\tau_4$  obtained by means of absorption spectroscopy describing the M decay and the recovery to the ground state.

The decay of the HRS intensity of wild-type BR occurs with a time constant of 0.45 ms. This value is lower than that of 1.8 ms measured by means of absorption spectroscopy. The rise in the HRS intensity is mainly determined by the time constant  $\tau_3$ .

In the case of the mutant T46C, the decay of the HRS intensity is determined by a time constant of 1 ms which is similar to that of 1.8 ms, describing the M decay. The rise of the HRS intensity is described by a time constant of 38 ms. This value is similar to the time constants  $\tau_3$ , and  $\tau_4$ . The biphasic rise of the HRS intensity could not be detected probably due to the bad signal-to-noise ratio of the signal.

The values of the decay and the rise of the HRS signal of the mutants R225C and R227C agree with those obtained by means of absorption spectroscopy with the exception of the time constant of 2.2 ms whose analogue could not be observed from the absorbance changes in the visible range. The biphasic relaxation of the HRS signal to the ground state was not found as well.

In the case of mutant D96C, the slowest rise of M was resolved, the value of which as well as the obtained time constant for the decay to the ground state are in good agreement with those obtained by means of absorption spectroscopy. A prolongation of the M decay for the mutants D85C, D96C is also observed.

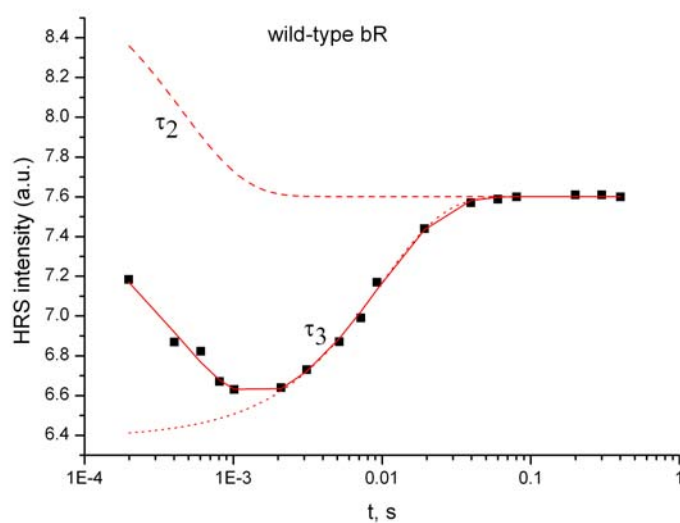


Figure 6.26. Hyper-Raleigh scattering intensity changes of BR during the photocycle. Exponential fit (*solid lines*) and the dominating time constants are included (*dashed lines*)

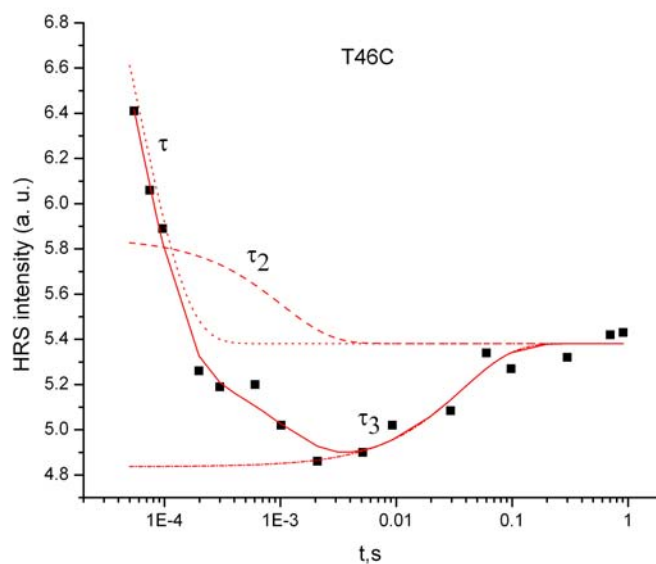


Figure 6.27. Hyper-Raleigh scattering intensity changes of mutant T46C during the photocycle. Exponential fit (*solid lines*) and the dominating time constants are included (*dashed lines*)

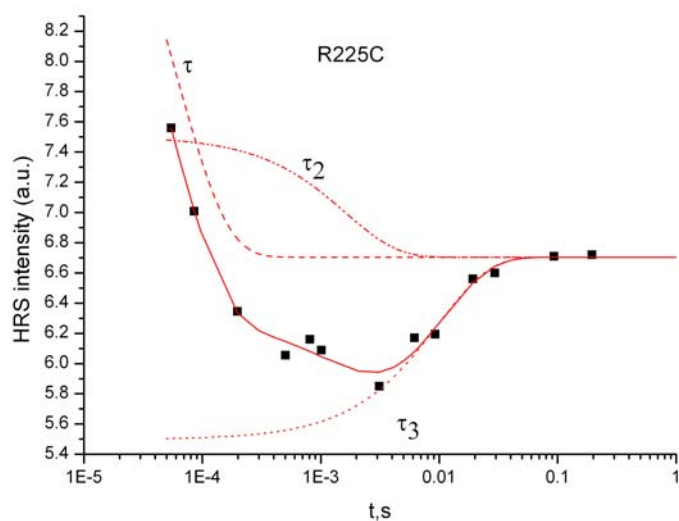


Figure 6.28. Hyper-Raleigh scattering intensity changes of mutant R225C during the photocycle. Exponential fit (*solid lines*) and the dominating time constants are included (*dashed lines*)

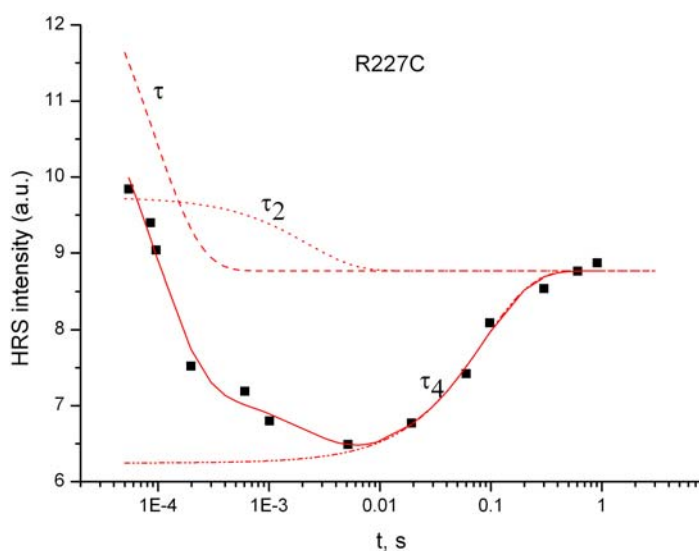


Figure 6.29. Hyper-Raleigh scattering intensity changes of mutant R227C during the photocycle. Exponential fit (*solid lines*) and the dominating time constants are included (*dashed lines*)

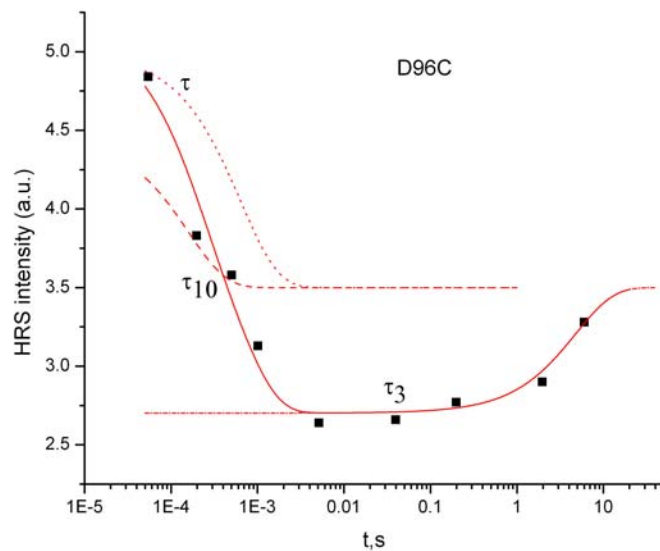


Figure 6.30. Hyper-Raleigh scattering intensity changes of mutant D96C during the photocycle. Exponential fit (*solid lines*) and the dominating time constants are included (*dashed lines*)

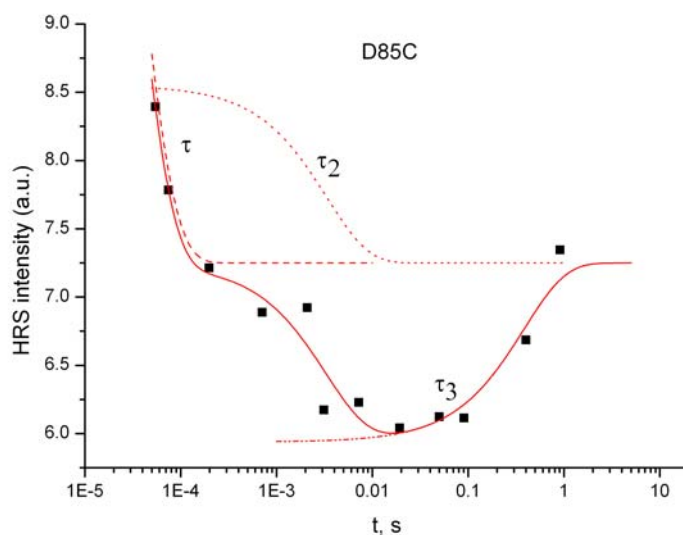


Figure 6.31. Hyper-Raleigh scattering intensity changes of mutant D85C during the photocycle. Exponential fit (*solid lines*) and the dominating time constants are included (*dashed lines*)

However, it has to be noted that the HRS intensity decreases during the M to N transition (described by the time constant  $\tau_2$ ) pointing out a fairly low  $\beta$  of the N state which was not expected. Indeed, the absorption maximum of the N intermediate lies at 550 nm. A similar absorption maximum characterizes the mutant W86F, which shows a high value of the first hyperpolarizability estimated both experimentally and theoretically to be 0.94-0.97 of wild-type BR. The origin of the discrepancy may be due to changes in the conformation of the membranes or their mutual reorientations that can contribute to the observed dependence of the HRS signal. Indeed, there exist some processes which occur on the same time scale. First of all, the release of protons to the extracellular membrane surface is a fairly fast process occurring during the L to M transition with a time constants of 10  $\mu$ s[145]. The pumping of the protons leads to an alteration of the charge distribution of the membrane surfaces, which disturb the short range distribution of the membrane sheets (which can exist owing to interaction of the permanent dipole moments of the membrane sheets[146;147]). However, the dynamic of proton transfer between the surface of purple membranes and the aqueous bulk, in other words, the discharge of the membranes, have been investigated by the *Laser Inducted Proton Pulse Method* to be of a few hundreds of microseconds[145]. This value is in good agreement with that observed by time-resolved HRS measurements.

Despite less likely, one reason for the observable dependence of the HRS signal could be due to the conformational changes of the protein occurring during the photocycle. Indeed, as was shown by Müh *et al*[148], the  $\alpha$ -helices of proteins possess a high dipole moment. They determine, therefore, the direction and the magnitude of the dipole moment of the membrane. As a result, any helix movement occurring during the conformational changes of the protein will also disturb the short range distribution of an ensemble of the membrane, resulting in a drop of the HRS intensity. A major conformational change occurring in the M or the N intermediates in BR was found by diffraction experiments[149-151]. These diffraction studies suggested that major changes occur at helices B, F, and G. Later, it was shown that the M intermediate is characterized by changes near helices B and G, whereas the main characteristics of N intermediate are changes near helices F and G[152]. The time-resolved analysis by means of electron

paramagnetic resonance spectroscopy gave detailed information on the kinetics of the structural dynamic at selected regions of the BR molecule. It was shown that the spectral change of a spin label attached at position 101 develops during the decay of the M-intermediate, and reverses upon return to the ground state, suggesting a movement of the C-D or E-F interhelical loops[153]. This is also consistent with result from time resolved FTIR spectroscopy, which revealed that the amide band changes occur during the M-to-N transition[154].



## Chapter 7

### Summary

The second-order nonlinear optical properties of modified bacteriorhodopsin were studied both theoretically and experimentally. The intrinsic origin of the unusually high nonlinearity of BR was discussed. It was mainly attributed to the positive charge near the retinal Schiff base which remains uncompensated in the protein interior as well as to the high polarizable aromatic residues of phenylalanine, tyrosine, and tryptophan, resulting in a considerable enhancement the first hyperpolarizability of BR.

For the first time a hybrid quantum mechanical/molecular mechanical-configuration interaction (QM/MM-CI) method has been used to determine the nonlinear behaviour of modified BR. The calculated structures are the ground state and M1 state of wild type BR, several BR variants, the BR mutants W86F, W189F, W182F, W138C, Y185F, and Y83F as well as a photoreceptor NpSRII. Despite a series of approximations with respect to *ab initio* methods, the high potentiality of the hybrid QM/MM method for (non)linear properties calculations (even absolute values) of the chromophore containing proteins has been demonstrated. The first hyperpolarizability of two available BR mutants W86F and D85C has been determined by means of HRS technique. The experimentally determined  $\beta$  value for the mutant W86F is in good agreement with that obtained theoretically.

pH dependence of the first-order nonlinearity of wild type BR is also presented. The titration experiments were carried out in the pH range from 1.7 to 11. The first hyperpolarizability shows a complex titration curve with two pKs around pH 3.5 and pH 8. The complex titration behaviour is similar to that obtained early by absorption spectroscopy. The calculated absorption maximum of BR at pH 2 (modelled by adding a

hydrogen atom to the carboxyl group of Asp85) of 602 nm indicates that there is no significant alteration in the structure relative to BR structure at normal pH, i.e. the 35 nm red shift is mostly caused by neutralization of the negative charge of Asp85.

Simultaneously with the time-resolved absorption spectroscopy measurements, the time-dependent HRS measurements were performed. Changes in the HRS signal during the photocycle were detected. The kinetics of time-resolved HRS and flash spectroscopy measurements of BR and the BR mutants T46C, R225C, R227C, D96C, and D85C were compared. The obtained kinetic constants are comparable with those determined by means of absorption spectroscopy. However, an unexpected decrease in the HRS intensity during the M to N transition was observed. The origin of the discrepancy may be due to the release of protons to the extracellular membrane surface occurring during the L to M transition disturbing the short range distribution of the membrane sheets. One other reason for the observable dependence of the HRS signal could be due to the conformational changes occurring during the photocycle. Any movements of  $\alpha$ -helices of proteins which possess a high dipole moment result in change of the direction and the magnitude of the dipole moment of the membrane. This could also disturb the short range distribution of an ensemble of the membrane resulting in a drop of the HRS intensity.

## Reference List

- 1 Greenbaum E. J. Vectorial photocurrents and photoconductivity in methalized chloroplasts. *Phys.Chem.* 94, 6151-6153. 1990.
- 2 Birge R.R. Photophysics and molecular electronic applications of the rhodopsins. *Annu.Rev.Phys.Chem.*41,683-733,1990
- 3 Lee I., Lee J. W. Greenbaum E. E. Biomolecular electronics: Vectorial arrays of photosynthetic reaction centers. *Phys.Rev.Lett.* 79, 3294-3297. 1997.
- 4 Vsevolodov N.N. Biomolecular electronics. An Introduction via Photosensitive Proteins. Birkhauser:Boston.1998.
- 5 Lewis A., Khatchaturiants A. Treinin M. Chen Z. Peleg G. Friedman N. Bouevith O. Rhothman Z. Loew L. Sheres M. Second-harmonic generation of biological interfaces: probing the membrane protein bacteriorhodopsin and imaging membrane potential around GFP molecules at specific sites in neuronal cells of *C.elegans*. *Chemical Physics* 245, 133-144.1999.
- 6 Birge R.R., Zhang C. F. Lawrence A. F. Optical random access memory based on bacteriorhodopsin. *NewYork*,369-379.1989.
- 7 Marwan W., Hegemann P. Oestrhelt D. Single photon detection by an archaebacterium. *J.Mol.Biol.*, 199, 663-664. 1988.
- 8 Rayfield G. Ultrahigh-speed bacteriorhodopsin photodetectors. *New York*, 361-368. 1989.
- 9 Mobarry C., Lewis A. Implementations of neural networks using photoactivated biological molecules. *Proc.SPIE*, 700, 304-314. 1986.
- 10 Hampp N., Bröuchle C. Oesterhelt D. Bacteriorhodopsin wildtype and variant aspatate-96 asparagine as reversible holographic media. *Biophys.J.* 58, 83-93. 1990.

- 11 Birge R.R. Protein-based optical computing and memories. *IEEE Comput.* 25, 56-57. 1992.
- 12 Thoma R., Happ N. Bröuchle C. Oesterhelt D. Optical limiting by chemically enhanced bacteriorhodopsin films. *Opt.Lett.* 18, 775-777. 1991.
- 13 Zhang Y.H., Song Q. W. Tseronis C. Birge R. R. Real-time holographic imaging with a bacteriorhodopsin film. *Opt.Lett.* 20, 2429-2431. 1995.
- 14 Oesterhelt, D. and W. R. Stoeckenius. Rhodopsin-like protein from the membrane of *Halobacterium Halobium*. *Natur.NewBiol.* 233, 149-152. 1971.
- 15 Grigorieff, N. T. A. Ceska K. H. Downing J. M. Baldwin and R. Henderson. Electron-crystallographic refinement of the structure of bacteriorhodopsin. *J.Mol.Biol.* 259, 393-421. 1996.
- 16 Henderson, R. J. M. Baldwin T. A. Ceska F. Zemlin E. Beckmann and K. H. Downing. Model for the structure of bacteriorhodopsin based on high-resolution electron cryomicroscopy. *J.Mol.Biol.* 213, 899-929. 1990.
- 17 Lücke, H. Atomic resolution structures of bacteriorhodopsin photocycle intermediates: the role of discrete water molecules in the function of this light-driven ion pump. *Biochim. Biophys.Acta* 1460,133-156.2000.
- 18 Birge, R. R. The Nature of the primary photochemical events in rhodopsin and bacteriorhodopsin. *Biochim.Biophys.Acta* (1016), 293-327. 1990.
- 19 Lanyi, J. K. Proton translocation mechanism and energetics in the light-driven pump bacteriorhodopsin. *Biochim.Biophys.Acta* 1183, 241-261. 1993.
- 20 Lanyi, J. K. and G. Varror. The photocycles of bacteriorhodopsin. *Isr.J.Chem.* 35, 365-385. 1995.

- 21 Mathies, R. A., Lin J. B. Ames and W. T. Pollard. From femtoseconds to biology: mechanism of bacteriorhodopsin's light-driven proton pump. *Annu.Rev.Biophys.Biophys.* 20, 491-518. 1991.
- 22 Rothschild, K. J. FTIR difference spectroscopy of bacteriorhodopsin: toward a molecular model. *J.Bioenerg.Biomembr.* 24, 147-167. 1992.
- 23 Balashov, S. P. Photoreactions of the photointermediates of bacteriorhodopsin. *Isr.J.Chem.* 35, 415-428. 1995.
- 24 Chizhov, I. D. S. Chernavskii M. Engelhard K. H. Mueller B. V. Zubov and B. Hess. Spectrally silent transitions in the bacteriorhodopsin photocycle. *Biophys.J.* 71, 2329-2345. 1996.
- 25 Lanyi, J. K. Understanding structure and function in the light-driven proton pump bacteriorhodopsin. *J.Struct.Biol.* 124, 164-178. 1998.
- 26 Blaurock, A. E and Stoeckenius W. Structure of the purple membrane. *Nature New Biol.* 233, 152-155. 1971.
- 27 Ovchinnikov Yu A, Abdulaev N. G. Feigina M. Y. Kiselev A. V. Lobanov N. A. The structural basis of the functioning of bacteriorhodopsin: an overview. *FEBS Lett.* 100, 219-224. 1979.
- 28 Khorana H.G., Gerber G. E. Herlihy W. C. Gray C. P. Amino acid sequence of bacteriorhodopsin. *Proc.Natl.Acad.Sci.U.S.* 76, 5046-5052. 1979.
- 29 Stoeckenius W. Bacterial rhodopsins: evolution of a mechanistic model for the ion pumps. *Protein Science.* 8, 447-459. 1999.
- 30 Henderson R., Unwin PNT. Three-dimensional model of the purple membrane obtained by electron microscopy. *Nature* 257, 28-32. 1975.

- 31 Luecke H., Schobert B. Richter H. T. Cartailler J. P. Lanyi J. K. Structure of bacteriorhodopsin at 1.55Å resolution. *J.Mol.Biol.* 291, 899-911. 1999.
- 32 Belrhali H., Nollert P. Royant A. Menzel C. Rosenbuch J. P. Landau E. M. and Pebay-Peyroula E. *Structure* 7, 909-917. 1999.
- 33 Hess B., Kuschmitz D. The photochemical reaction of the 412nm chromophore of bacteriorhodopsin. *Nature* 258, 766-768. 1977.
- 34 Groma G.I., Dancshyzy. How many M forms are there in the bacteriorhodopsin photocycle? *Biophys.J.* 50, 357-366. 1986.
- 35 Varo G., Lanyi J. K. Thermodynamics and energy coupling in the bacteriorhodopsin photocycle. *Biochemistry* 30, 5016-5022. 1991.
- 36 Perking G., Liu Ed Burkard F. Berry E. A. Glaeser R. M. Characterization of the Conformation Change in the M1 and M2 substrates of bacteriorhodopsin by the combined use of the visible and infrared spectroscopy. *J.Struct.Biol.* 109(142), 151. 1992.
- 37 Lanyi, J. K. and Schobert B. Crystallographic structure of the retinal and the protein after deprotonation of the Schiff base: the switch in the bacteriorhodopsin photocycle. *J.Mol.Biol.* 321, 727-737. 2002.
- 38 Rosenfeld T., Honig B. Ottolenghi M. Hurley J. and Ebrey T. G. Cis-trans isomerization in the photochemistry of vision *Pure Appl.Chem.* 49, 341-351. 1977.
- 39 Hurley J., Ebrey T. G. Honig B. and Ottolenghi M. Temperature and wavelength effects on the photochemistry of rhodopsin, isorhodopsin, bacteriorhodopsin and their photoproducts *Nature (London)* 270, 540-542. 1977.
- 40 Sharkov A.V., Pakulev A. V. Chekalin S. V. Matveetz Yu. A. Primary events in bacteriorhodopsin probed by subpicosecond spectroscopy. *Biochim.Biophys.Acta* 808, 94-102. 1985.

- 41 Mathies R.A., Lin S.W., Ames J.B., and Pollard W.T. From Femtoseconds to Biology: Mechanism of Bacteriorhodopsin's Light-Driven Proton Pump *Rev.Biophys.Chem.* 20, 491-518. 1991.
- 42 Balashov, S. P. and Imasheva E.S., Govindjee R. and Ebrey T. G. Quantum yield ratio of the forward and back light reactions of bR at low temperature and photosteady state concentration of the bathoproduct K. *Photochem.Photobiol.* 54, 955-961. 1991.
- 43 Lozier R.H. and Niederberger W. The photochemical cycle of bacteriorhodopsin. *Fed.Proc.* 36, 1805-1809. 1977.
- 44 Xie A. Quantum efficiencies of bacteriorhodopsin photochemical reactions. *Biophys.J.* 58, 1127-1132. 1990.
- 45 StoECKENIUS W and Lozier R.H. Light energy conversion in *Halobacterium halobium*. *J.Supramol.Struct.* 2, 769-774. 1974.
- 46 Balashov, S. P. and Litvin F.F. Primary photochemical reactions of bacteriorhodopsin in purple membranes and cells of *Halobacteria* at 4K. *Bio-organic Chemistry* 2, 565-566. 1976.
- 47 Tokunaga F., Isawa T. The photoreaction cycle of bacteriorhodopsin: Low temperature spectrophotometry. *Meth.Enzymol.* 88, 163-167. 1982.
- 48 Balashov, S. P. and Ebrey T. Trapping and Spectroscopic Identification of the Photointermediates of Bacteriorhodopsin at Low Temperatures. *Photochem.Photobiol.* 73(5), 453-462. 2001.
- 49 Balashov, S. P., Imasheva E.S., Litvin F. F., and Lozier R.H. The N intermediate of bacteriorhodopsin at low temperatures. Stabilization and photoconversion. *FEBS Lett.* 271, 93-96. 1990.
- 50 Drachev L.A., Kaulen A. D. Skulachev V. P. Zorina V. V. The mechanism of H<sup>+</sup> transfer by bacteriorhodopsin: the properties and the function of intermediate P. *FEBS Lett.* 226, 139-

144. 1987.

51 Gergely C.L., Zimanyi L. and Varo G. Bacteriorhodopsin intermediate spectra determined over a wide pH range . *J.Phys.Chem.B* 101, 9390-9395. 1997.

52 Hampp N. Bacteriorhodopsin as a Photochromic Retinal Protein for Optical Memories. *Chem.Rev.* 100, 1755-1776. 2000.

53 Oesterhelt D., Schulmann L. Reconstitution of bacteriorhodopsin. *FEBS Lett.* 44, 262-265. 1974.

54 Sarma S.D., Rajbhandary U. L. Khorana H. G. Bacterio-opsin mRNA in wild type and bacterio-opsin deficient mutation in *Halobacterium halobium* starins. *Proc.Natl.Acad.Sci.U.S.* 81, 125-129. 1984.

55 Feng Y., Minick D. R. Katz B. Beischel C. J. Hazard E. S. Misra S. Ebrey T. G. Couch R. K. Probing of the retinal binding site of bacteriorhodopsin by affinity labeling. *Biochemistry* 38, 11624-11630. 1993.

56 Steinberg G., Friedman N. Sheves M. Ottolenghi M. Isomer composition and spectra at the dark and light adapted forms at artificial bacteriorhodopsin. *Photochem.Photobiol.* 54, 969-976. 1991.

57 Fang J.M., Carriker J. D. Balogh-Nair V. Nakanishi K. Evidence for the necessity of double bond (13-ene) isomerization in the proton pumping of bacteriorhodopsin. *J.Am.Chem.Soc.* 105, 5162-5164. 1983.

58 Nakanishi K., Crouch R. Application of artificial pigments to structure determination and study of photoinduced transformation of retinal proteins. *Isr.J.Chem.* 35, 253-272. 1995.

59 Oesterhelt D., Krippahl G. Phototrophic growth of halobacteria and its use for isolation of photosynthetically deficient mutants. *Ann.Microbiol.(Inst.Pasteur)* 134B, 137-150. 1983.



- 60 Soppa J., Oesterhelt D. Bacteriorhodopsin mutans of Halobacterium spec. GRB.I. The 5-bromo-2-deoxyuridin-selection as a method to isolate point mutans in Halobacteria. *J.Biol.Chem.* 264, 13043-13048. 1989.
- 61 Soppa J., Otomo J. Straub J. Tittor J. Meessen S. Oesterhelt D. Bacteriorhodopsin mutans of Halobacterium spec. GRB.II. Characterization of mutans. *J.Biol.Chem.* 264, 13049-13056. 1989.
- 62 Greenhalgh D.A., Farrens D. L. Subramanian S. Khorana H. G. Hydrophobic amino acids in the retinal-binding pocket of bacteriorhodopsin. *J.Biol.Chem.* 27, 20305-20311. 1993.
- 63 Mogi T., Stern L. J. Marti T. Chao B. H. Khorana H. G. Aspartic acid substitution affects proton translocation by bacteriorhodopsin M. *Proc.Natl.Acad.Sci.U.S.* 85, 4148-4152. 1988.
- 64 Hackett N.H., Stern L. J. Chao B. H. Kronis K. A. Khorana H. G. Structure-function studies on bacteriorhodopsin, V. Effects of amino acid substitutions in the putative helix F. *J.Biol.Chem.* 262, 9277-9284. 1987.
- 65 Subramanian S., Marti T. Khorana H. G. Protonation state of Asp (Glu)-85 regulates the purple-to-blue transition in bacteriorhodopsin mutans Arg82-Ala and Asp85-Glu: The blue form is inactive in proton translocation. *Proc.Natl.Acad.Sci.U.S.* 87, 1013-1017. 1990.
- 66 Otto H., Marti T. Holz M. Stern L. J. Engel F. Khorana H. G. Heyn M. P. Substitution of amino acids Asp85, Asp212, and Arg 82 in bacteriorhodopsin affects the proton release phase of the pump and PK of the Schiff base. *Proc.Natl.Acad.Sci.U.S.* 87, 1118-1022. 1990.
- 67 Stern L.J., Khorana H. G. Structure-function studies on bacteriorhodopsin. X. Individual substitution of arginine residues by glutamine affect chromophore formation, photocycle, and proton translocation *J.Biol.Chem.*264, 14202-14208. 1989.
- 68 Delaney J.K., Schweiger U. Subramaniam S. Molecular mechanism of protein-retinal coupling in bacteriorhodopsin. *Proc.Natl.Acad.Sci.U.S.* 92, 11120-11124. 1995.

- 69 Subramaniam S., Greenhalgh D. A. Rath P. Rothschild K. J. Khorana H. G. Replacement of leucine-93 by alanine or threonine slows down the decay of the N and O intermediates in the photocycle of bacteriorhodopsin: Implications for proton uptake and 13-cis-retinal-all-trans-retinal reversion. *Proc.Natl.Acad.Sci.U.S.* 88, 6873-6877. 1991.
- 70 Roosenheek K., Brith-Linder M. Linder P. Zakaria A. Caplan S. Proteolysis and flash photolysis of bacteriorhodopsin in purple membranes fragments. *Biophys.Struct.Mech.* 4, 301-313.1978.
- 71 Hristova S.G., Der A. Varo G. Kesthelyi L. Effect of pH on photocycle and electric signal kinetics in the purple membrane subjected to digestion with proteolytic enzymes. *Photobiochem.Photobiophys.* 12, 231-241. 1986.
- 72 Lukashov E.P., Kononenko N. G. Abdulaev N. G. Ebrey T. G. Retardation of the photocycle in bacteriorhodopsin by cyclohexanedione. *Bio-organic Chemistry* 19, 395-405. 1992.
- 73 Abdulaev N.G., Feigina M. Yu. Kiselev A. V. Ovchinnikov Yu. A. Drachev L. A. Kaulen A. D. Khitrina L. V. Skulachev V. P. Products of limited proteolysis of bacteriorhodopsin generate a membrane potential. *FEBS Lett.* 90, 190-194. 1978.
- 74 Beence D., Bronw S. F. Czege J. et al. Effect of viscosity on the photocycle of bacteriorhodopsin. *Photochem.Photobiol.* 33, 517-522. 1981.
- 75 Eisenstein L. Effect of viscosity on the photocycle bacteriorhoopsin. *Meth.Enzymol.* 88, 297-305. 1982.
- 76 Neugebauer D.Ch., Blaurock A. E. Worcester D. L. Magnetic orientation of purple membrane demonstration by optical measurements and neutron scattering. *FEBS Lett.* 78, 31-35. 1977.
- 77 Shinar K., Drukmann S. Ottolenghi Korenstein. Electric field effect in bacteriorhodopsin. *Biophys.J.* 19, 1-6. 1977.

78 Borisevitch G.P., Lukashev E. N. Kononenko A. A. Rubin A. B. Bacteriorhodopsin BR570 bathochromic band shift in an external electric field. *Biochim.Biophys.Acta* 549, 171-174. 1979.

79 Varo G., Lanyi J. K. Distortion in the photocycle of bacteriorhodopsin at moderate dehydration. *Biophys.J.* 59, 313-322. 1991.

80 Korenstein R., Hess B. Hydration effect on the photocycle bacteriorhodopsin in thin layers of purple membrane. *Nature* 270, 184-186. 1977.

81 Dyukova T.V., Vsevolodov N. N. Chekulaeva L. N. Changing of bacteriorhodopsin photochemical activity in the polymeric matrix at dehydration. *Biophysics* 30, 613-616. 1985.

82 Lazarev Yu.A., Terpugov E. Effect of water on the structure of bacteriorhodopsin and photochemical processes in purple membrane. *Biochim.Biophys.Acta* 590, 324-328. 1980.

83 Tanny G., Caplan S. P. Eisenbach M. Interaction of purple membrane with solvents. I. Applicability of solubility parameter mapping. *Biochim.Biophys.Acta* 554, 269-278. 1979.

84 Eisenbach M., Caplan R. Interaction of purple membrane with solvents: II Mode in interaction. *Biochim.et Biophys.Acta* 554, 281-292. 1979.

85 Hwang S.B., Stoeckenius W. Purple membrane vesicles: morphology and proton translocation. *Membrane Biol.* 33, 325-350. 1977.

86 Dencher N.A., Heyn M. P. Formation and properties of bacteriorhodopsin monomers in the non-ionic detergents octyl- $\beta$ -D-glucoside, Triton X-100. *FEBS Lett.* 96, 322-326. 1978.

87 Padros E., Dumach M. Sabes M. Induction of the blue form of bacteriorhodopsin by low concentrations of sodium dodecylsulfate. *Biochim.et Biophys.Acta* 769, 1-7. 1984.

88 Huang J.Y., Chen Z. Lewis A. Second-Harmonic Generation in Purple Membrane-Poly(vinyl alcohol) Films: Probing the Dipolar Characteristics of the Bacteriorhodopsin

Chromophore in bR570 and M412. *J.Phys.Chem.*93, 3314-3320.1989.

89 Birg R.R., Zhang C. F. Two-photon double resonance spectroscopy of bacteriorhodopsin. Assignment of the electronic and dipolar properties of the low-lying 1Ag-like and 1Bu-like pi-pi states. *J.Chem.Phys.* 92, 7178-7195. 1990.

90 Clays K., Hendrickx E. Triest M. Verbiest T. Persoons A. Dehu C. Bredas J. L. Nonlinear optical properties of proteins measured by Hyper-Rayleigh scattering in solution . *Science* 262, 1419-1422. 1993.

91 Clays K., Elshocht S. V. Bacteriorhodopsin: a natural (nonlinear) photonic bandgap material. *Optics letters* 25, 1391-1393. 2000.

92 Clays K., Elshost V. Chi M. Bacteriorhodopsin: a natural, efficient (nonlinear) photonic crystal. *J.Opt.Soc.Am.B* 18, 1474-1482. 2001.

93 Bazhenov V.Yu., Soskin M. S. Taranenko V. B. Vasnetsov M. V. *Optical processing and Computing* . New York . 1989.

94 Hampp N., Bröuchle C. in Dürr H. Bouas-Laurent H. *Photochromism: Molecules and system*, 954. 1990.

95 Chemla D.S., Zyss J. *Nonlinear optical properties of organic molecules and crystals*. Academic Press, INC. 1987.

96 Kanis D.R., Ratner M. A. and Marks T. J. Design and Constaruction of Molecular Assemblies with Large Second-Order Optical Nonlinearities. *Quantum Chemical Aspects*. *Chem.Rev.* 94, 195-242. 1994.

97 Amstrong J.A., Bloemberg N. Ducuing J. and Pershan P. S. Interactions between light waves in a nonlinear dielectric *Phys.Rev.*127, 1918. 1962.

- 98 Terhune R.M., Maker P. D. and Savage C. M. Measurements of nonlinear light scattering  
Phys.Rev.Letters 14, 681. 1965.
- 99 Kielich S., Lalanne J. R. and Martin F. B. Double-photon elastic light scattering by liquids  
having centrosymmetric molecules. Phys.Rev.Letters 26, 1295. 1971.
- 100 Clays K., Persoons A. Hyper-Rayleigh scattering in solution. Rev.Sci.Instrum. 63(6),  
3285-3289. 1992.
- 101 Andrews D.L. Modern nonlinear optics. Adv.Chem.Phys. 85(3), 545. 1994.
- 102 Wortmann R. Habilitationsschrift, Johannes Gutenberg-Universität. Mainz . 1993.
- 103 Clays K., Persoons A. Hyper-Raleigh scattering in solution. Phys.Rev.Letters 66, 2980-  
2983. 1991.
- 104 Jensen F. Introduction to Computational Chemistry. JOHN WILEY & SONS. 1999.
- 105 Molecular orbital package MOS-F V7.0. User's manual. Fujitsu. 2006.
- 106 M.C.Zerner, G. H. Loew R. F. Kirchner and U. T. Mueller-Westerhoff. An intermediate  
neglect of differential overlap technique for spectroscopy of transition-metal complexes.  
J.Am.Chem.Soc. 102, 589. 1980.
- 107 W.P.Anderson, W. D. Edwards and M. C. Zerner. Calculated Spectra of Hydrated Ions of  
the First Transition-Metal Series Inorg.Chem. 25, 2728. 1986.
- 108 Sekino H., Barlett R. J.Chem.Phys. Frequency dependent nonlinear optical properties of  
molecules. 85, 976-989. 1986.
- 109 Luo Y., Agren H. Vahtras O. Jorgensen P. The hyperpolarizability dispersion of para-  
nitroaniline. Phys.Chem.Lett. 190, 194. 1993.

- 110 Ward J.F. (1965) Calculation of nonlinear optical susceptibilities using diagrammatic perturbation theory. *Rev.Mod.Phys.*, 37, 1-18.
- 111 Allen S., Morley J. O. Pugh D. Docherty V. J. *J.Proc.SPIE-Int.Soc.Opt.Eng.* 682, 20-26. 1987.
- 112 M.Born. *Physik* 1, 45. 1920.
- 113 L.Onsager. Electric moments of molecules in liquids *J.Am.Chem.Soc.* 58, 1486. 1936.
- 114 M.Cossi, V. Barone R. Cammi and J. Tomassi. Ab initio study of solvated molecules: a new implementation of the polarizable continuum model. *Chem.Phys.Lett.* 255, 327. 1996.
- 115 A.Klamt and G.Schuemann. COSMO: A New Approach to Dielectric Screening in Solvents with Explicit Expressions for the Screening Energy and its Gradient. *J. Chem. Soc. Perkin Transactions 2*, 799-805. 1993.
- 116 Gao J. Hybrid Quantum and Molecular Mechanical Simulations: An Alternative Avenue to Solvent Effects in Organic Chemistry.*J.Acc.Chem.Res.* 29, 298. 1996.
- 117 Monard G., Merz K. M. Combined Quantum Mechanical/Molecular Mechanical Methodologies Applied to Biomolecular Systems. *J.Acc.Chem.Res.* 32, 904. 1999.
- 118 Stewart J.J. Application of localized molecular orbitals to the solution of semiempirical self-consistent field equations *J.Quantum Chem.* 58, 133-136. 1996.
- 119 Molecular orbital package MOS-F V7.0 Users manual. 2005.
- 120 H.Houjou, Y. Inoue and M. Sakurai. Study of the Opsin Shift of Bacteriorhodopsin: Insight from QM/MM Calculations with Electronic Polarization Effects of the Protein Environment. *J.Phys.Chem.B* 105, 867-879. 2001.
- 121 Van der Steen, R. Biesheuvel P. L. Mathies M. A. Lugtenburg L. Retinal analogs with locked 6-7 conformations shows that bacteriorhodopsin require the 6-s-trans conformation of

the chromophore. *J. Am. Chem. Soc.* (108), 6410-6411. 1986.

122 Bassov T., Sheves M. Model compounds for the study of spectroscopic properties of visual pigments and bacteriorhodopsin. *J. Am. Chem. Soc.* 107, 7524-7533. 1985.

123 Irving C.S. and Byers G.W., Leermakers P. A. Spectroscopic model for the visual pigments. Influence of microenvironmental polarizability. *Biochemistry* 9, 858. 1970.

124 Hermann J.P., and Ducuing J. Third-order polarizabilities of long-chain molecules. *J. App. Phys.* 45, 5100-5102. 1974.

125 Hendrickx E., Clays K. Persoons A. Dehu C. and Bredas J. L. The Bacteriorhodopsin Chromophore Retinal and Derivatives: An Experimental and Theoretical Investigation of the Second-Order Optical Properties. *J. Am. Chem. Soc.* 117, 3547-3555. 2006.

126 Birge R.R., Masthay M. B. Stuart J. A. Tallent J. R. and Zhang C. F. Nonlinear Optical Properties of Bacteriorhodopsin: Assignment of the Third-order Polarizability Based on Two-Photon Absorption Spectroscopy. *SPIE* 1432, 129-140. 1991.

127 Kliger D.S., Milder S. J. Dratz E. A. Solvents effects on the spectra of retinal Schiff bases –I. Models for the bathochromic shift of the chromophore spectrum in visual pigments. *Photochem. Photobiol.* 25, 277. 1977.

128 Milder S.J., Kliger D. S. Solvents effects on the spectra of retinal Schiff bases-11. Models for convergence and clustering of visual pigment spectra. *Photochem. Photobiol.* 25, 287. 1977.

129 Ferrando E., Schweiger U. Oesterhelt D. Homologous bacterio-opsin-encoding gene expression via site-specific vector integration. *Gene* 125, 41-47. 1993.

130 Fischer U., Oesterhelt D. Chromophore equilibria in bacteriorhodopsin. *Biophys. J.* 28, 211-230. 1979.

131 Mowery P.C., Lozier R. H. Chae Q. Tsen Y. W. Taylor M. and Stoeckenius W. Effect of acid pH on the absorption spectra and photoreactions of bacteriorhodopsin . *Biochemistry* 18, 4100-4107. 1979.

132 Metz G., Siebert F. Engelhard M. Asp85 is the only internal aspartic acid that gets protonated in the M intermediate and the purple-to-blue transition of bacteriorhodopsin A solid-state<sup>13</sup>C CP-MAS NMR investigation. *FEBS Lett.* 303, 237. 1992.

133 Balashov S.P., Ebrey T. G. Bacteriorhodopsin: molecular mechanisms of transmembrane proton transfer. *The Spectrum* 7(3), 1-9. 1994.

134 Balashov S.P., Govindjee R. Kono M. Imasheva S. Lukachev E. Ebrey T. G. Crouch R. K. Menick D. R. Feng Y. Effect of the arginine-82 to alanine mutation in bacteriorhodopsin on dark adaptation, proton release, and the photochemical cycle. *Biochemistry* 32, 10331. 1993.

135 Brown L.S., Bonet L. Needleman R. Lanyi J. K. Estimated acid dissociation constants of the Schiff base, Asp-85, and Arg-82 during the bacteriorhodopsin photocycle. *Biophys.J.* 65, 124. 1993.

136 Balashov S.P., Govindjee R. Imasheva S. Misra S. Ebray T. G. Feng Y. Crouch R. K. Menick D. R. The two pKa's of aspartate-85 and control of thermal isomerization and proton release in the arginine-82 to lysine mutant of bacteriorhodopsin. *Biochemistry.* (34), 8820-8834, 1995.

137 Mathies R.A., Brito Cruz C. H. Pollard W. T. and Shank C. V. Direct observation of the femtosecond excited-state cis-trans isomerization in bacteriorhodopsin . *Science* 240, 777a. 1988.

138 Oesterhelt D., Schumann L. and Gruber H. Light-dependence reaction of bacteriorhodopsin withhydroxylamine in cell suspensions of *Halobacterium halobium*: demonstration of an apo-membrane. *FEBS Lett.* 44, 257-261. 1974.



- 139 Subramaniam S., Marti T. Roesslet S. J. Rothschild K. J. and Khorana H. G. The reaction of hydroxylamine with bacteriorhodopsin studied with mutants that have altered photocycles: Selective reactivity of different photointermediates. *Proc.Natl.Acad.Sci.U.S.* 88, 2583-2587. 1990.
- 140 Berne B.J., Pecora R. *Dynamic Light Scattering with applications to chemistry, biology, and physics.* JOHN WILEY & SONS. 1976.
- 141 Rouso I., Khatchatryan E. Brodsky I. Nachustai R. Ottolenghi M. Sheves M. Lewis A. Microsecond atomic force sensing of protein conformational dynamics: Implications for the primary light-induced events in bacteriorhodopsin. *Proc.Natl.Acad.Sci.U.S.* 94, 7937. 1997.
- 142 Xie A.H., Nagle J. F. Lozier R. H. Flash spectroscopy of purple membrane. *Biophys.J.* 51, 627-635. 1987.
- 143 Rink T., Pfeiffer M. Oesterhelt D. Gerwert K. Steinhoff H. J. Unraveling Photoexcited Conformational Changes of Bacteriorhodopsin by Time Resolved Electron Paramagnetic Resonance Spectroscopy. *Biophys.J.* 78, 1519-1530. 2000.
- 144 Rink T., Riesle J. Oesterhelt D. Gerwert K. Steinhoff H. J. Spin-Labeling Studies of the Conformational Changes in the Vicinity of D36, D38, T46, and E161 of Bacteriorhodopsin during the Photocycle. *Biophys.J.* 73, 983-993. 1997.
- 145 Schätzler B., Dencher N. Tittor J. Oesterhelt D. Yaniv-Checover S. Nachliel E. and Gutman M. Subsecond Proton-Hole Propagation in Bacteriorhodopsin. *Biophys.J.* 84, 671-686. 2003.
- 146 Dancshazy Zs., and Karvaly B. Incorporation of bacteriorhodopsin into a bilayer lipid membrane; a photoelectric-spectroscopic study. *FEBS Lett.* 72, 136-138. 1976.
- 147 Bamberg E., Dencher N. A. Fahr A. and Heyn M. P. Transmembraneous Incorporation of Photoelectrically Active Bacteriorhodopsin in Planar Lipid Bilayers. *Proc.Natl.Acad.Sci.U.S.* 78, 7702-7706. 1981.

- 148 Müh F., Madjet M. Adolphs J. Abdurahman A. Rabenstein B. Ishikita H. Knapp E. W. and Renger T. Alpha-Helices direct excitation energy flow in the Fenna-Matthews-Olson protein. PNAS 104(43), 16862-16867. 2007.
- 149 Dencher N., Dresselhaus G. Zaccai G. and Büldt G. Structural changes in bacteriorhodopsin during proton translocation revealed by neutron diffraction. Proc.Natl.Acad.Sci.U.S. 86, 7876-7879. 1989.
- 150 Subramaniam S., Gerstein M. Oesterhelt D. and Henderson R. Electron diffraction analysis of structural changes in the photocycle of bacteriorhodopsin. EMBO J. 12(1), 8. 1993.
- 151 Lücke H., Schobert B. Richter H. T. Cartailier J. P. Lanyi J. K. Structural changes in bacteriorhodopsin during ion transport at 2 angstrom resolution. Science 286, 255-260. 1999.
- 152 Kamikubo H. and Oka T., Imamoto Y. Tokunaga F. Lanyi J. K. and Kataoka M. The last phase of the reprotonation switch in bacteriorhodopsin: the transition between the the M-type and N-type protein conformation depends on hydration. Biochemistry 36, 12282-12287. 1997.
- 153 Steinhoff H.J., Mollaaghababa R. Altenbach C. Hideg K. Krebs M. Khorana H. G. Hubell WL. Time-resolved detection of structural changes during the photocycle of spin-labeled bacteriorhodopsin. Science 266, 105-107. 1994.
- 154 Gerwert K., Souvignier G. and Hess B. Simultaneous monitoring of light-induced changes in protein side group protonation, chromophore isomerization and backbone motion of bacteriorhodopsin by time-resolved Fourier-transform infrared spectroscopy. Proc.Natl.Acad.Sci.U.S. 87, 9774-9778. 1990.

## **List of Publications Resulting From This Work**

Bordignon, E., Klare, J.P., Holterhues, J., Martell, S., Krasnaberski, A., Engelhard, M., Steinhoff, H.-J. Analysis of Light-Induced Conformational Changes Natronomonas pharaonis Sensory Rhodopsin II by Time Resolved Electron Paramagnetic Resonance Spectroscopy. Photochem. and Photobiol. 83: 263–272 (2007)

Borovykh I.V., Zielke V., Krasnaberski A., Pfeiffer M., Steinhoff H.-J. „Effect of various salts on the structure and function of bacteriorhodopsin: site-directed spin labelling study”. To be submitted.

## Acknowledgment

First of all I would like to thank my supervisor Prof. Dr. H.-J. Steinhoff for giving me the opportunity to carry out this very interesting PhD project at the University of Osnabrück and for his scientific guidance during the past three years.

The financial support from the Graduate College 695 “*Nonlinearities of Optical Materials*”, financed by the Deutsche Forschungsgemeinschaft and the Federal State of Niedersachsen, is gratefully acknowledged.

I am grateful to Prof. Dr. A. Mulkidjianian for giving me the opportunity to work with his facilities, useful advice connected with my work.

Many thanks go to my colleagues, Dr. I. Borovykh, Dr. E. Bordignon, Dr. J. Klare for a nice working atmosphere, help and advice.

I am thankful to mechanic and electronic workshops for excellent help in many problems related to the creation and reparation of the mechanical and electronical parts during experiments.

My apologies to the others who I have not mentioned by name, I am indebted to them for the many ways they helped me.

Finally, I would like to thank my wife Maryna and parents for their steady understanding and motivation.

### **Eidesstattliche Erklärung**

Hiermit erkläre ich an Eides Statt, die vorliegende Abhandlung selbständig und ohne unerlaubte Hilfe verfasst, die benutzten Hilfsmittel vollständig angegeben und noch keinen Promotionsversuch unternommen zu haben.

Osnabrück, den 5. Januar 2008

(A. Krasnaberski)